Material characterization using spectrofluorometers

By

Charles B. Nettles

A Dissertation
Submitted to the Faculty of
Mississippi State University
in Partial Fulfillment of the Requirements
for the Degree of Doctor of Philosophy
in Chemistry
in the Department of Chemistry

Mississippi State, Mississippi

December 2016

Material characterization using spectrofluorometers

By

Charles B. Nettles

Approved:

_____

Dongmao Zhang
(Major Professor)

_____

David O. Wipf
(Committee Member)

_____

Todd E. Mlsna
(Committee Member)

_____

Nicholas C. Fitzkee
(Committee Member)

_____

Stephen C. Foster
(Graduate Coordinator / Committee Member)

_____

Rick Travis
Interim Dean
College of Arts & Sciences

Name: Charles B. Nettles

Date of Degree: December 9, 2016

Institution: Mississippi State University

Major Field: Chemistry

Major Professor: Dongmao Zhang

Title of Study: Material characterization using spectrofluorometers

Pages in Study 107

Candidate for Degree of Doctor of Philosophy

The use of spectrofluorometers to examine nanomaterials is quite popular using either fluorescence or synchronous measurements. However, understanding how a material's optical properties can influence spectral acquisition are of great importance to accurately characterize nanomaterials. This dissertation presents a series of computational and experimental studies aimed at enhancing the quantitative understanding of nanoparticle interactions with matter and photons. This allows for more reliable spectrofluorometer based acquisition of nanoparticle containing solutions.

Chapter I presents a background overview of the works described in this dissertation. Correction of the gold nanoparticle (AuNP) inner filter effect (IFE) on fluorophore fluorescence using PEGylated AuNPs as an external reference method is demonstrated in Chapter II. The AuNP IFE is corrected to quantify tryptophan fluorescence for surface adsorbed proteins. We demonstrate that protein adsorption onto AuNPs will only induce ~ 20% tryptophan fluorescence reduction instead of the commonly assumed 100% reduction.

Using water Raman intensities to determine the effective path lengths of a spectrofluorometer for correction of fluorophore fluorescence is discussed in Chapter III.

Using $Ni(NO_3)_2$ and $K_2Cr_2O_7$ as Raman IFE references, the excitation and emission path lengths are found to exhibit chromophore and fluorophore independence, however path lengths are spectrofluorometer dependent.

Finally, ratiometric resonance synchronous spectroscopy (R_2S_2) is discussed in Chapter IV. Using a combination of UV-vis and R_2S_2 spectroscopy, the optical cross sections of a wide range of nanomaterials were determined. Also on-resonance fluorescence in solution is demonstrated for the first time. The nanoparticles discussed range from photon absorbers, scatterers, simultaneous photon absorbers and scatterers, all the way to simultaneous photon absorbers, scatterers, and emitters.

ACKNOWLEDGEMENTS

This dissertation would not be possible without the help and support of many wonderful people.

First and foremost, I would like to thank Dr. Dongmao Zhang for his mentoring throughout the course of my Ph. D. studies. His guidance and direction has helped me through many difficult academic times.

I am grateful to my committee members Dr. Stephen C. Foster, Dr. David O. Wipf, Dr. Todd E. Mlsna, and Dr. Nicholas C. Fitzkee for their helpful suggestions and discussions.

Lastly, I want to thank my current and past lab members including Dr. Karthikeshwar Vangala, Dr. Siyam Ansar, Dr. Fathima Ameer, Dr. Manuel Gadogbe, Ganganath Perera, and Kumudu Siriwardana.

DEDICATION

I would like to dedicate this doctoral dissertation to my wife, Whitnee Nettles, my son, Brays Monroe Nettles, and my parents, Bruce Nettles, Glenda Nettles, and Mandy Nettles.

TABLE OF CONTENTS

LIST OF TABLES

LIST OF FIGURES

LIST OF SCHEMES

CHAPTER I

INTRODUCTION

1.1 Fluorescence and Spectrofluorometers

The typical spectrofluorometer has an instrumental setup for detection at a 90^{o} angle compared to the 180^{o} detection for absorption spectroscopy. This instrument configuration allows for detection of both fluorescence and scattering with limits of detection approximately three orders of magnitude lower than absorbance spectroscopy.[1] Figure 1.1 illustrates a partial energy-level diagram or Jablonski diagram, that represents the typical energy transitions that occur for fluorescence molecules. The heavier lines of S_0, S_1, and S_2 represent the lowest vibrational state of each electronic state while the lighter lines are higher energy vibrational states. Molecules can absorb photons of a given frequency while at their lowest energy electronic state, ground state (S_0), to any number of excited electronic states (denoted S_1 and S_2). Regardless of frequency that corresponds to photon absorption, fluorescence emission can only occur once the molecules have relaxed to the lowest electronic excited state (ground vibrational energy level of S_1). Stokes-shifted fluorescence emission results when the molecule is excited at a higher frequency relative the emission frequency. Resonance fluorescence results when emission occurs at the same frequency as the excitation frequency. There is a lack of information available on resonance fluorescence for species in solution and most information pertains to resonance fluorescence for dilute atomic vapors.[2-4] The lack of

information on resonance fluorescence for species in solution is possibly due to the fact that off-resonance or Stokes-shifted fluorescence can arise from a multitude of excitation frequencies with fluorescence detection due to emission/relaxation at a variety of different vibrational ground states. However, the energy distribution of the processes responsible for resonance fluorescence require that excitation and emission frequencies exactly match. As demonstrated in Chapter 4, this can account for the drastic decrease in resonance fluorescence quantum yields compared to Stokes-shifted fluorescence quantum yields.

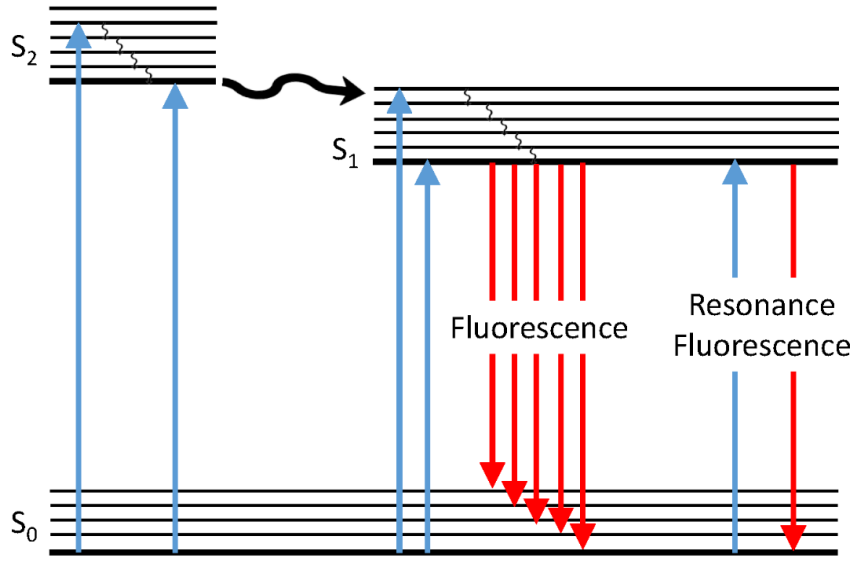

Figure 1.1 Fluorescence Jablonski diagram.

Both Raman and Rayleigh scattering can be detected using a spectrofluorometer. The energy level diagram depicted in Figure 1.2 illustrates the energy changes that occur for both Raman and Rayleigh scattering processes.[1] The most important note for scattering processes is that molecules are excited to a short-lived, unobservable virtual

state. Meaning that each virtual state has an associated energy but no direct measurement of its energy is possible. The difference between Rayleigh and Raman scattering stem from the difference between the excitation photons and the scattered photons. Rayleigh scattering is detected when the frequency difference is zero while Raman scattering is detected at frequencies greater than or less than that of the excitation frequency.

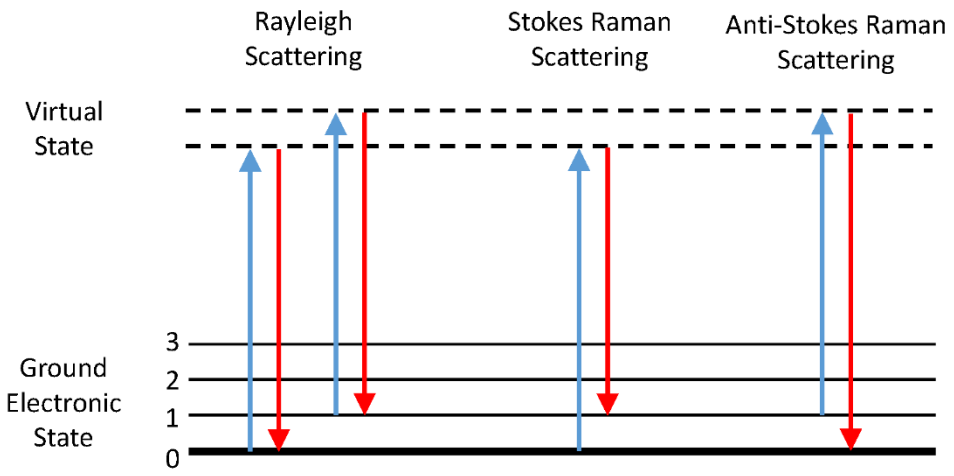

Figure 1.2 Raman and Rayleigh scattering energy diagram.

Resonance light scattering (RLS) observed in the literature from nanomaterials or aggregated species in solutions are the most commonly encountered scattering spectra acquired using spectrofluorometers.[5-8] Most RLS data contains inherent interferences pertaining to the solvent medium and instrumental artifacts as demonstrated in the experimental data acquired in Figure 1.3. The series of peaks centered at 467 nm are characteristic of instrumental artifacts due to the excitation monochromator of a Horiba Fluoromax-4 spectrofluorometer. Therefore, our group developed a ratiometric resonance synchronous spectroscopy (R_2S_2) technique that utilizes a solvent spectrum as

an internal reference to correct for these interferences. This allowed for the acquisition of resonance scattering or resonance fluorescence.[9] The R_2S_2 technique can be used on any spectrofluorometer while in synchronous mode set to a 0 nm wavelength offset in which the excitation and detection wavelengths are the same.

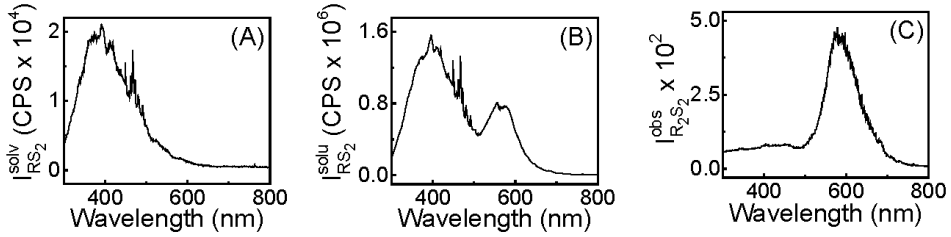

Figure 1.3 Resonance synchronous spectra (RS_2) of water and AuNPs in water to determine the ratiometric resonance synchronous spectra (R_2S_2) of AuNPs.

Notes: Resonance synchronous spectra (RS_2) of water (A) and AuNP dispersed in water (B), respectively. (C) AuNP R_2S_2 spectra without instrumental or solvent artifacts.

1.2 Gold Nanoparticles

Colloidal gold nanoparticles (AuNP) are a suspension of nanometer-sized gold particles and their use in stained glass dates back to over 2000 years.[10] AuNP research did not pick up until after Michael Faraday's discovery that colloidal gold has different properties than bulk gold.[11] AuNPs with diameters ranging from 10-90 nm exhibit an intense red color due to localized surface plasmon resonance (LSPR) from the collective oscillation of conduction electrons across the nanoparticle (NP) excited by incoming photons from an electromagnetic field at visible wavelengths.[12-15] The oscillation of conduction electrons upon interacting with an electromagnetic field is depicted in Figure 1.4.[13] AuNPs with a particle size around 10 nm in diameter have a strong UV-vis extinction maximum around 520 nm in aqueous solution due to their LSPR. As the NP

diameter increases, the LSPR band red-shifts due to electromagnetic retardation in larger particles.

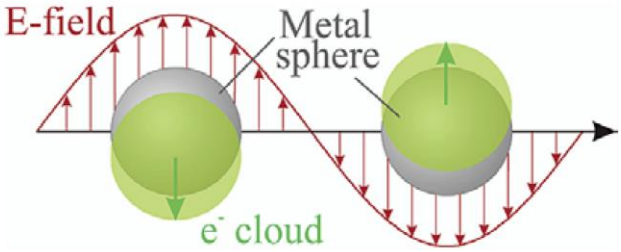

Figure 1.4 Schematic representation of plasmon oscillation for a metal sphere, where the displacement of the conduction electron cloud is relative to the nuclei.

Through theoretical and experimental studies, the AuNP LSPR is known to be a contribution of both photon absorption and scattering in which the AuNP absorption and scattering cross-section changes according to the size, shape, and composition of the NP.[16-18] The general theory of light scattering induced by spherical particles was originally developed by Mie.[19,20] The scattering cross-section of a particle with radius "*r*" much smaller than the wavelength of light (more accurately $2\pi r << \lambda$), varies as r^6, while the absorption cross-section varies as r^3. Therefore, as the radius of the nanoparticle increases, the scattering cross-section drastically increases as shown in Eq. 1.1.[19] Where σ_{scatt} is the NP scattering cross-section and m is the ratio of refractive indices of the particle and the medium in which the particle is dispersed.

$$\sigma_{scatt} = \frac{128\pi^5}{3\lambda^4} r^6 \left| \frac{m^2 - 1}{m^2 + 2} \right|^2 \qquad \text{Eq. 1.1}$$

1.3 Near- and Far-Field Effects

AuNPs exhibit both near- and far-field effects on fluorophore fluorescence. AuNP near-field effects (NFE) typically come into play if the fluorophore is in direct contact with or within ~10 nm of the AuNP surface.[21,22,23,24] NFEs range from surface resonance energy transfer (SET) and Forster resonance energy transfer (FRET) to static and dynamic quenching. NFEs can either result in fluorophore fluorescence reduction or enhancement.[23,25,26] Static and dynamic quenching are characteristic of a fluorophore directly in contact to the NP surface. AuNP induced static or dynamic quenching results when the AuNP acts as a quencher to reduce the fluorophore fluorescence. Static quenching occurs when the fluorophore is chemically or physically bound to the AuNP surface while dynamic quenching occurs upon collision of the fluorophore with the AuNP surface.[27] FRET and SET occur when the AuNP LSPR band overlaps with the emission band of a fluorophore allowing the excited-state fluorophore to interact with free electrons of the metal. FRET involves the non-radiative transfer of excitation energy from an excited donor fluorophore to a proximal ground-state acceptor in which the AuNP acts as the acceptor.[28] Therefore, AuNP FRET reduces the fluorophore fluorescence. SET can increases the fluorophore fluorescence intensity by altering the fluorophore's quantum yield based on the fluorophore's proximity to the surface.[29] FRET and SET efficiencies are dependent on the distance separating the fluorophore from the NP surface. FRET and SET efficiencies follow a sixth and fourth power dependence, respectively. As shown in Eq. 1.2 and 1.3, ϕ represents energy transfer efficiency, d represents the distance separating the fluorophore from the NP surface, and d_0 represents the distance at which energy transfer efficiency is 50%. Therefore, FRET

efficiency diminishes at shorter distances compared to SET efficiencies. Despite extensive experimental and theoretical works on the various NP NFEs, quantitative decoupling of the contribution of individual NFEs to the overall NP induced fluorescence signal variation is currently impossible. This is especially true for fluorophores in large molecules such as proteins in which different fluorophores in the same protein molecule can experience different NP NFEs.[29] The current understanding of NP NFEs on fluorophore fluorescence is investigated through the collective or ensemble averaged effect.

$$\phi_{FRET} = \frac{1}{1+(\frac{d}{d_0})^6} \qquad \text{Eq. 1.2}$$

$$\phi_{SET} = \frac{1}{1+(\frac{d}{d_0})^4} \qquad \text{Eq. 1.3}$$

The NP far-field effects (FFEs) refer to interactions that can change fluorescence signals of all fluorophores in solution, regardless of fluorophore and nanoparticle distance.[30,31,32,33,34] AuNP far-field effects are subcategorized into either inner filter effects (IFE) or multipath effects (MPE). IFE is well-known in fluorescence and Raman spectroscopy and is attributed to the attenuation of excitation and emission light intensities induced by photon absorbers in the sample solution that can cause spectral distortion and nonlinearity between fluorescence signal intensity and fluorophore concentration.[31,35-42] IFE results from photon absorption that can reduce the number of excitation photons that reach the fluorophore and/or reduce the number of emission

photons that reach the detector. IFEs are an inherent issue for all fluorophores since photon absorption must occur to induce fluorescence emission. The effect of IFEs on a simple fluorophore (2-aminopurine) in solution is illustrated in Figure 1.5. Even though the absorbance is linearly related to molecular concentration, the corresponding fluorescence emission does not exhibit a linear relation at high fluorophore concentrations.

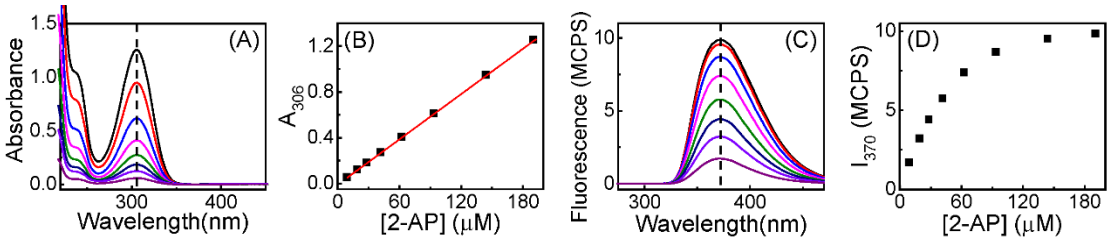

Figure 1.5 UV-vis and fluorescence measurements for 2-aminopurine.

Notes: (A) UV-vis and (C) fluorescence spectra for solutions containing 2-aminopurine. (B) and (D) illustrate peak absorbance and peak fluorescence intensities for spectra shown in (A) and (C) respectively.

Correcting the AuNP IFE is critically important since AuNPs exhibit broad spectrum absorption from 200 to 600 nm. Modelled UV-vis extinction spectra for AuNPs of 10, 30, 50, and 70 nm diameter are shown in Figure 1.6. The UV-vis spectra are broken into their absorbance and scattering counterparts. UV-vis spectral acquisition can detect both absorbance and scattering. For solutions that are known to only absorb light, the corresponding spectra have a y-axis label of absorbance. However, solutions such as nanoparticles are known to both absorb and scatter light and the corresponding UV-vis spectra have a y-axis label of extinction. As illustrated in Figure 1.6, even when the AuNP diameter is as large as 70 nm, the absorbance component in UV-vis

measurements is still significant with ~ 70% of the LSPR extinction peak attributed to photon absorption. Therefore, the larger AuNPs can significantly impose IFEs on fluorescence measurements. Correction for IFE becomes vital when the photon absorbing species has a UV-vis absorbance above 0.05.[43-47] . Over the past 50 years, there has been a substantial amount of research aimed at correcting fluorescence IFE.[44,48-56] However, many of these correction strategies utilize specialized instrumentation or tedious mathematical manipulation. A simpler correction scheme that is broadly applicable is highly desirable.

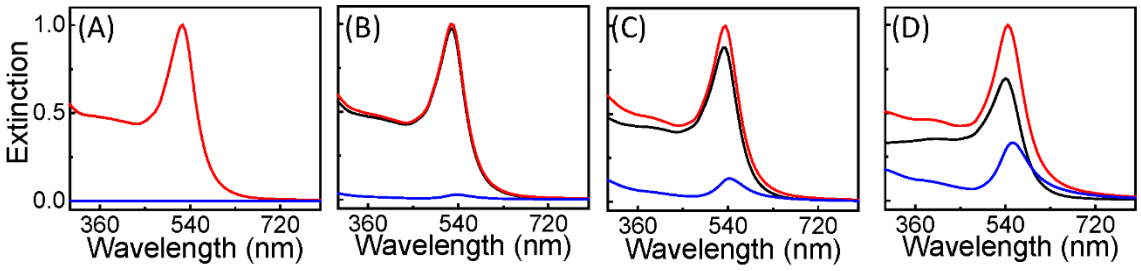

Figure 1.6 Computationally modelled AuNP UV-vis spectra for AuNPs of different diameters.

Notes: Extinction, absorption, and scattering spectra for AuNPs with particle diameters of (A) 10 nm, (B) 30 nm, (C) 50 nm, and (D) 70 nm, respectively. Extinction, absorbance, and scattering are shown in red, black, and blue lines, respectively.

Most of the current literature investigating nanoparticle interfacial phenomena using fluorescence, either does not consider the NP FFE or the only NP FFE considered is the fluorescence inner filter effect (IFE) imposed by NPs.[32,31,57,58,59] In the latter cases, the NPs were commonly treated as molecular chromophores and their FFE on fluorophore fluorescence was corrected on the basis of the UV-vis extinction of the NP-containing solutions without considering the NP scattering contribution to the UV-vis

extinction.[57,58,60] The AuNP multipath effect (MPE) results from photon scattering off the NP surface that increases the path length of photons in the solution medium. Scattering of emitted photons should have no significant effect on the number of photons reaching the detector since the distribution of the total number of photons in the cuvette is dominated by the number of excitation photons. However, scattering of excitation photons can have two competing effects (Scheme 1.1). On one hand, scattering of excitation photons reduces the number of photons that can interact with fluorophores in solution of the probed volume, reducing the detected fluorescence intensity (Scheme 1.1 (A)).[61] On the other hand, it can increase the possibility of individual excitation photons to interact with fluorophores in solution by scattering excitation photons back and forth (Scheme 1.1 (B)).[62,63] The latter effect is termed the multipath effect (MPE) because it enhances the fluorescence signal through the NP multiplicative scattering effect.

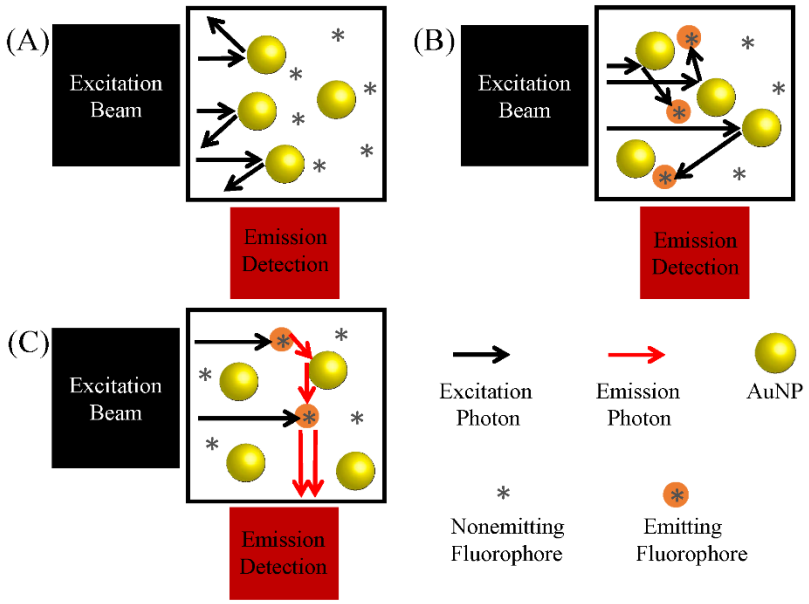

Scheme 1.1 Illustration of the competing dual effects (reducing and enhancing) of light scattering NPs on fluorophore fluorescence.

Notes: (A) Reducing fluorescence intensity by reducing the number excitation photon interactions with fluorophores at the probed volume. (B) Enhancing fluorescence emission by increasing the number of excitation photon interactions with fluorophores in the probed volume. (C) Enhancing fluorescence emission by simulated emission induced by scattering of emission photons. For the sake of simplicity, the NPs were assumed to be pure scatterers, and the fluorescence detection was at a 90-degree collection as commonly used in commercial spectrofluorometers.

Figure 1.7 illustrates the relation of AuNP absorption and scattering cross-sections as a function of NP diameter as calculated using Mie Theory.[64] The effect of AuNP scattering on spectrofluorometer measurements becomes increasingly significant as the AuNP diameter increases thereby increasing the AuNP MPE. Light absorption at the fluorescence excitation and emission wavelengths invariably reduce fluorescence intensities, and the degree of signal attenuation can be understood straightforwardly on the basis of Beer's Law. However, the effect of light scattering on fluorescence signals is

highly complicated and depends on instrument geometry and the light scattering efficiency at the excitation and emission wavelengths.[9,16,18,24,65]

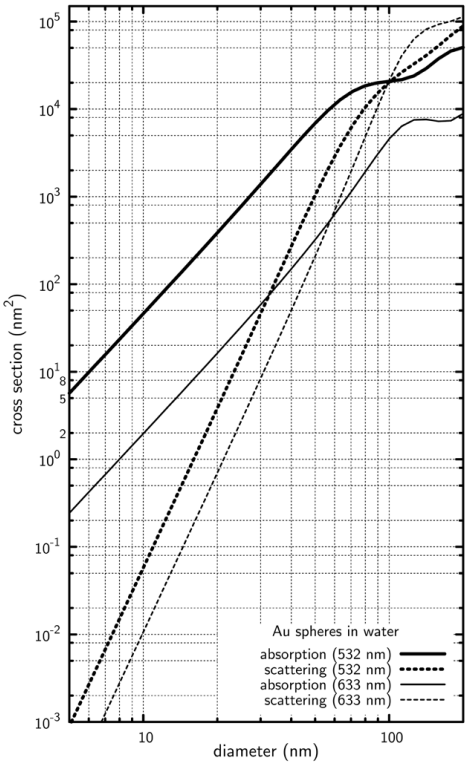

Figure 1.7 Absorption and scattering cross-sections for AuNPs as a function of AuNP diameter calculated using Mie Theory and two different excitation wavelengths.[64]

Notes: The bold lines pertain to calculations using a 532 nm excitation wavelength. The lighter lines pertain to using a 633 nm excitation wavelength. Solid lines and dashed lines represent absorption cross-sections and scattering cross-sections, respectively.

As illustrated in Scheme 1.1, photon scattering in solution can lead to two competing effects resulting in either fluorescence reduction or enhancement. Scattering of excitation photons away from fluorophores in solution or scattering of emission photons away from the fluorescence detector would exhibit fluorescence reduction. Fluorescence can be enhanced by increasing the number of photon interactions with

fluorophores. Following this train of thought, two enhancement possibilities are the most likely as outlined in Scheme 1.1. First, the number of excitation photon interactions with fluorophores in solution can increase (Scheme 1.1 (B)). Secondly, fluorescence enhancement can occur due to stimulated emission induced by scattered emission photon interactions with other fluorophores already in their excited-state (meaning the emission photon energy matches the energy of the excited state fluorophore) (Scheme 1.1 (C)).[66] Stimulated emission is the same phenomenon that occurs in lasers. An electron at an excited-electronic state interacts with an incoming photon for which the quantum energy is equal to the energy difference between its present level and lower ground state level. This incoming photon causes the excited state electron to drop down to ground state stimulating the release of an emission photon of equal energy as the incoming photon as shown in Figure 1.8.[67] The effect of scattering from a turbid medium on fluorophore fluorescence has been previously investigated, however, the correction methods implemented require special instrumentation capable of acquiring reflectance or complex modelling to estimate the photon path in the medium.[56,68] It is vital to quantitatively understand NP absorption and scattering to accurately probe fluorophore fluorescence in the presence of AuNPs.

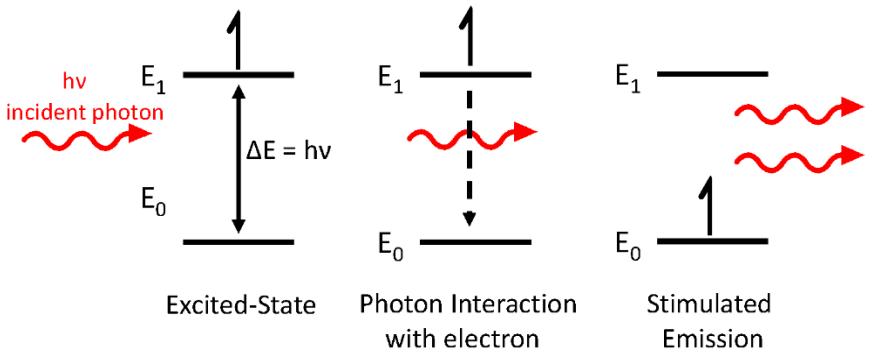

Figure 1.8 Partial energy diagram illustrating stimulated emission.

Notes: An incoming photon interacts with an excited state electron stimulating the relaxation of excited electron down to ground state with the release of two emission photons.

The effect of nanoparticles (NP) on fluorophore fluorescence can be highly complicated depending on the type of NP and the structure of the fluorophore-containing molecules. This is especially true when considering protein tryptophan fluorescence on AuNPs where both fluorescence enhancement and quenching has been proposed in literature[39,40,69-75] with large discrepancies in the degrees of fluorescence enhancement or quenching factors.[75] One common belief is that AuNPs induce static or dynamic fluorescence quenching.[57,73,76-82] Such quenching is commonly modelled with the Stern-Volmer equation to estimate the AuNP/protein binding rate or binding affinity constants. The Stern-Volmer equation is shown in Eq. 1.4.

$$\frac{F_0}{F} = 1 + K_{SV}[Q] \qquad \text{Eq. 1.4}$$

Where Q is the quencher or AuNP concentration, F_0 is the fluorophore fluorescence without a quencher present, and F is the fluorophore fluorescence intensity in the

presence of quencher. The Stern-Volmer constant or binding constant (K_{SV}) is extrapolated by linear fitting $\frac{F_0}{F}$ as a function of AuNP concentration ($[Q]$).

The Stern-Volmer equation is applicable when monitoring the binding of simple molecular species with AuNPs. However, protein/AuNP binding can alter protein fluorophore fluorescence through multiple pathways such as changing the protein secondary and tertiary conformations,[77,83-86] modifying the quantum yields of protein fluorescence,[87] or by charge and energy transfer.[57,71] A protein fluorophore in *direct* contact with the NP surface will have its fluorescence drastically reduced due to charge-transfer induced static quenching. However, a protein-conjugated fluorophore in close vicinity to (but not in direct contact with) the NP can have its fluorescence intensity enhanced or reduced, depending on the competitive electromagnetic enhancement of AuNP and fluorescence signal attenuation due to the Forster resonance energy transfer.[38,46,58,60,88,89]

Mechanistic understanding of the effect of NPs on fluorophore fluorescence is exceedingly challenging due to the fact that NPs can modify fluorophore fluorescence concurrently through multiple near- and far-field effects.[62,31] Presented in the proceeding chapters are a series of experimental and computational studies aimed at mechanistically understanding nanoparticle interactions with matter and photons to increase the reliability of spectrofluorometer based measurements. AuNP surface effects on fluorophore fluorescence have been evaluated using PEGylated AuNPs as an external reference for AuNP FFEs. Secondly, systematic evaluation of water Raman IFE has allowed for determination of a spectrofluorometer's effective path lengths. Lastly, the R_2S_2

technique was used to determine the optical cross-sections such as extinction, scattering, and on-resonance fluorescence cross-sections of a variety of nanomaterials. These studies provide critical information increasing the understanding of NP optical properties and their effects on fluorophores in solution regardless of direct interaction with the NP surface.

CHAPTER II

A GENERALIZED MODEL ON THE EFFECTS OF NANOPARTICLES ON FLUOROPHORE FLUORESCENCE IN SOLUTION

This work has been previously published: Zhang, D.; Nettles, C. B. A Generalized Model on the Effects of Nanoparticles on Fluorophore Fluorescence in Solution. *J. Phys. Chem. C*, **2015**, *119*, 7941–7948

2.1 Abstract

Nanoparticles (NP) can modify fluorophore fluorescence in solution through multiple pathways that include fluorescence inner filter effect (IFE), dynamic and static quenching, surface enhancement, and fluorophore quantum yield variation associated with structural and conformational modifications induced by NP binding. The latter three effects are termed the collective near-field effect as 1) they affect only fluorophore fluorescence in molecules close to the NPs, and 2) it is impossible to differentiate these effects with steady-state fluorescence measurements. A generalized model ($F_0^{corr} / F_{NP}^{corr} = (1 + K[NP])/(1 + K[NP]\ S)$ was developed for determination of the NP collective near-field effect S on the fluorophore fluorescence in the surface-adsorbed molecules. The popular Stern-Volmer equation ($F_0^{corr} / F_{NP}^{corr} = 1 + K[NP]$) used in current fluorescence studies of NP interfacial interactions is a special case of this generalized model, valid only under situations in which the surface-bound molecules are completely fluorescence inactive (S=0). In addition, we excluded the possibility of NPs

inducing significant dynamic fluorescence quenching under realistic experimental conditions on the basis of a simple dynamic quenching calculation (Eq. 2.1). Furthermore, using an external reference fluorescence IFE correction method developed in this work, we demonstrated that gold nanoparticles (AuNPs) only slightly attenuate, but do not completely quench the fluorescence signal of the protein bovine serum albumin (BSA) on AuNP. This result undermines the reliability of the BSA/AuNP binding constants calculated using the Stern-Volmer equation in earlier studies of BSA/AuNP interfacial interactions. The methodology and insights provided in this work should be of general importance for fluorescence study of nanoparticle interfacial interactions.

2.2 Introduction

The effect of nanoparticles (NP) on fluorophore fluorescence can be highly complicated depending on the types of NP and the structure of the fluorophore-containing molecules. Taking protein tryptophan fluorescence on plasmonic gold NPs (AuNPs) as examples, both fluorescence enhancement and quenching has been proposed in literature,[39,40,69-75] and there are large discrepancies in the degrees of fluorescence enhancement or quenching factors.[75] One common belief is that AuNPs induce static or dynamic fluorescence quenching.[57,73,76-82] Such quenching is commonly modelled with the Stern-Volmer equation to estimate the AuNP/protein binding rate or binding affinity constants.

Despite its popularity, the general applicability of the Stern-Volmer equation for fluorophore interactions with NPs is highly questionable. Indeed, the Stern-Volmer equation is applicable only in situations in which fluorophore fluorescence is completely

quenched in the dynamic and static fluorophore/quencher complex. Such a scenario is unlikely to occur for general NPs such as silica, graphene, two-dimensional nanosheets, or plasmonic AuNPs. Using protein binding to AuNPs as an example again, AuNPs can alter protein fluorophore fluorescence through multiple pathways. First, protein binding with AuNP can change protein secondary and tertiary conformations,[77,83-86] modifying the quantum yields of protein fluorescence.[87] This effect is well-known for protein tryptophan fluorescence. Second, AuNPs can change fluorophore fluorescence through charge and energy transfer.[57,71] When a protein fluorophore residue is in *direct* contact with the NPs, its fluorescence activity should be drastically reduced due to charge-transfer induced static quenching. However, when a protein-conjugated fluorophore is in close vicinity to, but not in direct contact with the NP, its fluorescence intensity can be enhanced or reduced, depending on the competitive electromagnetic enhancement of AuNP, and fluorescence signal attenuation due to the Forster resonance energy transfer.[38,46,58,60,88,89] The degree of fluorescence enhancement or reduction of individual fluorophores in a specific protein molecule depends on parameters such as fluorophore-AuNP distance, the molecule orientation relative to AuNP surface, polarization of photon excitations, and the optical spectral features of the fluorophore and AuNPs.[23,90-97]

There are further complications in the NP effect on protein fluorescence in that each protein can contain multiple intrinsic tryptophan fluorophores or externally labeled fluorophores. The distances between the NP and individual protein fluorophores are likely different from one to another. Therefore, individual fluorophores in the same protein can experience different degrees of fluorescence signal perturbations induced by NPs. The experimentally measured fluorescence signal modification induced by NPs is

an ensemble measurement of the overall effect of NPs on each individual fluorophore in all protein molecules.

All the effects described above are NP near-field effects because they only change the fluorescence intensity in molecules that are in direct contact or extremely close vicinity to the NP surfaces. It is currently impossible to disentangle individual contributions of these different near-field effects on fluorophore fluorescence. Therefore, these effects are referred to as the collective NP surface effect that contains the combined contribution of all the NP near-field effects.

Besides the collective NP surface effect, NPs also modify fluorophore fluorescence through the fluorescence inner filter effect (IFE). IFE is well-known in fluorescence and Raman spectroscopy and is attributed to the attenuations of excitation and emission light intensities induced by photon absorbers and scatterers in the sample solution.[31,35-42] Critically, fluorescence IFE is in play for all fluorophores in the NP-containing solution regardless of whether or not the fluorophore is adsorbed onto NPs. In addition, all NPs can impose strong fluorescence IFE on the fluorophore fluorescence. This is because NPs are invariably drastically stronger light scatters than molecular species because the scatter cross-section is proportional to the 6^{th} power of the particle size. In addition, many NPs including plasmonic AgNPs and AuNPs, semiconductor quantum dots, and graphene are stronger light absorbers. As such, the fluorescence IFE effects induced by these NPs are even more prominent. Unfortunately, the fluorescence IFE has been overlooked in many recent reports on the fluorescence study of NP interfacial interactions.[38,79,88,89,98]

The goal of this study is to develop a quantitative understanding of the effect of NPs on the fluorophore fluorescence by disentangling the collective NP surface effect from the fluorescence signal variation induced by NP-imposed fluorescence IFE. We first excluded the possibility of NPs inducing any detectable dynamic fluorophore fluorescence quenching on the basis of a simple calculation shown in Eq. 2.1 where a NP concentration as high as 10 μM is required to induce dynamic quenching. Therefore illustrating that the use of the Stern-Volmer equation to derive the fluorophore/NP binding rates is not reliable. We then derived a general model for determination of the collective NP surface effect on the fluorescence signal for the surface adsorbates, and demonstrated the condition under which this general model can be simplified into the popular Stern-Volmer equation. An example application of the generalized model is demonstrated by quantifying the collective AuNP surface effect on tryptophan fluorescence in protein bovine serum albumin (BSA). This study revealed that the AuNPs only attenuate, but do not completely eliminate fluorescence signal of the surface adsorbed BSA on the AuNPs with particle sizes of 10, 30 and 50 nm in diameters. For the sake of simplicity, we used the notation of A/B in the text to represent the mixture solution of A and B.

2.3 Experimental

2.3.1 AuNP synthesis and characterization

Both in-house synthesized and commercial AuNPs were used in this work. The in-house AuNPs were prepared using the citrate reduction method and it has an average size of 13 nm in diameter.[99] The concentration of the prepared AuNPs was 10.5 nM, calculated using the molar extinction coefficient of 2.7×10^8 M^{-1} cm^{-1} for 13 nm AuNPs

and the UV−vis spectrum of the as-synthesized AuNPs.[100] The commercial citrated-reduced 10 nm, 30 nm, and 50 nm AuNP were obtained from Nanocomposix. AuNP concentrations and particle sizes were provided by the vendor, but the particle size was verified in-house with UV-vis measurements and TEM images (Figure 2.1).

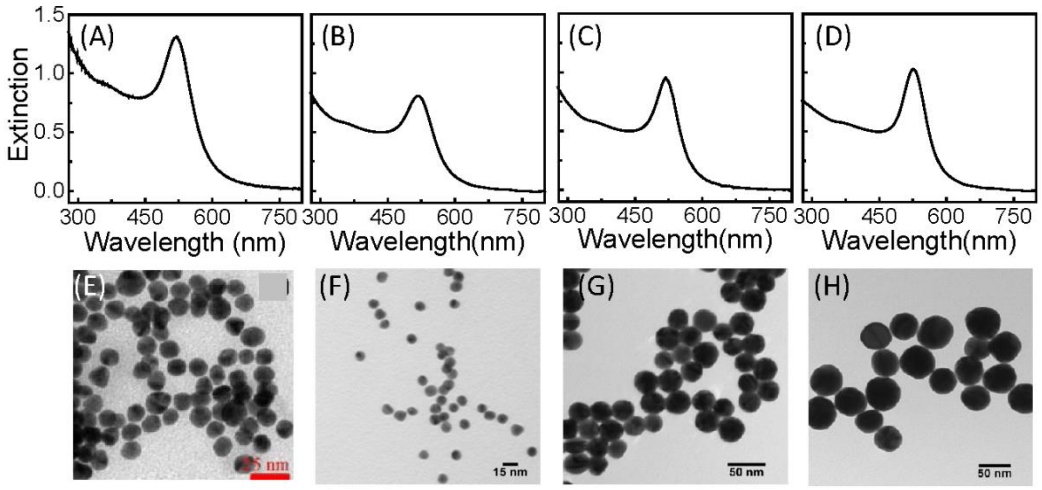

Figure 2.1 UV-visible and TEM characterization of 10, 13, 30, and 50 nm AuNPs.

Notes: (A)-(D) UV-vis spectra of AuNPs with diameters of 13 nm, 10 nm, 30 nm, and 50 nm, respectively. (E)-(H) TEM images of AuNPs with diameters of 13 nm, 10 nm, 30 nm, and 50 nm, respectively.

2.3.2 AuNP PEGylation

Two types of PEGylated AuNPs (p_{2k}AuNPs and p_{30k}AuNPs) were used in this work, which were prepared with thiolated polyethylene glycol (PEG) with average molecular weight of 2,000 g/mol and 30,000 g/mol. respectively. Before use, the PEG molecules were dialyzed against water. pAuNP stock solutions was prepared by the addition of 5 mL of 120 μM PEG-SH to 10 mL of AuNPs and mixture solution were them kept at 4 ^{o}C refrigerator for at least 12 h before use within one week.

2.3.3 Preparation of BSA/AuNP, BSA/pAuNP, and BSA controls

BSA concentration is kept constant at 1 μM in all the examples, but the AuNP concentrations of the 13 nm AuNPs in the BSA/AuNPs and BSA/pAuNP samples varies. The BSA/AuNP and BSA/pAuNP samples were prepared in parallel so that the BSA and AuNP concentrations and AuNP sizes in the two sets of parallel samples were identical. Four types of BSA controls were prepared and evaluated in which the solvents were nanopure water, centrifugation supernatant of colloidal AuNPs, 30 μM PEG solution and centrifugation supernatant of PEGylated AuNPs. Since all the controls have essentially identical BSA fluorescence spectra (Figure 2.2), only the BSA dissolved in nanopure water is used in subsequent experiments as the control for evaluation of the effect of AuNP and pAuNP on the BSA fluorescence. All fluorescence measurements were conducted with a Horiba Fluoromax 4 spectrofluorometer using a standard 4 mL 1 cm x 1 cm cell path length. The amount of BSA adsorbed onto the AuNPs and pAuNPs were estimated by fluorescence quantification of BSA in the centrifugation supernatant in the AuNP/BSA or pAuNP/BSA samples. The centrifugations were conducted using a Fisher Scientific Marathon 21000R centrifuge at 9000 rpm for 75 min at 15 ^{o}C or until the AuNP LSPR peak (~520 nm) was no longer detectable in the supernatant. All the UV-vis and fluorescence measurements were conducted within one day of the sample preparations.

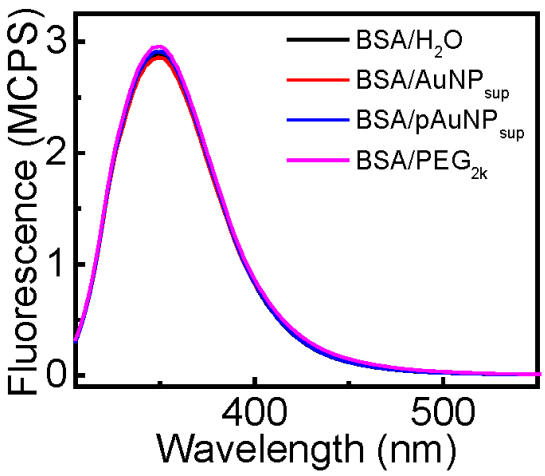

Figure 2.2 Fluorescence spectra of 1 μM BSA in different solvents.

Notes: Fluorescence spectra of 1 μM BSA dissolved in water (BSA/H_2O), centrifugation supernatant of colloidal AuNPs (BSA/$AuNP_{sup}$), centrifugation supernatant of PEGylated AuNPs (BSA/$pAuNP_{sup}$), and 30 μM PEG with molecular weight of 2,000 g/mol (BSA/PEG_{2k})..

2.4 Theoretical Considerations

2.4.1 NP-induced dynamic fluorescence quenching

One common belief in recent literature is that NPs induce dynamic fluorescence quenching.[76,82,89] However, such a possibility can be readily ruled out with a simple calculation that incorporates the experimental conditions employed in the literature as shown in Eq. 2.1. Dynamic fluorescence quenching is due to the formation of transient fluorophore/quencher complexes that lead to non-radiative relaxation of the excited fluorophore.[27,44] Mathematically, the degree of dynamic fluorescence quenching can be expressed with Eq. 2.1 where I_0 and I_Q are the fluorescence intensities of the sample without and with quencher,[44] τ_f is the fluorescence lifetime without the quencher, $[Q]$ represents the quencher concentration, k_c is the rate constant of fluorophore/quencher

collision, and K_q is the dynamic quenching efficiency, that is, the probability that such collisions lead to complete non-radiative relaxation of the excited fluorophores.

$$\frac{I_0}{I_Q} = 1 + k_c \, K_q \tau_f \, [Q] \tag{3.1}$$

In order to achieve effective dynamic quenching, the quencher and fluorophore-containing molecules have to be highly mobile so they can have a high collision rate constant (large k_c) and each collision has to have high a probability to induce non-radiative fluorophore relaxation (K_q close to 1, for example). Even under these conditions, the quencher molecules have to be at a relatively high concentration (*[Q]* is mM or above).[44,46,58] This is because dynamic quenching has to compete with the fluorescence process that usually occurs on a nanosecond (10^{-9} s) timescale. However, in typical NP/ligand binding experiments, especially with NPs that have high optical activity such as light absorption and scattering, the NP concentration is commonly in the low nM range.[39,41,72,73,76,81,82,86,89] For example, the highest AuNP concentration used in protein/AuNP binding experiments is usually significantly below 10 nM in order to avoid excess AuNP-imposed fluorescence IFE and ensure the viability of UV-vis measurements. Furthermore, the NP diffusion coefficient is inevitably much smaller than that for small molecule fluorescence quenchers because of the much larger size of the NPs. Assuming (1) the dynamic fluorescence quenching in NP/fluorophore solutions is entirely diffusion-limited ($K_q = 1$, every collision leads to non-radiative relaxation of the excited fluorophore), and (2) the k_c for NP/fluorophore collision rate constant is as large as 1×10^{10} $M^{-1}s^{-1}$ (the highest collision rate for common small molecules in aqueous solution),[44] the minimum NP concentration that can lead to detectable dynamic

fluorescence quenching is ~100 μM. Further assumptions used for this calculation include (1) the fluorophore fluorescence life-time in the fluorophore-containing molecule is 10 ns, (2) relative errors in fluorescence measurements are significantly smaller than 0.01, which is significantly better than practical fluorescence measurement, and (3) the NP diffusion coefficient is as high as that for oxygen and tryptophan in water.[44,101,102] Considering that NP concentrations used in practical NP binding experiments are usually in low nM, more than four orders of magnitude lower than this threshold concentration, and the collision rate between NP and fluorophore should be significantly smaller than that for oxygen and tryptophan, the possibility for NPs to induce significant dynamic fluorescence quenching is entirely negligible.

2.4.2 Effect of NPs on fluorophore fluorescence in solution

The exclusion of the possibility for NPs to induce significant dynamic fluorescence quenching enables us to use Eq.2.2 to model the effect of NPs on fluorophore fluorescence in NP-containing solutions. The first term in parenthesis on the right-hand side of this equation is for fluorophores adsorbed onto NPs, and the second term is for fluorophores that are away from the NP surface.

$$\frac{F_{NP}^{obsd}}{F_0^{obsd}} = [\frac{1}{M\chi_F N}(\sum_k^{M\chi_F}\sum_i^N P_{k,i}) + (1-\chi_F)]\frac{\eta_{NP}}{\eta_0} \qquad (3.2)$$

Here $F_{NP}^{obsd} / F_0^{obsd}$ is the ratio of the experimental measured fluorescence intensity of the samples with and without NPs. $P_{k,i}$ defines the collective NP surface effect on the fluorescence signal of fluorophore *i* in surface-adsorbed molecule *k*. To ensure the general applicability of Eq. 2.2 to systems where each surface adsorbate (such as protein)

can contain multiple fluorophores, we assumed that each molecule contains N fluorophores and NP binding can have a different effect on the fluorescence intensities of individual fluorophores. The $P_{k,i}$ value can be smaller or larger than, or equal to 1, corresponding to situations where the NP quenches, enhances, or has no significant near-field effect, respectively, on the fluorescence signal of the specified fluorophore. M is the total number of fluorophore-containing molecules in the sample. χ_F represents the fraction of the fluorophore-containing molecules adsorbed onto the NPs and is calculated by division of AuNP-fluorophore supernatant fluorescence (AuNP/BSA or pAuNP/BSA) by fluorophore control fluorescence (H_2O/BSA). Only the fluorophores in NP-bound molecules experience fluorescence signal perturbation induced by the collective NP surface effect that includes FRET, surface plasmonic resonances, and NP-binding-induced structural and conformational modifications. η_{NP} and η_0 represent the fluorescence IFE in the sample solutions with and without NPs, respectively. Both the fluorophore-containing molecules and NPs can impose fluorescence IFE, while the latter attenuates fluorescence intensity of molecules in solution regardless of whether they are attached to or away from the NPs. Each η can take any value between 0 and 1, corresponding to fluorescence IFE from high to low, respectively. Although, η_0 is commonly approximated as 1 (no IFE) when the total UV-vis absorbance of the sample at the fluorescence excitation and the emission wavelengths is less than 0.05.[44,60]

Eq. 2.2 can be simplified into Eq. 2.3 in which F_{NP}^{corr} and F_0^{corr} are the fluorescence intensities of the NP-containing and NP-free samples after correcting their fluorescence IFE by using Eq. 2.4 and 2.5, respectively

$$\frac{F_{NP}^{corr}}{F_0^{corr}} = 1 - \chi_F + \chi_F S \tag{3.3}$$

$$F_{NP}^{corr} = F_{NP}^{obsd} / \eta_{NP} \tag{3.4}$$

$$F_0^{corr} = F_0^{obsd} / \eta_0 \tag{3.5}$$

$$S = \frac{1}{M \chi_F N} \left(\sum_k^{M \chi_F} \sum_i^N P_{k,i} \right) \tag{3.6}$$

S represents the ensemble-averaged collective NP surface effect on all the fluorophores in the surface adsorbates. It is critical to note that the value of *S* can be larger, smaller, or equal to 1, corresponding to situations where the NP enhances, reduces, or has no significant effect on the fluorescence signal of the molecular adsorbates on NPs.

Using the assumption that ligand binding with NPs can be described with an equilibrium chemical reaction (Eq. 2.7a and 2.7b) in which K_{eq} is the equilibrium binding constant between a NP and fluorophore-containing molecule *M*, one can determine χ_F with Eq. 2.8b. The latter equation can be derived with simple mathematical manipulation on the basis of the mathematic definition of K_{eq}. $\rightleftharpoons$

(A) $$NP + F \rightleftharpoons F - NP$$

(B) $$K_{eq} = \frac{[F - NP]}{[NP][F]} \tag{3.7}$$

(A) $$\chi_F = \frac{[F-NP]}{[F]+[F-NP]}$$

(B) $$\chi_F = \frac{K_{eq}[NP]}{1+K_{eq}[NP]} \quad (2.8)$$

Eq. 2.9 is derived by substitution of χ_F in Eq. 2.3 with that defined by Eq. 2.8b, and with a simple mathematic manipulation.

$$\frac{F_0^{corr}}{F_{AuNP}^{corr}} = \frac{1+K_{eq}[NP]}{1+K_{eq}[NP]\ S} \quad (3.9)$$

Critically, Eq. 2.9 can be reduced to the popular Stern-Volmer equation $F_0^{corr}/F_{AuNP}^{corr} = 1+K[NP]$ when all fluorophores in all the surface-bound molecules are entirely fluorescence inactive (*S=0*). The model described in Eq. 2.9 is more broadly applicable than the Stern-Volmer equation for modeling the effect of NPs on fluorophore fluorescence as it has no constraint on the degree of fluorescence enhancement or quenching imposed by NPs on fluorophores in surface-bound molecules. Furthermore, the fluorescence IFE is explicitly considered in the generalized model. This is in contrast to the Stern-Volmer equation in which fluorescence signal reduction is entirely attributed to complete dynamic and static quenching.

The generalized model described in Eq. 2.9 and the Stern-Volmer equation facilitate conceptual understanding of the effect of NPs on fluorophore fluorescence. However, using these models to predict the NP binding constants or assemble-averaged collective NP surface effect of fluorophore fluorescence is extremely challenging in practical NP binding experiments. This is because the NP concentration in the Eq. 2.9 and in the Stern-Volmer equation is the equilibrium concentration of ligand-free NPs, but

not the total NP concentration used in most of the existing literature.[40,41,72,76-82] Unfortunately, it is currently impossible to determine the equilibrium concentration of free NP (without bound ligands) in NP binding experiments.

Using the concentration of total NPs as the concentration of ligand-free NPs in the Stern-Volmer equation or the general model of Eq, 2.9 can be highly problematic because this approximation may be valid only when the NP concentration is much higher than the concentration of ligand molecules. However, in practical fluorescence studies of NP binding experiments, the NP concentration is usually much lower than that of the ligand to avoid excess NP-induced fluorescence IFE. As an example, the AuNP concentration is usually more than two orders of magnitude lower than that of protein in the fluorescence studies of protein/AuNP binding.[41,76-79,81,82] It is, therefore, unreliable to use the total NP concentration to determine the NP/protein binding equilibrium constants.

Even without determining the fluorophore/NP binding constant and the free NP concentration, one can still quantify the ensemble-averaged collective NP surface effect on the fluorescence signal of fluorophores in surface-bound molecules by using Eq. 2.10 The latter is equivalent to Eq. 2.9 and it is derived by rearranging Eq. 2.3. Eq. 2.10 implies that one has to be able to reliably correct the fluorescence IFE in the NP-free and NP-containing samples, and the fraction of fluorophore-containing molecules attached onto the NP surface in order to determine the collective NP surface effect (enhancing, quenching, or complete eliminating) on the fluorescence signal of the fluorophores in the molecules located on the NP surfaces,

$$S = \frac{F_{NP}^{corr} - (1-\chi_F) F_0^{corr}}{\chi_F F_0^{corr}} \tag{3.10}$$

2.5 Results and Discussion

Example application of Eq. 2.10 for determination of the NP surface effect on fluorophore fluorescence was demonstrated for BSA adsorbed onto AuNPs. The effect of AuNPs on BSA tryptophan fluorescence has been one of the most popular systems for studying the effect of NP binding on protein fluorescence.[57,73-77,82,89] Unfortunately, in many of these studies, the NP-induced fluorescence IFE effect has not been considered, or deemed insignificant without experimental verification. In addition, dynamic fluorescence quenching has been commonly invoked in those studies as the main pathway for AuNP induced protein tryptophan fluorescence signal reduction,[76,82,89] even though the AuNP concentrations used in those reports is far below the concentration threshold needed for producing dynamic fluorescence quenching.

In this work, we developed and validated a new method for correction of fluorescence IFE in BSA/AuNP samples by using samples prepared with BSA mixed with PEGylated (BSA/pAuNP) as the external references. The performance of this external reference method were compared with that of two popular mathematical fluorescence IFE removal methods used in recent literature.[38,44,80] The key theoretical foundation of this external reference method is the fact the BSA adsorption is kinetically restricted onto the PEGylated AuNPs (pAuNP), therefore the pAuNP can only change the BSA fluorescence through the AuNP-imposed fluorescence IFE. The latter was experimentally confirmed with our control experiments shown below. The collective AuNP surface effect on tryptophan fluorescence of the BSA adsorbed onto the AuNPs were quantified for AuNPs with particle sizes of 10 nm, 30 nm, and 50 nm in diameter

2.5.1 Correction of fluorescence IFE effect

Figure 2.3(A)-(C) show the UV-Vis spectra of a series of BSA/AuNP, BSA/p_{2k}AuNP, and BSA/p_{30k}AuNP solutions using 13 nm AuNPs, respectively. p_{2k}AuNP and p_{30k}AuNP refer to the AuNPs that were PEGylated with thiolated polyethylene with molecular weight of 2,000 g/mol and 30,000 g/mol, respectively. The UV-vis spectra of the BSA/AuNP solutions are very similar to their corresponding BSA/p_{2k}AuNP and BSA/p_{30k}AuNP samples that contain the same amount of BSA and AuNPs. Therefore, the fluorescence IFE in the BSA/AuNP samples should be very similar to that in their corresponding BSA/pAuNP samples. This is because the fluorescence IFE is caused by photon adsorption and scattering, the significance of which is measured by the sample UV-vis spectrum. Importantly, fluorescence intensities of the centrifugation supernatants of the BSA/p_{2k}AuNP and BSA/p_{30k}AuNP solutions are almost entirely independent of the pAuNP concentration, confirming that there is no BSA adsorption onto AuNPs that are PEGylated by either 2,000 g/mol or 30,000 g/mol PEG-SH. The slight deviation in fluorescence intensity for the supernatant pAuNP containing solutions can be attributed to changes in the AuNP localized surface plasmon resonance band upon passivation with PEG which could alter that absorbance efficiency of AuNPs. In contrast, the fluorescence intensity in the centrifugation supernatants of BSA/AuNP samples decreases monotonically with increasing NP concentration (Figure 2.3(G)), showing the BSA adsorption onto AuNPs. These experimental data indicate that observed fluorescence signal variation of the BSA/AuNP samples are due to the combined effect of the NP-induced fluorescence IFE effect and the collective NP surface effect, while that in BSA/p_{2k}AuNP and BSA/p_{30k}AuNP is due only to the NP-induced

fluorescence IFE. It is important to note that since the highest AuNP concentration used in this study is below 10 nM, it is impossible for NPs to induce any detectable dynamic fluorescence quenching in any of the AuNP- and pAuNP-containing samples.

$$\eta_{pAuNP} = \frac{F_{pAuNP}^{obsd}}{F_0^{obsd}} \eta_0 \tag{3.11}$$

pAuNP changes BSA fluorescence only through AuNP-induced fluorescence IFE effect. Therefore, one can determine the fluorescence IFE in the BSA/pAuNP samples on the basis of the fluorescence signal variation induced by PEGylated AuNPs as shown with Eq. 2.11. Mathematically, Eq. 2.11 can be obtained from Eq. 2.2 by eliminating the first term in the right-hand side of the equation, and setting $\chi_F = 0$ in the second term. This is because no BSA is adsorbed onto the PEGylated AuNPs (Figures 2.3(H) and 2.3(I)). The fluorescence IFE in the AuNP-free samples is negligible because of their low UV-vis absorbance (A < 0.05) in the BSA control solution (Figure 2.3(A)). $\eta_0 = 1$ in this case. Furthermore, since UV-vis spectra of BSA/AuNP samples are highly similar to those of their corresponding BSA/p_{2k}AuNP or BSA/p_{30k}AuNP samples, one can set $\eta_{AuNP} = \eta_{pAuNP}$. Consequently, the IFE- corrected fluorescence intensity in BSA/AuNP samples can be calculated with Eq. 2.12 by replacing η_{AuNP} in Eq. 2.11 with η_{pAuNP} calculated with Eq. 2.4.

$$F_{AuNP}^{corr} = \frac{F_0^{obsd}}{F_{pAuNP}^{obsd}} F_{AuNP}^{obsd} \tag{3.12}$$

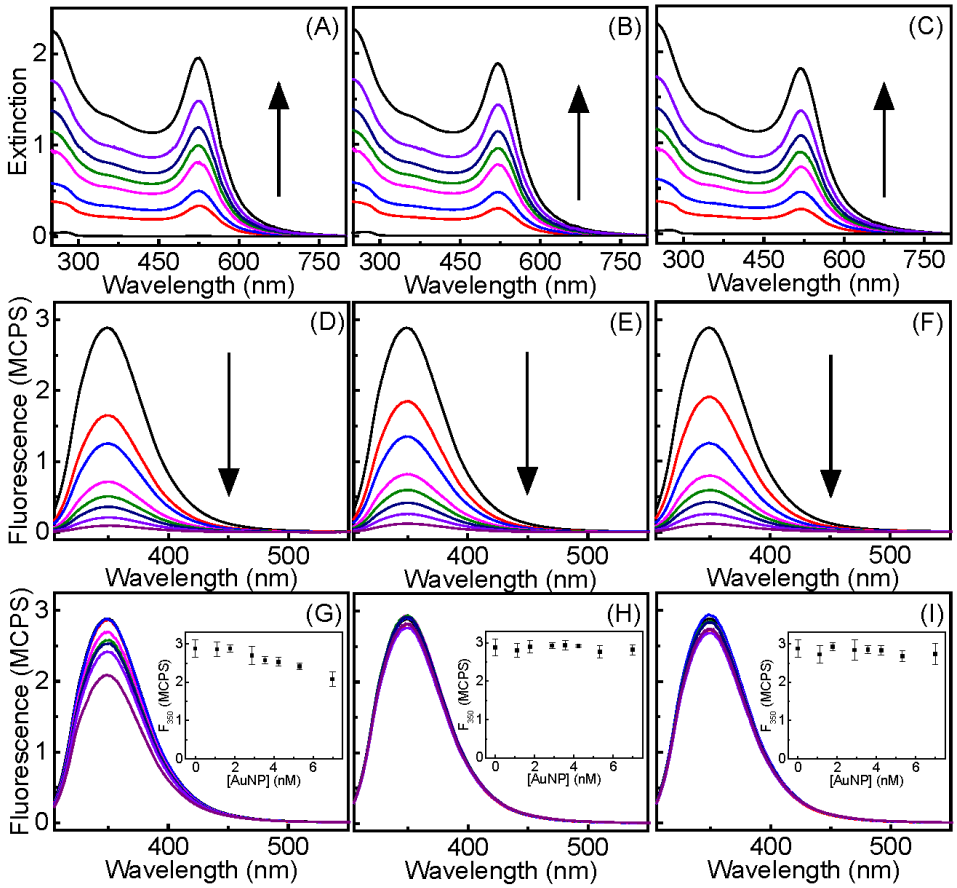

Figure 2.3 UV-vis and fluorescence spectra of a series of BSA/AuNP, BSA/p_{2k}AuNP, and BSA/p_{30k}AuNP solutions.

Notes: (A), (B), and (C) UV-vis spectra obtained with BSA/AuNP, BSA/p_{2K}AuNP, and BSA/p_{30K}AuNP, respectively. (D), (E), and (F) Fluorescence spectra for samples shown in (A), (B), and (C), respectively. (G), (H), and (I) Fluorescence spectra of the centrifuge supernatants of (D), (E), and (F), respectively. The data plotted in the same column were acquired with the same set of samples. The BSA and AuNP concentrations in the corresponding BSA/AuNP, and BSA/p_{2K}AuNP, and BSA/p_{30K}AuNP samples are exactly the same. The concentration of BSA is 1 μM in all the samples, but the AuNP concentration increases from 0, 1.11, 1.77, 2.89, 3.56, 4.24, 5.32, to 6.99 nM as shown by the arrows in plots (A) to (F). The inset in (G), (H), and (I) shows the fluorescence intensities as a function of AuNP concentration in the fluorescence spectra obtained with the centrifugation supernatants of BSA/AuNP, BSA/p_{2K}AuNP, and BSA/p_{30K}AuNP, respectively. Error bars represent one standard deviation of three independent measurements. 13 nm AuNPs were used for all samples.

The data shown in Figure 2.3 indicates both BSA/p_{2k}AuNP and BSA/p_{30k}AuNP can serve as the external reference for correcting the fluorescence IFE effect in the BSA/AuNP samples because no BSA adsorption were observed in these two samples. In this work, we use BSA/p_{2k}AuNP as the external reference for correcting the fluorescence IFE effect in the BSA/AuNP solutions, and the BSA/p_{30k}AuNP samples were used as independent validation samples for evaluation of the performances of the external reference method and two mathematical methods employed in recent literature.[38,44] Those mathematical techniques correct the fluorescence IFE effect on the basis of UV-vis absorbance of the samples and the instrumental setup of the spectrofluorometer. However, independent validation of those methods has, to our knowledge not been possible for correcting NP-imposed fluorescence IFE.

Eq. 2.13 and Eq. 2.14 describe the two literature mathematical methods that are evaluated in this work. Eq.2.13 is for the fluorescence spectra obtained with the standard 4 mL cuvette with path length of 1 cm, while Eq. 2.14 considered the photon excitation and collection geometries in the spectrofluorometer.[38,44,60] A_x and A_m are the UV-vis absorbances at the fluorescence excitation and emission wavelength of the fluorescence sample, while *d, g,* and *s* in Eq. 2.14 are instrument specific parameters (Figure 2.4).[58]

$$\frac{F_{AuNP}^{corr}}{F_{AuNP}^{obsd}} = 10^{0.5A_x + 0.5A_m} \tag{3.13}$$

$$\frac{F_{AuNP}^{corr}}{F_{AuNP}^{obsd}} = \frac{2.3\,d\,A_x}{1-10^{-d\,A_x}} 10^{g\,A_m} \frac{2.3\,s\,A_m}{1-10^{-d\,A_m}} \tag{3.14}$$

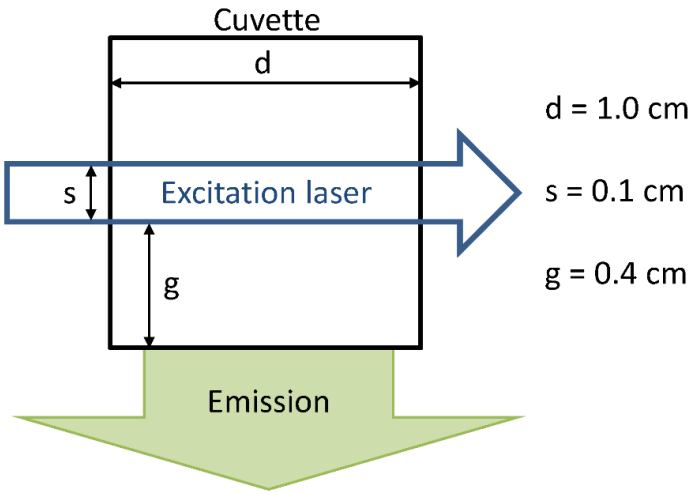

Figure 2.4 Instrumental parameters d, g, and s for the fluorescence IFE correction using Eq. 14.

Notes: Top view of 3 mL fluorescence cuvette used to determine values of d, g, and s used in Eq. 14 to correct for AuNP IFE.

Near perfect fluorescence IFE corrections were achieved in the BSA/p_{30k}AuNP samples by using the BSA/p_{2k}AuNP samples as the external references as shown in Figure 2.5B. This is because the IFE-corrected BSA fluorescence intensities in the BSA/p_{30k}AuNP samples are entirely independent (within measurement error) of the AuNP concentration. This result is consistent with the fact that BSA cannot be adsorbed onto the PEGylated AuNPs and fluorescence signal reduction induced by the p_{30k}AuNPs is due exclusively to the AuNP-imposed fluorescence IFE. This data provides critical validation of the external reference method. In contrast, the two mathematical methods described with Eq. 2.13 and Eq. 2.14 under-correct the fluorescence IFE in BSA/p_{30k}AuNP samples (Figure 2.5(C and D)), especially for the samples that contain relatively high AuNP concentrations. The IFE- corrected fluorescence intensities of the BSA/p_{30k}AuNP samples are significantly lower than the fluorescence intensities of their

centrifugation supernatants (Figure 2.3(I)). The latter are entirely independent of the AuNP concentrations. Indeed, if these mathematical correction models are correct, the PEGylated AuNPs have to quench the tryptophan fluorescence in BSA molecules that are dispersed in solution. Such an event is impossible given BSA and pAuNP concentrations used in these samples. The possibility that PEG induces BSA tryptophan fluorescence quenching has also been experimentally excluded (Figure 2.2).

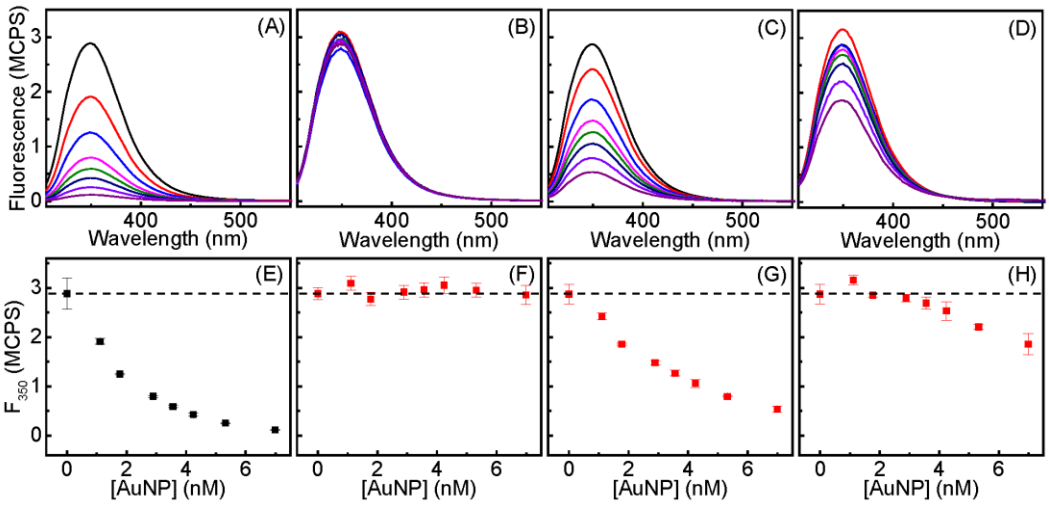

Figure 2.5 Comparison of IFE correction methods for BSA/p_{30k}AuNP (13 nm) samples using either our external reference method, Eq. 2.13, or Eq. 2.14.

Notes: (A) as-acquired and (B), (C), and (D) IFE-corrected fluorescence spectra obtained for BSA/p_{30k}AuNP using either the external reference method devised in this work, or mathematical methods described by Eq. 2.13 and 2.14, respectively. (E-H) Fluorescence intensities as a function of the AuNP concentration for spectra as shown in A-D, respectively. The external references used for correcting the fluorescence IFE in BSA/p_{30k}AuNP are the BSA/ p_{2k}AuNP samples. UV-vis spectra from Figure 2.3C were used for mathematical correction of fluorescence IFE in Eq. 2.13 and Eq. 2.14. The dash line represents the fluorescence intensities for perfect IFE correction. Each standard derivation was calculated from three independent measurements.

2.5.2 Collective AuNP effect on BSA tryptophan fluorescence

The effect of AuNPs on the tryptophan fluorescence signal in the surface adsorbed BSA were investigated for AuNPs with particle sizes of 10 nm, 30 nm, and 50 nm in diameter. For each BSA/AuNP sample, a different set of BSA/pAuNP samples were prepared as the external reference to correct the fluorescence IFE in their corresponding BSA/AuNP samples. The BSA concentrations, and AuNP sizes and concentrations in the BSA/AuNP samples are identical to their respective counterparts in their corresponding BSA/pAuNP external references. This is critical to ensure the fluorescence IFE in each BSA/AuNP sample and its corresponding BSA/pAuNP external reference are the same.

Figure 2.6 shows the UV-vis and fluorescence spectra obtained with the BSA/AuNP and their corresponding BSA/p_{2k}AuNP external reference. The fact that the fluorescence intensity of the supernatant of BSA/p_{2k}AuNP is identical to the fluorescence intensity of the BSA control confirms no BSA adsorption to the PEGylated AuNPs of different particle sizes. Furthermore, the UV-vis spectra of the BSA/AuNP and their corresponding BSA/p_{2k}AuNP are highly similar, which justifies using BSA/p_{2k}AuNP as an external reference for correcting the fluorescence IFE in BSA/AuNP samples.

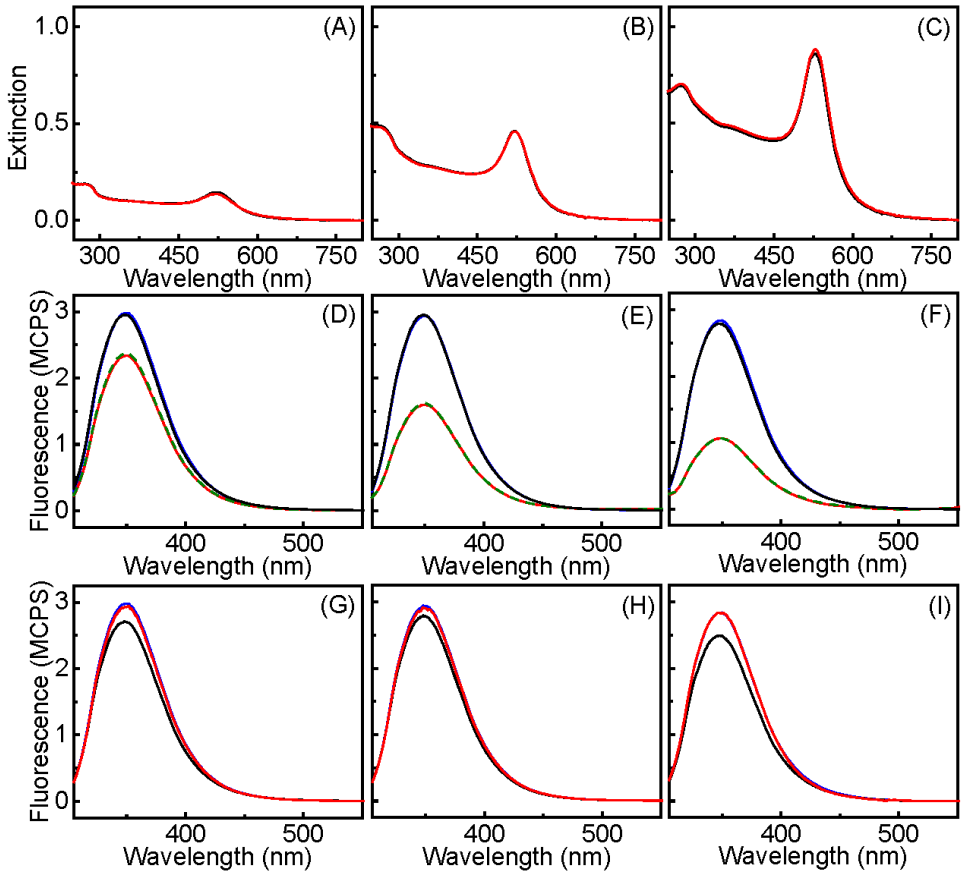

Figure 2.6 UV-vis and fluorescence spectra for BSA/AuNP and BSA/p_{2k}AuNP external references using 10, 30, or 50 nm diameter AuNPs.

Notes: (A), (B), and (C) UV-vis spectra obtained with (red) BSA/AuNP and (black) BSA/p_{2k}AuNP. AuNP sizes are (A) 10 nm, (B) 30 nm, and (C) 50 nm diameter, respectively. (D), (E), and (F) Fluorescence spectra obtained with (blue) BSA control, (red) BSA/AuNP, (green dash) BSA/p_{2k}AuNP, and (black) centrifugation supernatant of BSA/p_{2k}AuNP. (G), (H), and (I) Fluorescence spectra obtained with (black) centrifugation supernatant of BSA/AuNP, (blue) BSA control, and (red) the IFE-corrected BSA/AuNP fluorescence spectra. BSA concentration is 1 μM in all samples, and the AuNP concentrations are 1.13, 0.12, and 0.043 nM for the 10 nm, 30 nm, and 50 nm AuNPs, respectively.

BSA adsorption onto AuNPs was observed for AuNPs of all three different sizes. The fraction of BSA adsorbed was calculated on the basis of the fluorescence intensity difference between the BSA control and the centrifugation supernatants of each BSA/AuNP solution (Figure 2.6(G, H, and I)). Using the fluorescence-IFE corrected

fluorescence intensity of the BSA/AuNP samples, the effect of AuNPs on the tryptophan fluorescence intensity of the surface adsorbed protein is quantified (Figure 2.7). The most notable conclusion is that AuNPs have neither drastically enhanced nor quenched the tryptophan fluorescence in the surface adsorbed BSA. Indeed, the value of collective AuNP surface effect *S* on the fluorescence signal of the protein adsorbates is very modest, which varies from 0.70 ± 0.02 to 0.99 ± 0.05 for the AuNPs of the three difference sizes. This indicates that the fluorescence activity of the protein adsorbed onto AuNPs are only slightly modified, but not completely quenched as assumed in much of the recent literature. The fact that protein molecules on AuNP can remain fluorescence active undermines the general applicability of the Stern-Volmer equation for fluorescence study of protein binding to AuNPs.

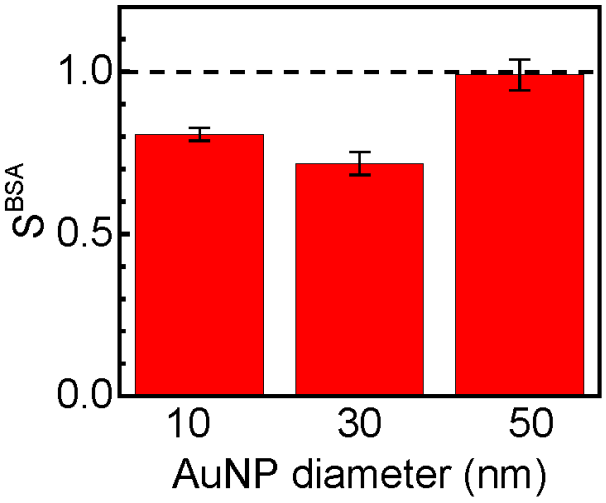

Figure 2.7 Collective AuNP surface effect on tryptophan fluorescence in BSA adsorbed onto AuNPs of different particle sizes.

Notes: Standard deviation is calculated from three independent measurements.

2.6 Conclusions

In summary, a generalized model was developed for conceptual understanding of the effect of NPs on fluorophore fluorescence in solution. This model explicitly considered the NP- and fluorophore-imposed fluorescence IFE. The popular Stern-Volmer equation ($F_0^{corr} / F_{NP}^{corr} = 1 + K[NP]$) used extensively in literature is a special case of this generalized model, valid only under situations in which the surface-bound molecules are completely fluorescence inactive (S=0). An example application of this generalized model is demonstrated with BSA protein adsorbed onto AuNPs. The fact that AuNP binding only attenuates, but does not eliminate the protein tryptophan fluorescence undermines the reliability of using the Stern-Volmer equation to study the protein/AuNP binding constant and dynamic quenching kinetics. The methodology and insights provided in this work should be of general importance for nanoscience research given the popularity of fluorescence spectroscopy in studying NP interfacial phenomena.

CHAPTER III

USING WATER RAMAN INTENSITIES TO DETERMINE THE EXCITATION AND EMISSION PATH LENGTHS OF SPECTROFLUOROMETERS FOR CORRECTING FLUORESCENCE INNER FILTER EFFECT

This work has been previously published: Nettles, C. B.; Hu, J.; Zhang, D. Using Water Raman Intensities to Determine the Effective Excitation and Emission Path Lengths of Fluorophotometers for Correcting Fluorescence Inner Filter Effect. Anal. Chem., 2015, 87, 4917-4924

3.1 Abstract

Fluorescence and Raman inner filter effects (IFE) cause spectral distortion and nonlinearity between spectral signal intensity with increasing analyte concentration. Convenient and effective correction of fluorescence IFE has been an active research goal for decades. Presented herein is the finding that fluorescence and Raman IFE can be reliably corrected using the equation $I^{corr}/I^{obsd} = 10^{d_x A_x + d_m A_m}$ when the effective excitation and emission path lengths d_x and d_m of a spectrofluorometer are determined by simple linear curve-fitting of Raman intensities of a series of water Raman reference samples that have known degrees of Raman IFEs. The path lengths derived with one set of Raman measurements at one specific excitation wavelength are effective for correcting fluorescence and Raman IFEs induced by any chromophore or fluorophore, regardless of the excitation and emission wavelengths. The IFE-corrected fluorescence intensity can

be linearly correlated to fluorophore concentration even when the sample UV-vis absorbance is a high as ~5 (normalized to 1 cm cuvette). This water Raman-based method is easy to implement. It doesn't involve complicated instrument geometry determination or mathematical data manipulation. This work should be of broad significance to physical and biological sciences given the popularity of fluorescence techniques in analytical applications.

3.2 Introduction

Fluorescence is one of the most broadly used techniques in physical and biological sciences. One well-known problem in fluorescence measurements is, however, the fluorescence inner filter effect (IFE) that can cause fluorescence spectral distortion and nonlinearity between fluorescence signal intensity and fluorophore concentration. Fluorescence IFE occurs whenever there are photon absorbers and scatterers in the sample solution,[37,41,58,76,103] and it is in effect even without extrinsic molecular or nanoparticle-based light absorbers or scatterers. This is because fluorophores must absorb excitation photons in order to emit. The fluorescence IFE can be deemed insignificant only in samples for which the total UV-vis absorbance at the fluorescence excitation and emission wavelengths are significantly smaller than 0.05.[43-47] This imposes a significant constraint on the general applicability of this otherwise highly convenient technique. Indeed, without reliable fluorescence IFE correction, it is essentially impossible to get reliable fluorescence acquisition for fluorophores that have relatively low fluorescence quantum yields and for studying chromophore-fluorophore interactions. For the latter case, the chromophore can change fluorophore fluorescence through static and dynamic quenching, and fluorescence IFE.

It has been long realized that the degree of the fluorescence IFE is related to the sample UV-vis absorbance at the excitation and emission wavelengths, and the effective excitation and emission path lengths of the spectrofluorometers.[37,44-46,49,104] While UV-vis absorbance of the samples can be determined straightforwardly from the sample UV-vis spectrum, determination of the effective excitation and emission path length of a spectrofluorometer is a nontrivial task.[105] Figure 3.1 shows a typical instrument configuration of a spectrofluorometer in which the emitted photons are collected with a 90 degree angle relative to the excitation beam. The optical pathways for the excitation and emission photons at one specific sampling point in solution can be significantly different from their respective counterparts at another sampling point in the same sample. Therefore, the degrees of excitation and emission intensity attenuation due to the fluorescence IFE can differ from one sampling point to another.

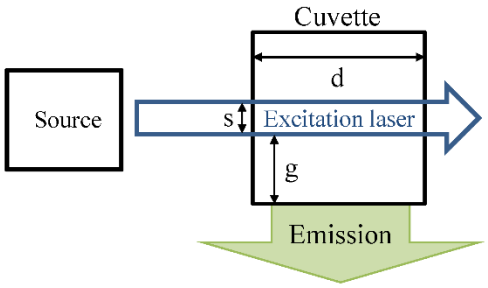

Figure 3.1 Sampling geometry in a typical spectrofluorometer.[58]

Notes: *d, s,* and *g* are the cuvette length, photon excitation beam width, and the nominal emission beam path length, respectively.

$$\frac{I^{corr}}{I^{obsd}} = 10^{0.5A_x + 0.5A_m} \tag{3.1}$$

$$\frac{I^{corr}}{I^{obsd}} = \frac{2.3\, d\ A_x}{1-10^{-d\ A_x}}\, 10^{g\ A_x}\, \frac{2.3\, s\ A_m}{1-10^{-s\ A_m}} \tag{3.2}$$

Numerous fluorescence IFE correction methods have been proposed in the past several decades.[45,56,58,105-111] Eqs. 3.1 and 3.2 describe two example methods that appear most frequently in recent literature, presumably because of their relative simplicity.[44,58,60,82,105,112,113] I^{obsd} and I^{corr} are the fluorescence intensities before and after the IFE correction. A_x and A_m are the UV-vis absorbance of the fluorescence samples at the excitation and emission wavelengths, respectively. Eq. 3.1 is used for correcting the fluorescence IFE in spectra obtained with a 1 cm × 1 cm fluorescence cuvette.[44] In this case the effective excitation and emission path lengths are both assumed to be 0.5 cm. The correction parameters of *d, s,* and *g* in Eq. 3.2 are the cuvette length, photon excitation beam width, and the nominal emission beam path length (Figure 3.1).

These methods are conceptually simple and applied extensively in recent literature.[41,43,44,60,82,105,106,112] However, independent and robust evaluation of the reliability of these fluorescence IFE correction methods is challenging. This is because of the difficulty in preparing the standards that have known degrees of fluorescence IFE. Indeed, besides fluorescence IFE, there are many competitive photochemical and physicochemical processes that can change fluorophore fluorescence. Examples of such processes include fluorescence photobleaching, fluorophore/fluorophore interactions through π-π stacking or other intermolecular interactions,[114-118] and dynamic or static fluorescence quenching induced by solvent impurities including oxygen.[119,120]

As demonstrated later and in Chapter 2, neither method produces satisfactory results when applied to independent validation samples that have a known degree of

Raman IFE. Indeed, besides cuvette size and the nominal excitation and emission photon beam sizes that are considered in Eq. 1 and 2, there are many other instrument parameters that affect the fluorescence IFE but are impossible to characterize.[48,51,105] For example, imperfections in the optics and optical alignments can change the excitation and emission angles, which inevitably modify the fluorescence IFE. Photon energy distributions across the excitation and emission beam should also affect the average fluorescence IFE experienced by the fluorophore in solution. Therefore, fluorescence IFE-correction methods derived on the basis of measurable instrumental parameters such as the ones described in Eq. 2 are unlikely to be effective for reliable fluorescence IFE correction.

$$\frac{I^{corr}}{I^{obsd}} = 10^{d_x A_x/L + d_m A_m/L} \tag{3.3}$$

Reported herein is a performance-based method for determination of the effective excitation and emission path lengths (d_x and d_m in Eq. 3.3) of spectrofluorometers for correcting fluorescence and Raman IFEs. L in Eq. 3.3 is the path length of the UV-vis cuvette used for taking the UV-vis spectra of the fluorescence sample to determine the sample UV-vis absorbance at the fluorescence excitation and emission wavelengths (A_x and A_m). For applications in which UV-vis acquisitions are conducted with a 1 cm cuvette, one can directly apply the UV-vis absorbance A_x and A_m to determine the effective fluorescence excitation and emission path lengths in cm. For convenience, we hereafter drop the L term in Eq. 3.3 and use Eq. 3.4 instead. It is emphasized that in this case A_x and A_m are implicitly normalized by the UV-vis path length (A/L). Normalization is important to ensure that the exponent term in Eq. 3.4 is unitless.

$$\frac{I^{corr}}{I^{obsd}} = 10^{d_x A_x + d_m A_m} \tag{3.4}$$

Mathematically, Eq. 3.4 is very similar to Eq. 3.1 and 3.2. However, it differs significantly from the latter ones in its underlying principle and method for determination of path length parameters. d_x and d_m in Eq. 3.4 are determined by optimization of the Raman IFE correction for a series of chromophore-containing solutions. Since the presence of a chromophore has negligible effect on the water concentration, the water Raman signal reduction in chromophore-containing solutions can be fully attributed to the Raman IFE induced by chromophore UV-vis absorption at the Raman excitation and scatter wavelengths. The latter should be true as long as the chromophore is diluted enough so that it has no significant effect on the water Raman cross-section. Also, the chromophore Raman signal should be negligible in comparison to the water Raman signal. These conditions can easily be met considering the fact that the concentration of water is an aqueous solution is ~55 M. In contrast, the chromophore concentration is most commonly below 10 mM in practical UV-vis and fluorescence measurements.

The origin of the Raman IFE is exactly the same as that for fluorescence IFE, that is, attenuation of excitation and Raman or fluorescence photon intensity by light absorbers and scatters in sample solutions. Therefore, the effective path lengths derived from water Raman measurements are directly applicable for correcting the fluorescence IFE, as long as the instrument configuration of the spectrofluorometer remains unchanged during water Raman and fluorescence measurements. The key advantage to using water Raman, instead of fluorophore fluorescence, to determine the effective excitation and emission path lengths for a spectrofluorometer is that the degree of water Raman IFE in a

chromophore-containing sample can be reliably quantified by dividing the water Raman control signal (no chromophore) by that of the chromophore-containing signal. This is in stark contrast to the fluorescence method for which it is impossible to conduct fluorescence-IFE-free measurements. The latter is due to the fact that the fluorophore has to absorb photons in order to emit. No such photon absorption is involved in chromophore-free water Raman samples. Furthermore, water Raman measurements are much more robust than fluorescence acquisition. Unlike fluorescence signals that can be susceptible to light and environmental oxygen, there is no water Raman photobleaching or static/dynamic quenching.

Using water Raman to correct fluorescence signal variations has been demonstrated before.[121-124] These corrections are mainly for compensating fluorescence signal variation induced by the fluctuations in excitation laser power and detector photon energy collection, as well as, for normalizing the fluorescence cuvette or instruments from different vendors.[121-124] However, using Raman IFEs to determine the effective path lengths of spectrofluorometers for fluorescence IFE correction has, to our knowledge, not been demonstrated.

3.3 Theoretical Considerations

I^{corr} and I^{obsd} in Eq. 3.4 are the Raman intensities of the water control (chromophore-free), and chromophore-containing sample, respectively. A_x and A_m are the path length-normalized UV-vis absorbance of the chromophore-containing sample at the excitation and Raman photon wavelengths. Each UV-vis spectra has individual A_x and A_m values corresponding to the excitation and Raman wavelengths, respectively. Since all these variables are experimentally measurable, one may think at first glance that it is

possible to determine the values of d_x and d_m with two or more water Raman samples that contain only one chromophore in solution with different chromophore concentrations. This approach is however, problematic because the A_m and A_x are linearly related to each other ($A_m = k A_x$) if the water Raman samples contain only one chromophore or a chromophore mixture in which the chromophore concentration ratio doesn't change. This can be understood by Beer's Law in which the absorbance of a chromophore at one wavelength is always directly proportional to its absorbance at another wavelength since that molecule's molar absorptivity or extinction coefficient are determined based on the absorbance wavelength. Under this condition, Eq. 3.5 is equivalent to Eq. 3.2 in which d_x and d_m can't be independently quantified.

$$\frac{I^{corr}}{I^{obsd}} = 10^{mA_x} \tag{3.5}$$

Such collinearity can be readily resolved by including two or more chromophores in the water Raman samples in which the chromophore concentration ratio differs from each other. Defining $\frac{I^{corr}}{I^{obsd}}$ as the water Raman correction factor *F, i* as the index of the chromophore-containing sample, one can derive Eq. 3.6 from Eq. 3.4 with simple mathematical manipulation.

$$\frac{logF_i}{A_{x,i}} = d_x + d_m \frac{A_{m,i}}{A_{x,i}} \tag{3.6}$$

With this approach, the effective excitation and emission path lengths are the intercept and slope in the linear equation obtained by linear fitting of $\frac{logF_i}{A_{x,i}}$ as a function of $\frac{A_{m,i}}{A_{x,i}}$.

3.4 Experimental

3.4.1 Reagents

$K_2Cr_2O_7$ was obtained from Fisher Scientific. $Ni(NO_3)_2$, Mercaptobenzimidazole (MBI), 2-aminopurine (2-AP), and Coomassie Brilliant Blue R (CBBR) were obtained from Sigma-Aldrich. All solutions were prepared with nanopure water (18 mΩ cm).

3.4.2 UV-vis, Raman, and fluorescence measurements

All UV-visible measurements were conducted with a Shimadzu UV-2550 UV-vis spectrophotometer and with samples contained in 1 cm × 1 cm cuvettes. The Raman and fluorescence spectra were acquired with a Horiba Jobin Yvon FluoroMax-4 spectrofluorometer. Unless stated otherwise, all Raman and fluorescence spectra were acquired with a 1 cm × 1 cm fluorescence cuvette, and the excitation and emission monochromator slit width in the spectrofluorometer were kept at 5 nm (default setting). Two fluorescence cuvettes were used in this work, and their sizes are 1 cm × 1 cm and 1 cm × 0.17 cm, respectively.

3.4.3 Error Propagation for Linear Fit of Water Raman Data

All water Raman measurements were conducted in triplicate allowing for calculation of standard deviation of the mean (s) for I^{corr} and I^{obsd}. Error propagation was

calculated for F_i or I^{corr}/I^{obsd} using $s_{F_i} = F_i(\sqrt{(\frac{s_{I^{corr}}}{I^{corr}})^2 + (\frac{s_{I^{obsd}}}{I^{obsd}})^2}$. Error propagation was calculated for log(F_i) using $s_{\log(F_i)} = 2.303(logF_i)(s_{F_i})$.

3.5 Results and Discussion

3.5.1 Determination of the effective path lengths using water Raman IFE

The two chromophores used for determining the effective excitation and emission path lengths of the spectrofluorometer used in this work are $Ni(NO_3)_2$ and $K_2Cr_2O_7$. Figure 3.2 shows the UV-vis and Raman spectra of the $Ni(NO_3)_2$ and $K_2Cr_2O_7$ mixture solutions. When Raman excitation and Raman photon wavelengths are in the region where the chromophore absorbs, the water Raman signal intensity monotonically decreases with increasing chromophore concentration. This is evident from the experimental data obtained when the Raman excitation wavelength is set at 300 nm (Figure 3.2B). However, when the excitation wavelength moves to 482 nm at which neither $Ni(NO_3)_2$ nor $K_2Cr_2O_7$ is a strong light absorber, the water Raman intensity can be deemed independent of the chromophore concentration (Figure 3.2(C)). These results conclusively demonstrate that the Raman signal reduction in these chromophore-containing samples observed in Figure 3.2B is indeed due exclusively to the Raman IFE.

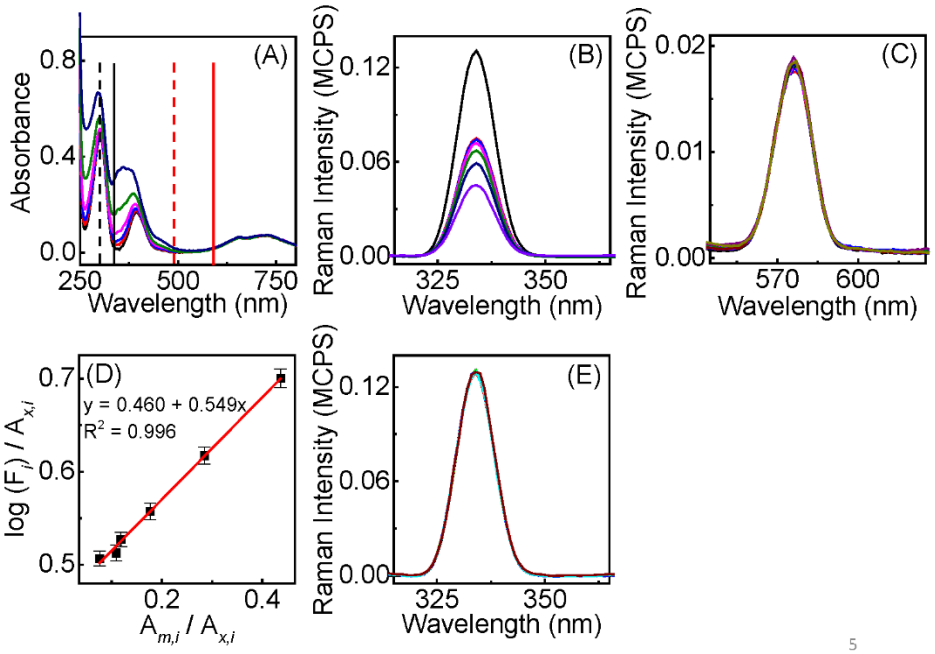

Figure 3.2 Determination of water Raman effective path length using $Ni(NO_3)_2$ and $K_2Cr_2O_7$ chromophores to induce inner filter effects.

Notes: (A) UV-vis spectra of a series of $Ni(NO_3)_2$ and $K_2Cr_2O_7$ mixture solutions. The $Ni(NO_3)_2$ concentration was held constant at 1.54 mM, but $K_2Cr_2O_7$ concentration varied from 0, 0.005 mM, 0.01 mM, 0.02 mM, 0.05 mM, and 0.1 mM. The black dashed and solid vertical lines indicate the excitation and water Raman photon wavelengths for the Raman spectra acquired with an excitation wavelength of 300 nm. The red dashed and solid lines indicate the excitation and water Raman photon wavelengths for Raman spectra acquired with an excitation wavelength of 482 nm. (B) and (C): Raman spectra obtained with $Ni(NO_3)_2$ and $K_2Cr_2O_7$ mixture solutions with excitation wavelength of 300 nm and 482 nm, respectively. The black spectrum is acquired with the water control. (D) Curve-fitting determination of the effective excitation and emission path length, d_x (intercept) and d_m (slope), using Eq. 3.6 and the experimental data shown in (A) and (B). (E) Raman IFE corrected spectra of the $Ni(NO_3)_2$ and $K_2Cr_2O_7$ solutions. 5 nm excitation and emission slit widths were used to obtain Raman spectra. Standard deviations were calculated by propagation of error in $\log(F_i)$, in which the error in F_i was calculated from three independent water Raman measurements.

The effective excitation and emission path lengths were successfully determined through linear-curve fitting of the water Raman data shown in Figure 3.2. The slope and the intercept from this curve-fitting are 0.549 ± 0.009 and 0.460 ± 0.003, respectively (Figure 3.2), indicating that the effective excitation and emission path lengths of the

spectrofluorometer are 0.460 cm and 0.549 cm, respectively. The fact that the IFE-corrected water Raman intensity is totally independent of the chromophore concentration used in these samples (inset in Figure 3.2(D)) indicates that the effective path lengths are at least effective for correcting the water Raman IFE in the chromophore-containing samples used for determining the path lengths.

Independent validation of the effective path lengths, 0.460 and 0.549, for fluorescence and Raman IFE correction are first demonstrated with water Raman measurements (Figure 3.3**)** in which the Raman IFE were induced by chromophore $Ni(NO_3)_2$, mercaptobenzimidazole (MBI), and $K_2Cr_2O_7$, respectively. Importantly, these validation samples have completely different chromophore composition from the samples used for the path length determination in Figure 3.2. Again, the IFE-corrected water Raman intensities are independent of the chromophore concentration in all three series of samples (Figure 3.3). This result indicates that the effective path lengths determined with one set of water Raman measurements are totally effective for correcting the Raman IFE, regardless of the chromophore and Raman excitation wavelength used. The latter indicates that the effective path lengths are instrument-specific, but sample independent.

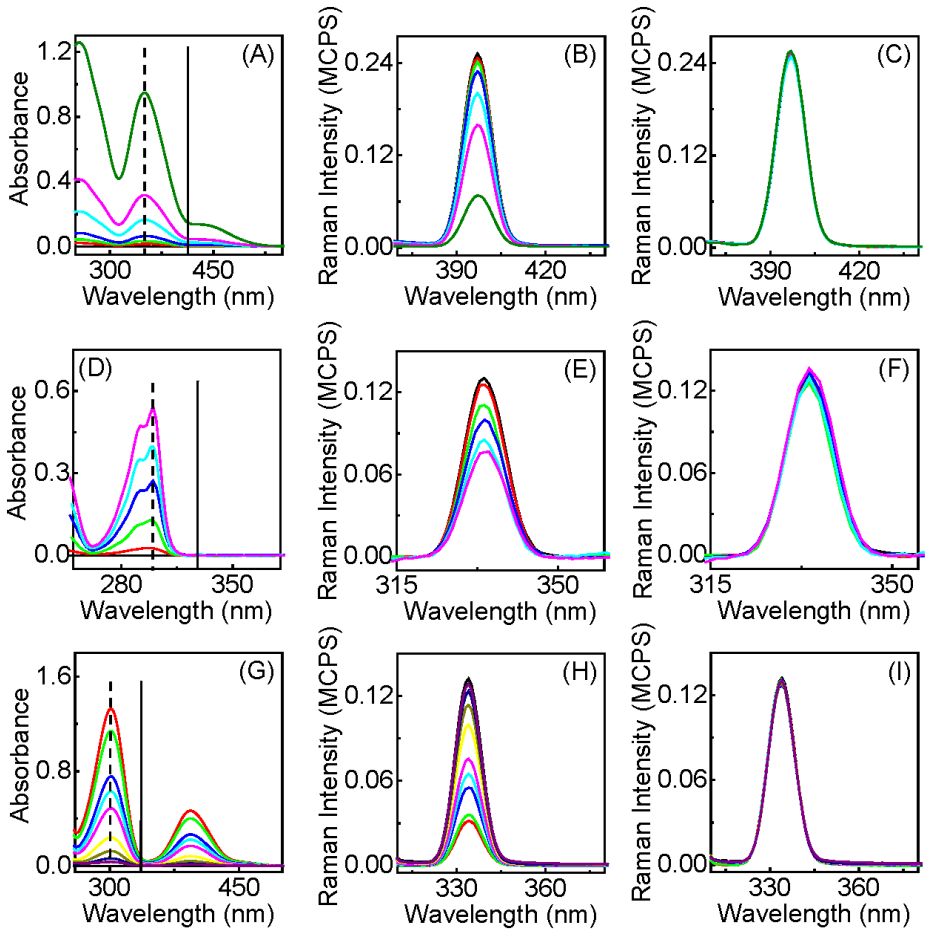

Figure 3.3 Independent validation of effective path lengths determined in Figure 3.2 for correcting the water Raman IFE induced by $K_2Cr_2O_7$, MBI, and $Ni(NO_3)_2$, respectively.

Notes: (A), (D), and (G): UV-vis spectra of $K_2Cr_2O_7$, MBI, and $Ni(NO_3)_2$ solutions, respectively. The dash and solid vertical line indicates the water Raman excitation and scatter wavelengths, respectively. The concentration of the chromophore varies from 0 to 0.3 mM for $K_2Cr_2O_7$, 0 to 19.8 μM for MBI, and 0 to 4.41 mM for $Ni(NO_3)_2$. (B), (E), and (H) Raman spectra obtained with the samples shown in (A), (D), and (G), respectively. The excitation wavelength for the Raman spectra in (B), (E), and (H) are 350 nm, 300 nm, and 300 nm, respectively. (C), (F), and (I) shows the Raman IFE corrected spectra for the data shown in (B), (E), and (H), respectively. 5 nm excitation and emission slit widths were used to obtain Raman spectra.

3.5.2 Correction of fluorescence IFE

The effective path lengths obtained with the water Raman measurements are directly applicable for correcting the fluorescence IFE in fluorescence spectra acquired with the same spectrofluorometer. This conclusion is drawn from a series of fluorescence measurements conducted with two examples fluorophores, 2-aminopurine (2-AP) and Coomassie Brilliant Blue-R (CBBR). Figure 3.4 shows the UV-vis and fluorescence spectra of 2-AP and CBBR as a function of fluorophore concentration. The peak fluorescence intensities of the as-acquired spectra have a poor linear correlation to the fluorophore concentration for both fluorophores. In contrast, their IFE-corrected fluorescence intensities obtained by applying Eq. 3.4 with the effective path lengths determined from the water Raman measurements have an excellent linear correlation to fluorophore concentration. The fact that excellent IFE-correction is achieved for these two fluorophores that differ in both their excitation and emission wavelengths provides further evidence that the effective path lengths are instrument-specific, but sample-independent. The fact that the same pair of effective excitation and emission path lengths enables both reliable Raman and fluorescence IFE correction validates the hypothesis that the origins of Raman and fluorescence IFE are the same.

Neither of the two previous example methods shown with Eqs. 3.1 and 3.2 give satisfactory results when they were applied for correcting the fluorescence IFE in the same fluorescence spectral data shown in Figure 3.4. The difference between the literature method described with Eq. 3.1 and the water Raman method devised in this work is especially striking giving the similarity in the path length values used for the correction. The effective excitation and emission path lengths obtained with the water

Raman measurements (Figure 3.2) are 0.460 ± 0.003 cm and 0.549 ± 0.009 cm, respectively, which are only ~ 10% smaller or larger than their respective counterparts used in Eq. 3.1. Furthermore, the sum of d_x and d_m from the water Raman method differs only by 1% from that in Eq. 3.1. However, the performance of these two methods is drastically different. The reason for this is that the path length parameters are in the exponent term of correction Eq. 3.1 and 3.3. Consequently, small errors in path length determination can lead to large error in fluorescence IFE correction. This result highlights the critical importance of reliable determination of the effective path lengths for effective fluorescence IFE correction.

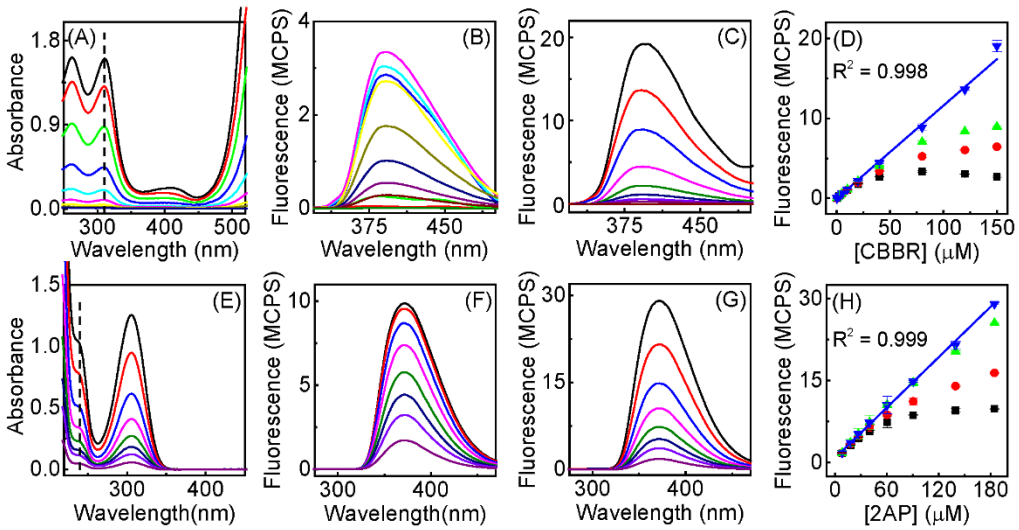

Figure 3.4 IFE correction applied to fluorescence measurements for model fluorophores, CBBR and 2AP using correction equations 3.1, 3.2, or the water Raman derived effective path lengths. .

Notes: Upper row is CBBR and lower row is 2AP. (A) and (E): UV-vis spectra of fluorophores with increasing fluorophore concentration. Dashed lines indicate the excitation wavelengths. (B) and (F): The as-acquired fluorescence spectra of samples shown in (A) and (E), respectively. (C) and (G): IFE-corrected fluorescence spectra using the effective path lengths obtained with the water Raman measurements shown in Figure 3.2. (D) and (H). Correlation between peak fluorescence intensity as a function of fluorophore concentration. Black dots: as-acquired fluorescence intensities, red and green dots are for IFE-corrected intensities for which the corrections were performed with Eq. 3.1 and Eq. 3.2, respectively. Blue dots: IFE-corrected intensities for which the correction was performed using the method presented in this work. 5 nm excitation and emission slit widths were used to obtain fluorescence spectra. Standard deviations were calculated from three independent measurements.

3.5.3 Parameters affecting effective path lengths

The effective path lengths determined with the water Raman measurements remain valid for correcting the fluorescence and Raman IFE as long as the instrumental configuration of the spectrofluorometer remains unchanged during Raman and fluorescence measurement acquisition. Indeed, the fluorescence and water Raman spectra shown in the Figures 3.2, 3.3, and 3.4 were acquired within a ~ 6-month time span. The fact that the Raman and fluorescence IFEs were reliably corrected for all these

samples with the same set of effective path lengths highlights the robustness of this water-Raman based method. However, changing the cuvette size and orientation (for non-square cuvettes) changes the effective path lengths. Figure 3.5 shows the Raman determination of the effective path lengths of the spectrofluorometer when a 1 cm × 0.17 cm fluorescence cuvette is used at two different orientations (Scheme 3.1). For simplicity, we refer hereafter to the cuvette orientation as long or short excitation when the non-square fluorescence cuvette is oriented such that nominal excitation path length is larger or smaller than the emission path length (Scheme 3.1), respectively. Evidently, the effective excitation and emission path lengths of the spectrofluorometer at these two cuvette configurations are different from each other even though the only difference is in the cuvette orientation.

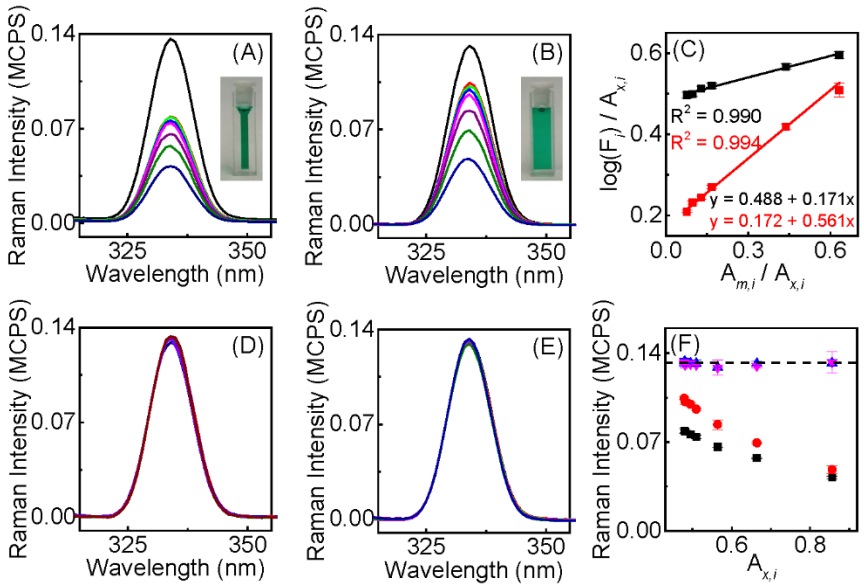

Figure 3.5 Water Raman determination of the effective path lengths for the spectrofluorometer when a 1 cm × 0.17 cm fluorescence cuvette is used with either a short excitation or long excitation orientation.

Notes: (A) and (B) water Raman spectra obtained with the same series of $Ni(NO_3)_2$ and $K_2Cr_2O_7$ mixture solutions used in Figure 3.2. (A) is oriented with a long excitation configuration, and (B) a short excitation. (C) curve-fitting determination of the excitation and emission path lengths of the spectrofluorometer associated with the two orientations of the fluorescence cuvette. (D) and (E): IFE-corrected water Raman spectra when the cuvette was oriented with long or short excitation, respectively. (F) Correlation between the water Raman intensity as a function of the sample UV-vis absorbance at the excitation wavelengths. Black and red dots represent as-acquired data. Blue and pink dots represent IFE corrected data. 5 nm excitation and emission slit widths were used to obtain Raman spectra.

It is important to note that changing the cuvette orientation may or may not change the water Raman intensity of the chromophore-free samples, but it has significant effect on water Raman intensity of the chromophore-containing samples. The significance of the effect of changing cuvette orientation on the water Raman signal depends on the sampling geometry of the spectrofluorometer and the UV-vis spectral feature of the samples. Scheme 3.1 shows two example instrument geometries in which the beam is perfectly centered and aligned for all orientations. The first case is that the

excitation and emission beam size are both smaller than the cuvette size (configuration (A) and (B)). In these configurations, changing the cuvette orientation should have negligible effect on the Raman signal of the chromophore-free samples. However, the Raman signal of the chromophore-containing sample obtained with configuration (A) should be significantly higher than that obtained with configuration (B) if the sample has strong UV-vis absorbance only at the excitation wavelength. On the contrary, the Raman signal of the chromophore-containing sample obtained with configuration (A) will be smaller than that obtained with configuration (B) if the sample has strong UV-vis absorbance only at the emission wavelength. This argument should also hold true for fluorescence samples.

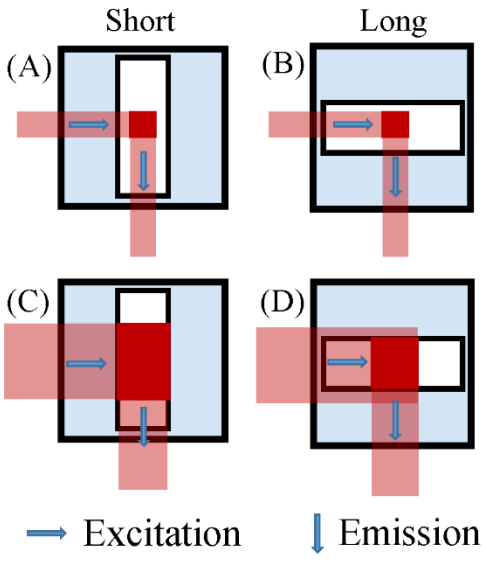

Scheme 3.1 Illustration of example instrument configurations when a non-square cuvette is oriented with short or long excitation.

Notes: A and C represent short excitation orientation. B and D represent long excitation orientation.

If one beam size is larger than the nominal excitation or emission path length of the fluorescence cuvette as shown in Scheme 3.1 (C) and (D), changing the orientation of the fluorescence cuvette can change water Raman intensity in both the chromophore-free and chromophore-containing samples. Again, the long excitation orientation reduces the IFE induced by sample absorption of the emission photons, while the short excitation orientation minimizes the IFE induced by sample absorption of the excitation photons. This characteristic is important for choosing cuvette orientation in practical fluorescence measurements for instrumental reduction of the fluorescence IFE. For fluorescence measurements conducted with excitation at a samples' peak UV-vis wavelengths, taking fluorescence with a cuvette's short excitation orientation can be preferable for concentrated samples.

Changing the slit widths of the excitation and emission monochromators can modify the effective excitation and emission path lengths of the spectrofluorometer. Figure 3.6 shows an example water Raman determination and fluorescence validation of the effective path lengths when the nominal excitation and emission slit widths are both set to 2 nm, not 5 nm as that used for the data shown in Figures 3.2. However, the same 1 cm square cuvette was used in both cases. The effective excitation and emission path lengths associated with the 2 nm slit width are 0.491 ± 0.005 and 0.453 ± 0.009 cm, respectively, which are significantly different from their respective counterparts (0.549 ± 0.009 and 0.460 ± 0.003 cm) associated for the 5 nm slit widths.

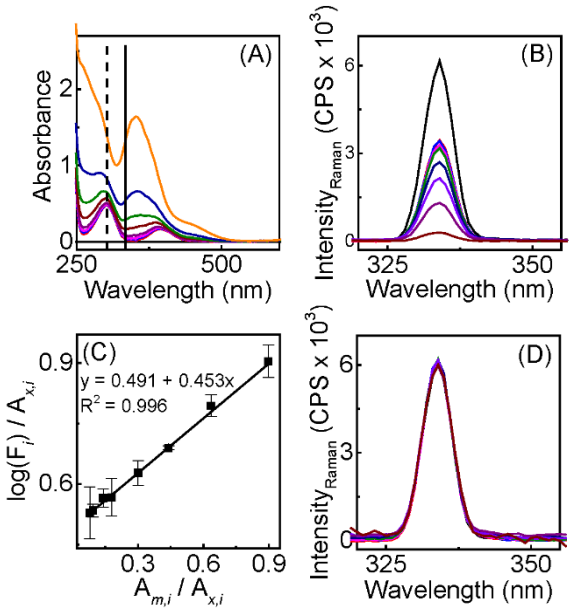

Figure 3.6 Water Raman determination of the effective path lengths of the spectrofluorometer in which 2 nm slit widths for both the excitation and emission monochromators were used for Raman acquistion.

Notes: (A) UV-vis, and (B) water Raman spectra obtained with the $Ni(NO_3)_2$ and $K_2Cr_2O_7$ mixture solutions. (C) curve-fitting determination of the effective excitation and emission path lengths of the spectrofluorometer. (D) IFE-corrected water Raman spectra of the $Ni(NO_3)_2$ and $K_2Cr_2O_7$ mixture solutions. All Raman measurements were conducted with a 1 cm × 1 cm square cuvette. 2 nm excitation and emission slit widths were used to obtain Raman spectra.

There are two reasons why the effective excitation and emission path lengths of a spectrofluorometer are related to the slit widths in the excitation and emission monochromators. The first is that changing the monochromator slit widths modify the excitation and emission beam sizes,[105] which can also change photon energy distribution across the excitation and emission beams. This can change the effective path lengths of the spectrofluorometer. The second reason, which is likely more significant, is that the monochromator slit widths are critically related to the fluorescence polychromatic effect. The polychromatic effect refers to the fact that the experimentally measured light

intensity of photons at a specified wavelength inevitably contain signal contribution from photons with wavelengths close to the specified wavelength. Therefore, the experimentally measured spectral intensities in all optical measurements at individual wavelengths are only an approximation of their true intensities. The larger the slit width, the more severe the polychromatic effect and the larger the deviation of the measurement results from the true intensities.

Reducing the monochromator slit widths reduces the polychromatic effect, which can drastically improve the reliability of the Raman and fluorescence IFE correction. For example, with the 5 nm slit widths, the largest correction factor for the water Raman IFE is ~5 for samples in a 1 cm square cuvette (Figure 3.3 (H)), while that for the 2 nm slit widths is ~25 (Figure 3.6 (B)). When using 5 nm slit widths the wavelength accuracy for selected excitation radiation deviates from the specified wavelength to much greater extent than the wavelength accuracy accociated when using 2 nm slit widths. Therefore, 5 nm slit widths are less monochromatic compared to 2 nm slit widths. The reasons why polychromatic effects have such a profound impact on the IFE correction are two-fold. First, the accuracy of the effective path lengths determined using Eq. 3.6 relies entirely on the reliability of the measured Raman and UV−vis absorbance of the water Raman samples at specified wavelengths. Second, even when the effective path lengths are perfectly correct, the IFE correction can still be erroneous for samples in which their fluorescence, Raman, and UV−vis absorbance cannot be reliably determined. In other words, polychromatic effects are critical for both path length determination and applications for IFE correction.

Besides slit widths, other instrument and sample parameters also affect the polychromatic effect.[1] These include the effective path lengths associated with UV−vis and fluorescence cuvettes, the spectral resolution of the monochromators of the spectrophotometers, and the sample concentrations. For optimal IFE correction, one should minimize the polychromatic effects in UV−vis and fluorescence spectroscopic acquisitions. The polychromatic effect in UV−vis measurements is usually small in comparison to fluorescence measurements. This is because the monochromator slit widths in UV−vis measurements are usually 1 nm or smaller, but the slit widths used in fluorescence spectroscopic analysis are usually in the range of 2 to 5 nm to ensure adequate light throughput.

Small slit widths combined with a fluorescence cuvette with short path lengths minimize polychromatic effects, which in turn enable optimal IFE corrections. Figure 3.7 shows the water Raman and fluorescence IFE correction for samples contained in a 1 cm × 0.17 cm cuvette. The slit widths of both the excitation and emission monochromators were kept at 2 nm for spectral acquisition. The IFE-corrected peak fluorescence intensities of 2-AP exhibit excellent linear correction to the 2- AP concentration from 5.9 nM all the way to 595 μM, spanning about 5 orders of magnitude. Increasing the 2-AP concentration to 1 mM or above leads to deviation of the linearity between IFE-corrected fluorescence intensity and 2-AP concentration. It is critical to note that this deviation does not necessarily imply failure of the IFE-correction. At this high fluorophore concentration, multiple physical and photochemical processes can induce change in the 2-AP fluorescence quantum yield, making the fluorescence intensity intrinsically nonlinear to fluorophore concentration.

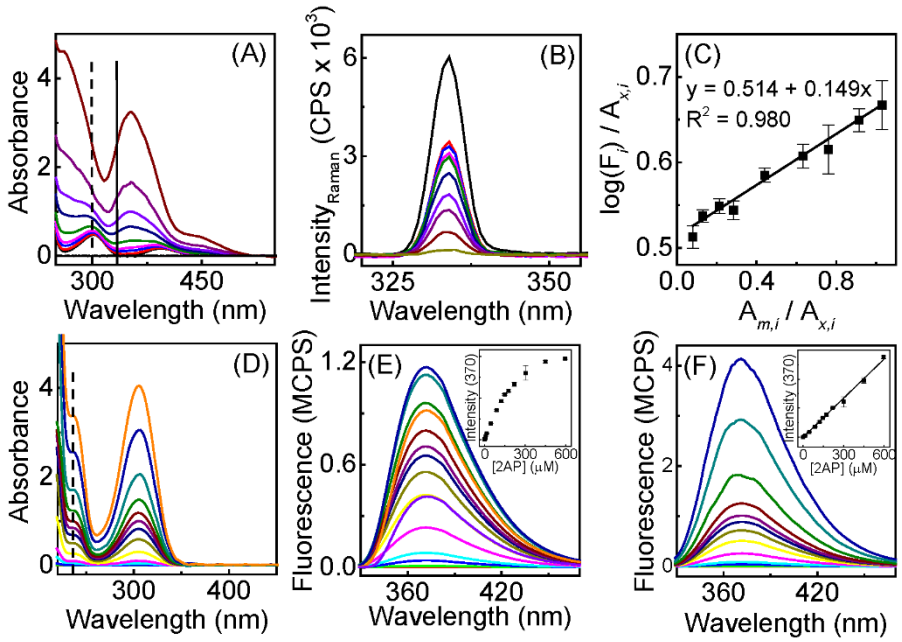

Figure 3.7 Water Raman determination of Raman IFE path lengths for correction of 2-aminopurine fluorescence IFE using a 1 cm × 0.17 cm cuvette and 2 nm slit widths.

Notes: (A) UV-vis, and (B) Raman spectra of water Raman solutions of $Ni(NO_3)_2$ and $K_2Cr_2O_7$ mixture solutions. The $Ni(NO)_3$ concentration is 1.54 mM and the $K_2Cr_2O_7$ concentration varied from 0, 0.01, 0.02, 0.05, 0.10, 0.20, 0.30, 0.50, and 1.0 mM. (C): Curve-fitting determination of the effective excitation (intercept) and emission (slope) path lengths of the spectrofluorometer. (D) UV-vis spectra of 2-AP solutions with different concentrations, (E) as-acquired 2-AP fluorescence spectra. Inset: correlation between the peak fluorescence intensity and 2-AP concentration. (F) IFE-corrected fluorescence spectra. Inset: correlation between the IFE-corrected peak fluorescence intensity versus 2-AP concentrations. All Raman and fluorescence measurements were conducted with identical instrument configuration. The excitation and emission monochromator slit widths are both 2 nm. The size of fluorescence cuvette is 1 cm × 0.17 cm, and it is oriented such that the nominal excitation path length is 0.17 cm. The spectral integration time is 2 s for all fluorescence spectra.

As discussed in the introduction section, water Raman IFE should provide a far more reliable estimator than fluorescence on the upper limit of the optical density of a fluorescence sample for which its IFE can be reliably corrected. The highest collective UV−vis absorbance at the excitation and emission wavelengths for the $Ni(NO_3)_2$ and $K_2Cr_2O_7$ mixture solution for which its Raman IFE was reliably corrected is 6.7. Since

the peak UV−vis absorbance in common fluorescence samples are usually lower than 2, the successful Raman IFE correction in water Raman samples with such high optical density strongly suggests that this water path length determination method should be totally adequate for fluorescence IFE correction in general fluorescence applications.

The effective path lengths are highly reproducible, indicating the rigidity of the spectrofluorometer used in this work. The most common instrument parameters one would change in fluorescence measurements include the excitation wavelength, monochromator slit width, spectral integration time, and cuvette size and orientation. The effective path lengths are independent of the spectral integration time. Preceding experimental data indicates that the effective path length is mostly independent of the excitation wavelengths. This is because the same pair of path lengths provide excellent water Raman IFE correction as shown in Figure 3.3. We found that the effective excitation and emission path lengths determined for a specific instrument configuration (cuvette size, orientation, and slit width) remain valid for correcting fluorescence for at least several months as long as the fluorescence spectra were taken with the specified instrument configuration. The instrument configuration can be changed between the path length determination and fluorescence measurements.

One can take advantage of the path length reproducibility to minimize the need for repeated path length determinations. It can be advantageous to determine effective path lengths associated with all foreseeable instrumental configurations for a specific spectrofluorometer. Whenever needed, one can simply use the predetermined effective path lengths for fluorescence IFE correction. New water Raman-based path length determination is needed only when a new instrument configuration (cuvette size and

orientation and slit width) is employed or the validity of the predetermined path lengths is in doubt. The fact that the same set of water Raman samples can be used for determination of the effective excitation and emission path lengths of a spectrofluorometer at any instrument configuration is another key advantage of this water Raman method. For convenience, one can prepare a series of water Raman standard stock solutions and acquire and digitally store their UV−vis spectra. Whenever needed, one can simply collect a new set of water Raman spectra with the existing stock water Raman standards and then perform the linear curve-fitting to determine or verify the effective path lengths. One example series of water Raman standards is the $Ni(NO_3)_2/K_2Cr_2O_7$ mixture solutions used in this work that are stable under ambient conditions for at least several months.

3.6 Conclusions

A water Raman based method has been developed for determination of the effective excitation and emission path lengths (d_x and d_m) of spectrofluorometers for fluorescence IFE correction. The latter is achieved by applying the correction equation of $I^{corr}/I^{obsd} = 10^{d_x A_x + d_m A_m}$. The effective excitation and emission path lengths determined with one set of water Raman measurements at one specific Raman excitation wavelength are globally applicable for correcting fluorescence and Raman IFEs induced by any chromophore in solution, regardless of excitation and emission wavelengths. The effective path lengths were determined with simple linear curve-fitting. No complicated instrument geometry characterization or difficult data manipulation is needed. The IFE-corrected fluorescence intensities are linearly correlated to fluorophore concentration

over 5 orders of magnitude (from 5.9 nM to 0.59 mM) for 2- aminopurine in a 1 cm × 0.17 cm fluorescence cuvette. The methodology provided in this work should be of broad significance in physical and biological sciences given the simplicity of the IFE-correction method and the popularity of fluorescence spectroscopy in analytical applications.

CHAPTER IV

UV-VIS RATIOMETRIC RESONANCE SYNCHRONOUS SPECTROSCOPY FOR DETERMINATION OF NANOPARTICLE AND MOLECULAR OPTICAL CROSS SECTIONS

This work has been previously published: Nettles, C. B.; Zhou, Y.; Zou, S.; Zhang, D. UV-Vis Ratiometric Resonance Synchronous Spectroscopy for Determination of Nanoparticle and Molecular Optical Cross Sections. *Anal. Chem*., **2016**, *88*, 2891-2898

4.1 Abstract

Demonstrated herein is a UV−vis Ratiometric Resonance Synchronous Spectroscopic (R_2S_2, pronounced as "R-two-S-two" for simplicity) technique where the R_2S_2 spectrum is obtained by dividing the resonance synchronous spectrum of a NP-containing solution by the solvent resonance synchronous spectrum. Combined with conventional UV−vis measurements, this R_2S_2 method enables experimental quantification of the absolute optical cross sections for a wide range of molecular and nanoparticle (NP) materials that range optically from pure photon absorbers or scatterers to simultaneous photon absorbers and scatterers, simultaneous photon absorbers and emitters, and all the way to simultaneous photon absorbers, scatterers, and emitters in the UV−vis wavelength region. Example applications of this R_2S_2 method were demonstrated for quantifying the Rayleigh scattering cross sections of solvents including water and toluene, absorption and resonance light scattering cross sections for plasmonic

gold nanoparticles, and absorption, scattering, and on-resonance fluorescence cross sections for semiconductor quantum dots (Qdots). On-resonance fluorescence quantum yields were quantified for the model molecular fluorophore Eosin Y and fluorescent Qdots CdSe and CdSe/ZnS. The insights and methodology presented in this work should be of broad significance in physical and biological science research that involves photon/matter interactions.

4.2 Introduction

Photon interactions with nanoparticle (NP) chromophores and fluorophores have been implicated in a broad range of NP applications including photocatalysis,[125-128] cancer therapy,[129-131] solar energy harvesting,[132-135] optoelectronics,[136-139] biosensing,[140-144] and optical spectroscopy.[145-147] A large number of NPs have been synthesized in recent decades that differ in size, shape, and chemical composition. These NPs optically range from pure photon absorbers that have negligible photon scattering, pure scatterers that have no significant photon absorption, simultaneous photon absorbers and scatterers, and all the way to simultaneous photon absorbers, scatterers, and emitters in the UV−vis wavelength region. However, experimental characterization of the NP optical properties remains a significant challenge in nanoscience research. This is especially true for NP fluorophores for which there is currently no measurement technique capable of resolving the interplay of NP photon absorption, scattering, and on-resonance fluorescence emission.

While determination of the NP UV−vis extinction cross section is straightforward with a simple UV−vis spectrophotometer, experimental decoupling of the NP absorption and scattering contribution to the NP photon excitation is challenging. This is because

photon absorption and scattering are highly convoluted processes. While photon absorption invariably reduces the scattered photon intensity due to the sample inner filter effect (IFE), the effect of photon scattering on the photon absorption is much more complicated. Qualitatively, photon scattering can both reduce and increase the path lengths of the individual photons inside the sample cell. The net effect of photon scattering on NP photon absorption depends critically on the NP properties and concentration as well as the geometry of the sample cell.

Determination of the NP absorption and scattering cross sections for NP fluorophores is even more challenging in comparison to that of NP chromophores. This is because the NP fluorophore can undergo on-resonance fluorescence that can be mistakenly treated as resonance light scattering. The latter is a special case of Rayleigh scattering and refers to photon scattering that occurs at the same wavelengths that the NP absorbs, even though the resonance light scattering does not involve photon absorption. In contrast, photon absorption must occur prior to on-resonance fluorescence by molecular and NP fluorophores. On-resonance fluorescence refers to fluorescence emission at the wavelength identical to that of the absorbed photon. While there is extensive work on molecular and nanoparticle resonance light scattering,[5,148,149] there is essentially no quantitative information on fluorophore on-resonance fluorescence.

Presented herein is the development and validation of a Ratiometric Resonance Synchronous Spectroscopic (R_2S_2) method for experimental determination of NP and molecular optical cross sections that includes the material's extinction, absorption, scattering, and on-resonance fluorescence emission cross sections. The model NPs include commercial plasmonic gold nanoparticles (AuNPs) with ~10, ~30, and ~50 nm

diameters, toluene soluble CdSe fluorescence quantum dots (Qdots) with a diameter of ~2.5 nm, and water-soluble CdSe/ ZnS core−shell Qdots with a particle size of ~10 nm diameter. Molecular chromophore $K_2Cr_2O_7$ and fluorophore Eosin Y were also used to model NP photon absorbers and simultaneous photon absorbers and emitters, respectively. Polystyrene nanoparticle (PSNP) beads with ~100 nm diameter were used to approximate NP photon scatterers that have negligible UV−vis absorption. The inclusion of this relatively large set of model NPs enables critical evaluation of the general applicability of this R_2S_2 method.

4.3 Theoretical Considerations

It is commonly assumed that scattered photon intensity is linearly related to the concentration of the scatterers ($I_{sca} = KC$). However, this equation is only applicable to situations in which the NPs are approximately pure photon scatterers with no significant photon absorption and emission. Otherwise, a large deviation occurs if the NPs or other components in the NP containing solution absorb photons in the wavelength region of interest. This photon absorption induces sample IFE that have been documented extensively in Rayleigh, Raman, surface enhanced Raman, and fluorescence spectroscopic measurements.[32,33,35,54]

Scattered and on-resonance fluorescence photons can be determined with a conventional spectrofluorometer in resonance synchronous spectral acquisition mode in which the excitation and emission wavelength are set to be identical during the entire synchronous spectral acquisition (wavelength offset = 0). For solutions containing NPs that are simultaneous photon absorbers, scatterers, and on-resonance emitters, the

resonance synchronous spectral intensity ($I_{RS_2}^{Solu}(\lambda)$) can be expressed as Eq. 4.1. The resonance synchronous intensity for the solvent alone is represented with Eq. 4.2.

$$I_{RS_2}^{Solu}(\lambda) = I_{exc}(\lambda)K(\lambda)[C_{Solv}\sigma_{Sca}^{Solv}(\lambda) + C_{NP}\sigma_{Sca}^{NP}(\lambda) + C_{NP}\sigma_{OFE}^{NP}(\lambda)]10^{-\eta(\lambda)E(\lambda)d_{eff}} \tag{4.1}$$

$$I_{RS_2}^{Solv}(\lambda) = I_{exc}(\lambda)K(\lambda)C_{Solv}\sigma_{Sca}^{Solv}(\lambda) \tag{4.2}$$

$I_{exc}(\lambda)$ is the excitation light intensity at the specified wavelength, d_{eff} is the effective path length of the excitation photons inside the cuvette that is related to parameters such as the cuvette geometry, instrument alignment, and monochromator slit width. C_{solv} and C_{NP} are the solvent and NP concentrations, respectively. $\sigma_{\mathrm{Sca}}^{\mathrm{Solv}}(\lambda)$, $\sigma_{\mathrm{Sca}}^{\mathrm{NP}}(\lambda)$, $\sigma_{\mathrm{OFE}}^{\mathrm{NP}}(\lambda)$ are the solvent and NP scattering cross sections and NP on-resonance fluorescence emission cross section, respectively. K(λ) is the instrument photon collection efficiency and detector quantum yield. E(λ) is the solution UV−vis extinction at the specified wavelength. η(λ) is the absorption fraction of the extinction, E(λ), at the specified wavelength. η(λ) is 1 if the photon extinction is due entirely to photon absorption and 0 if due entirely to scattering. Eqs 4.1 and 4.2 were derived on considerations similar to our previous publication that discussed in Chapter 3 where sample IFE on Raman measurements was used to determine the effective path lengths for correcting the sample IFE in fluorescence measurements.[54] We demonstrated there and latter in this work that the path length, $d_{eff,}$ is instrument-specific and independent of the excitation and emission wavelengths.

Dividing Eq. 4.1 with Eq. 4.2 leads to Eq. 4.3 in which $I_{R_2S_2}^{obs}(\lambda)$ is the experimentally observed R_2S_2 of the solution that contains simultaneous photon scatterers, absorbers, and on-resonance emitters.

$$I_{R_2S_2}^{obs}(\lambda) = \frac{I_{RS_2}^{Solu}}{I_{RS_2}^{Solv}} = \left[1 + \frac{C_{NP}(\sigma_{Sca}^{NP}(\lambda) + \sigma_{OFE}^{NP}(\lambda))}{C_{Solv}\sigma_{Sca}^{Solv}(\lambda)}\right] 10^{-\eta(\lambda)E(\lambda)d_{eff}} \tag{4.3}$$

$$\log I_{R_2S_2}^{obs}(\lambda) = \log\left[1 + \frac{C_{NP}}{C_{Solv}} \frac{\sigma_{Sca}^{NP}(\lambda) + \sigma_{OFE}^{NP}(\lambda)}{\sigma_{Sca}^{Solv}(\lambda)}\right] - \eta(\lambda)E(\lambda)d_{eff} \tag{4.4}$$

As implied in Eq. 4.3 and manifested by experimental data shown later in this work, the interplay of photon absorption, scattering, and emission can induce drastic deviation of linearity between the experimental R_2S_2 spectral intensity versus NP concentration and cause distortion of the R_2S_2 spectra as a function of NP concentration. However, such deviation and spectral distortion can be corrected once the correct $\eta(\lambda)$ is known. Eqs 4.5a or 4.5b are derived from Eq. 4.3 for calculating the IFE-corrected R_2S_2 spectrum ($I_{R_2S_2}^{corr}(\lambda)$). Evidently, the IFE-corrected R_2S_2 intensity is linearly proportional to the NP concentration with a baseline intensity of 1.

(A) $$I_{R_2S_2}^{corr}(\lambda) = I_{R_2S_2}^{obs}(\lambda) 10^{\eta(\lambda)E(\lambda)d_{eff}}$$

(B) $$I_{R_2S_2}^{corr}(\lambda) = 1 + C_{NP} \frac{\sigma_{Sca}^{NP}(\lambda) + \sigma_{OFE}^{NP}(\lambda)}{C_{Solv}\sigma_{Sca}^{Solv}(\lambda)} \tag{4.5}$$

The effective path length, d_{eff}, in the above equations can be reliably quantified on the basis of sample IFE imposed by molecular chromophores such as $K_2Cr_2O_7$ on water Rayleigh scattering. This is analogous to our recent work using water Raman scattering to determine the effective path lengths for Stokes-shifted fluorescence spectroscopy

mentioned in Chapter 3.[54] In this case, Eq. 4.4 can be simplified into Eqs 4.6 or 4.7 on the basis of the following considerations. First, $K_2Cr_2O_7$ has no detectable fluorescence activities ($\sigma_{OFE}^{NP}(\lambda) = 0$). Second, the Rayleigh scattering cross section of $Cr_2O_7^{2-}$ is likely similar to water, but the chromophore concentration (<1 mM) is drastically smaller than that of water (~55 M). As a result, the logarithm term in the right-hand-side of Eq. 4.4 is approximately 0. This, combined with the fact that $\eta = 1$ and $A(\lambda) = E(\lambda)$, leads to the conversion of Eq. 4.4 into Eqs 4.6 or 4.7. The latter shows the effective instrument path length is the slope of the linearly fitted curve of the logarithm of $1/I_{R_2S_2}^{obs}(\lambda)$ as a function of the chromophore UV−vis absorbance at the specific wavelength.

$$I_{R_2S_2}^{corr}(\lambda) = I_{R_2S_2}^{obs}(\lambda)10^{\eta(\lambda)E(\lambda)d_{eff}} \tag{4.6}$$

$$I_{R_2S_2}^{corr}(\lambda) = 1 + C_{NP}\frac{\sigma_{Sca}^{NP}(\lambda) + \sigma_{OFE}^{NP}(\lambda)}{C_{Solv}\sigma_{Sca}^{Solv}(\lambda)} \tag{4.7}$$

Once the effective photon path length is quantified, one can determine the experimental $\eta(\lambda)$ and $\frac{\sigma_{sca}^{NP}(\lambda) + \sigma_{OFE}^{NP}(\lambda)}{\sigma_{Sca}^{Solv}(\lambda)}$ values through a two-parameter fitting of the experimental R_2S_2 spectral intensity as a function of the NP concentration and its UV-vis extinction intensity. The $\eta(\lambda)$ value enables the decoupling of the NP photon absorption and scattering contributions to the NP extinction spectrum. Eqs 4.8 and 4.9 are derived on the basis of the definition of $\eta(\lambda)$ and the UV−vis extinction cross sections ($\sigma_{ext}(\lambda)$). N_A is Avogadro's constant.

$$\sigma_{abs}^{NP}(\lambda) = \eta(\lambda)\sigma_{ext}^{NP}(\lambda) = \eta(\lambda)\frac{E(\lambda)}{N_A C_{NP}} \tag{4.8}$$

$$\sigma_{sca}^{NP}(\lambda) = (1-\eta(\lambda))\sigma_{ext}^{NP}(\lambda) \tag{4.9}$$

The solvent Rayleigh scattering cross section can be readily determined using the NP external reference method by combining UV−vis and R_2S_2 measurements of a NP photon scatterer that have negligible photon absorption and photon emission. For a pure NP photon scatterer, Eq. 4.3 is simplified into Eq. 4.10. Since the absolute scattering cross section of a pure NP scatterer is equivalent to its NP extinction cross section, one can conveniently quantify the absolute solvent Rayleigh scattering cross section using Eq. 4.11.

$$I_{R_2S_2}^{obs}(\lambda) = 1 + \frac{C_{NP}\sigma_{Sca}^{NP}(\lambda)}{C_{Solv}\sigma_{Sca}^{Solv}(\lambda)} \tag{4.10}$$

$$\sigma_{sca}^{Solv}(\lambda) = \frac{E(\lambda)}{(I_{R_2S_2}^{obs}(\lambda)-1)C_{Solv}N_A} \tag{4.11}$$

One can also determine the solvent Rayleigh scattering cross section using a solvent external reference technique by measuring the R_2S_2 spectra between the targeted solvent and a solvent with known Rayleigh scattering cross section. Mathematically, the R_2S_2 spectrum between two solvents can be represented with Eq. 4.12 that is derived from Eq. 4.2, and the Rayleigh scattering of the target solvent can be calculated with Eq. 4.13 in which $I_{R_2S_2}^{1,2}(\lambda)$ is the R_2S_2 intensity between the two solvents (Solv. 1 and 2). This solvent external reference method is simpler in comparison to the NP reference technique discussed in the preceding section.

$$I_{R_2S_2}^{1,2}(\lambda) = C_{Solv,1}\sigma_{Sca}^{Solv,1}(\lambda) / C_{Solv,2}\sigma_{Sca}^{Solv,2}(\lambda) \tag{4.12}$$

$$\sigma_{Sca}^{Solv,1}(\lambda) = C_{Solv,2} I_{R_2S_2}^{1,2}(\lambda) \sigma_{Sca}^{Solv,2}(\lambda) / C_{Solv,1} \quad (4.13)$$

It is noted that using resonance synchronous spectroscopy for detecting the Rayleigh scattering and resonance light scattering has been demonstrated before.[5,6,18,150] However, in these applications, the solvent and possible on-resonance fluorescence contribution to the detected synchronous spectra have been neglected. In contrast, the R_2S_2 method provides a systematic approach to quantitatively decouple the interplay of photon absorption, scattering, and on-resonance emission of photon absorbers, scatterers, and emitters in the same sample.

4.4 Experimental

4.4.1 Reagents

Toluene, $K_2Cr_2O_7$, and Eosin Y were obtained from Sigma-Aldrich. AuNPs with diameters of 10, 30, and 50 nm were purchased from Nanocomposix. CdSe (2.5 nm) and CdSe/ZnS (10 nm) Qdots were purchased from NN-Lab Crystal Corporation. Polystyrene beads (PSNPs, 100 nm) were obtained from Polysciences, Inc. All solutions were prepared with nanopure water (18 MΩ cm) unless otherwise stated.

4.4.2 UV-vis, Stokes-shifted fluorescence, and resonance synchronous measurements

All UV-visible measurements were conducted with a Thermo Scientific Evolution 300 UV-vis spectrophotometer. UV-vis acquisition was conducted with samples contained in a 1 cm x 1 cm quartz cuvette and a scan rate of 120 nm/min. All resonance synchronous and Stokes-shifted fluorescence measurements were acquired using a Horiba FluoroMax-4 spectrofluorometer. Resonance synchronous spectra were acquired

by setting the offset to 0 nm between the excitation and detection wavelength. All synchronous spectra were acquired with a 1 cm × 1 cm fluorescence cuvette, excitation and detection monochromator slit widths of 1 nm, and the spectral integration time of 0.3 s for the entire spectral wavelength range from 300 to 800 nm.

In order to obtain the Stokes-shifted fluorescence spectrum in the UV−vis region from 300 to 800 nm without spectral interference from excitation photons, two Stokes-shifted fluorescence spectra were acquired for each fluorophore. The first spectrum is acquired with excitation wavelength of 290 nm, and emission was monitored from 300 to 500 nm. The second one is taken with an excitation of 400 nm, and the emission spectra was monitored from 450 to 795 nm. The two Stokes-shifted fluorescence spectra were then combined to give the Stokes-shifted fluorescence emission spectrum from 300 to 800 nm.

4.4.3 Computational Simulations

In the theoretical calculations, since the molecular and nanoparticle fluorophores are all small (equal or smaller than 10 nm in diameter), their indices of refraction were obtained from experimental UV-vis spectra using Kramer-Kronig transformation method.[151] Once the indices of refraction of the nanoparticles were obtained, their scattering, absorption, and extinction spectra were calculated using Mie theory.[19,20]

4.5 Results and Discussion

4.5.1 NP photon scatter

One can quantify the absolute scattering cross section of a NP photon scatterer directly on the basis of the NP UV−vis extinction spectrum. The combined NP UV−vis

and R_2S_2 spectral measurements, however, provide a simple way for quantifying the solvent Rayleigh scattering cross section as shown in Eq. 4.11 with the experimental data obtained with the surface-modified water-soluble polystyrene NPs (PSNPs) (Figure 4.1). These PSNPs have a nominal diameter of 100 nm, and they can be approximated as pure NP photon scatterers with no detectable fluorescence activity or UV−vis absorptivity in the detected wavelength range. This approximation is justified on the observation that the experimental R_2S_2 intensity of the PSNP at four different wavelengths are all linearly related to the NP concentration. If the PSNP has any significance photon absorption, the R_2S_2 intensity will deviate from the linear dependence of the NP concentration as predicted with Eq. 4.3 and as shown later with the experimental data obtained with NP photon absorbers.

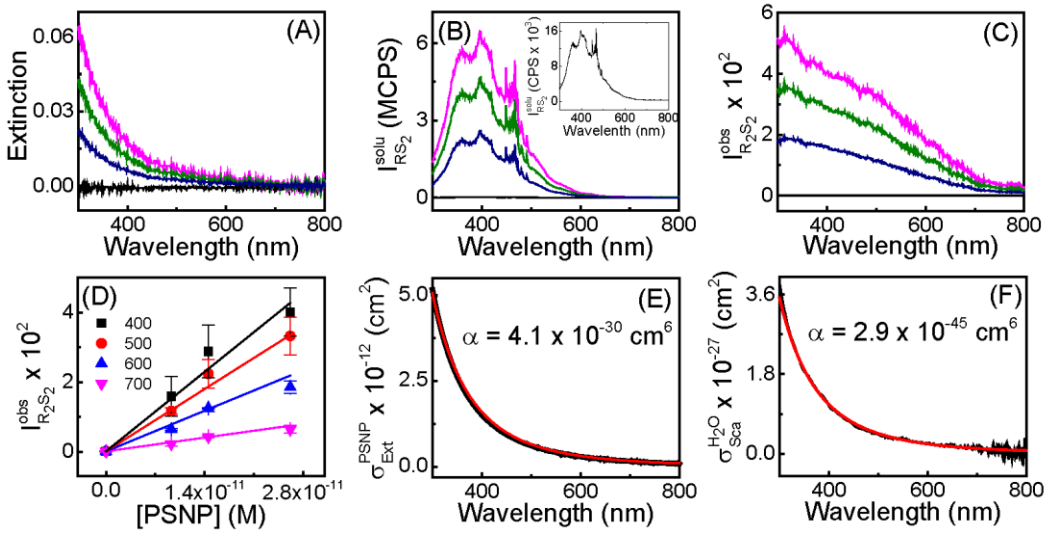

Figure 4.1 Combined UV-vis and R_2S_2 determination of PSNP and water Rayleigh scattering cross-sections.

Notes: (A), (B), and (C) Concentration dependent PSNP UV-vis extinction spectra, as-acquired resonance synchronous spectra, and R_2S_2 spectra, respectively. Inset in (B) is the solvent water resonance synchronous spectrum. (D) R_2S_2 spectral intensity as a function of the PSNP concentration at four different wavelengths. (E) and (F) show the Rayleigh scattering cross-section as a function of excitation wavelength for PSNP and solvent, respectively. The curves in black are the experimental Rayleigh scattering cross-sections, and the red curves are obtained by curve-fitting the experimental data with the equation of $\sigma = \alpha/\lambda^4$ and the α values are shown in the plots.

The experimental scattering cross sections for both PSNPs and water are exactly proportional to the reciprocal of the fourth power of the wavelength. This indicates that both PSNPs and water molecules predominantly undergo conventional Rayleigh scattering that is characterized by its $1/\lambda^4$ law, but with no significant contribution of Mie scattering for which the scattering cross section is approximately wavelength independent. Using water as the solvent external reference and the R_2S_2 spectral measurement as described in Eq. 4.13, we have also quantified the Rayleigh scattering cross section for toluene (Figure 4.2) which is the solvent for quantifying the optical cross sections of toluene-soluble CdSe Qdots. The wavelength dependence of the toluene

scattering cross section also follows the equation of $\sigma(\lambda) = \alpha/\lambda^4$. The α value for toluene is 4.3×10^{-43} cm^6, which is about 150 times larger than that for water.

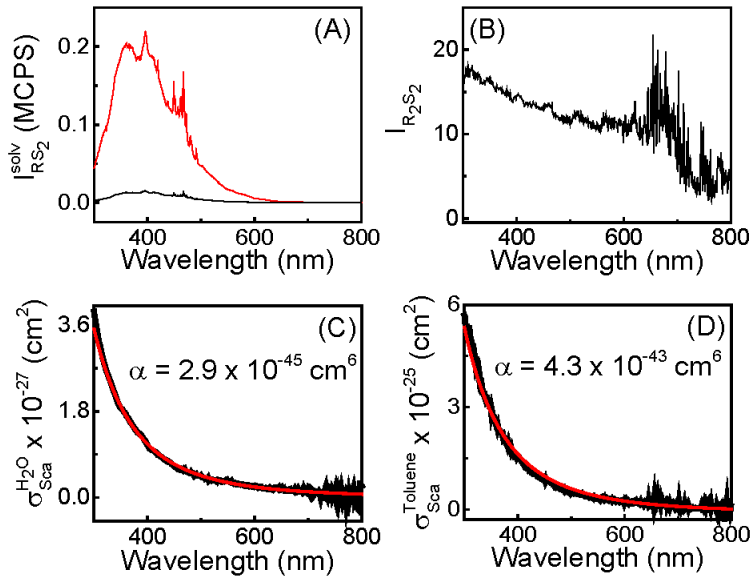

Figure 4.2 Determination of Rayleigh scattering cross-sections for toluene in the UV-vis wavelength region.

(A) Resonance synchronous spectra of water (black) and toluene (red). (B) R_2S_2 spectra of toluene. (C) Rayleigh scattering cross-sections of water determined with PSNPs. (D) Rayleigh scattering cross-sections of toluene calculated using Eq. 4.13.

4.5.2 NP photon absorber

Identifying model NPs that can be approximated as pure photon absorbers with no detectable photon scattering and fluorescence activity is challenging. This is because essentially all NPs have drastically larger sizes than solvent molecules, thereby their Rayleigh scattering or resonance light scattering cross sections can be significant in comparison to that of the solvent molecules. Furthermore, many ultrasmall NPs are fluorescence active.[152-154] In this work, we used a molecular chromophore, $K_2Cr_2O_7$, to model NP pure photon absorbers (Figure 4.3).

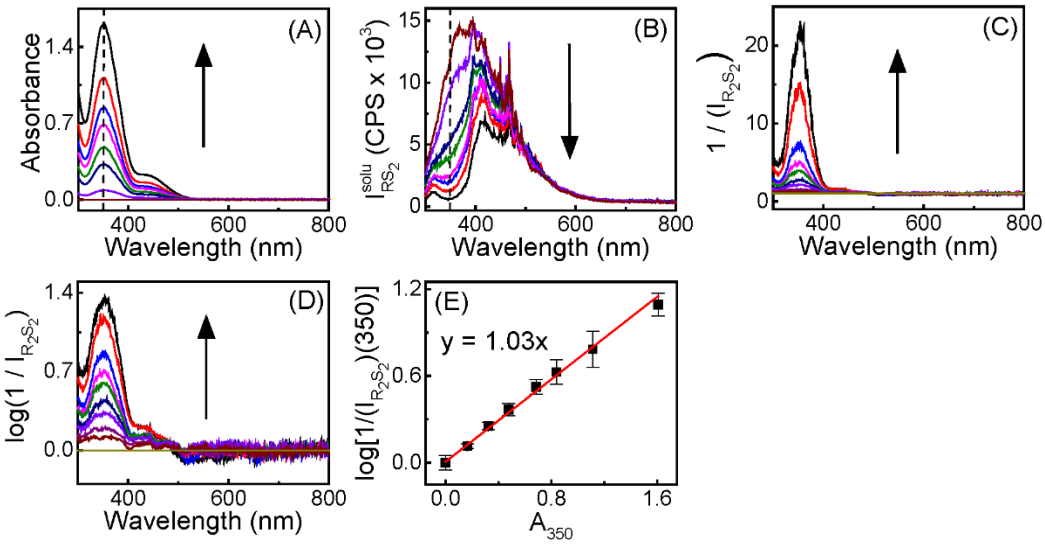

Figure 4.3 Determination of the R_2S_2 effective path length using $K_2Cr_2O_7$.

Notes: (A) UV−vis spectra, (B) RS_2 spectra, (C) reciprocal of R_2S_2 spectra of the $K_2Cr_2O_7$ samples, and (D) logarithm of the peak intensity of R_2S_2 reciprocal spectrum at 350 nm, all as a function of $K_2Cr_2O_7$ concentration. Arrows indicate increasing $K_2Cr_2O_7$ concentration in the plots. (E) Curve-fitting of the logarithm of the R2S2 reciprocal spectrum as a function of absorbance at 350 nm. The black dots are experimental data, and the red line is obtained from the linear curve- fitting of the experimental data with Eq. 4.7. The slope of the linear curve is the effective path length of the spectrofluorometer as shown in Eq. 4.7.

In sharp contrast to what has been observed with the PSNP photon scatterer in which the R_2S_2 intensity linearly increases with increasing PSNP concentration, the peak intensity of the reciprocal $K_2Cr_2O_7$ R_2S_2 spectra increases with increasing $K_2Cr_2O_7$ concentration (Figure 4.3). In other words, the R_2S_2 spectral intensity at the wavelength region where the $K_2Cr_2O_7$ absorbs decreases with increasing chromophore concentration. This is due to the sample IFE induced by $K_2Cr_2O_7$ photon absorption of incident and scattered photons. The logarithm of the reciprocal R_2S_2 peak intensity is linearly dependent on the chromophore UV−vis absorbance (Figure 4.3) as predicated with Eq.

4.7. The slope of this linearly fitted curve is 1.0 ± 0.2, which is the effective path length of the spectrofluorometer in R_2S_2 spectral acquisition.

4.5.3 NPs that are both photon scatterers and absorbers

The NP concentration dependence of the R_2S_2 spectra of AuNPs (Figure 4.4) that are simultaneous photon absorbers and scatterers is drastically more complicated than that for NP photon scatterers (Figure 4.1) or absorbers alone (Figure 4.3). For AuNPs of all three different sizes, neither R_2S_2 peak intensities nor their logarithm is linearly dependent on the NP concentration (Figure 4.4). Moreover, the R_2S_2 peak wavelength position varies with different NP concentrations. Both observations are due to the complex interplay of photon absorption and scattering. Such an interplay is prominent even when the sample optical density is as low as 0.5.

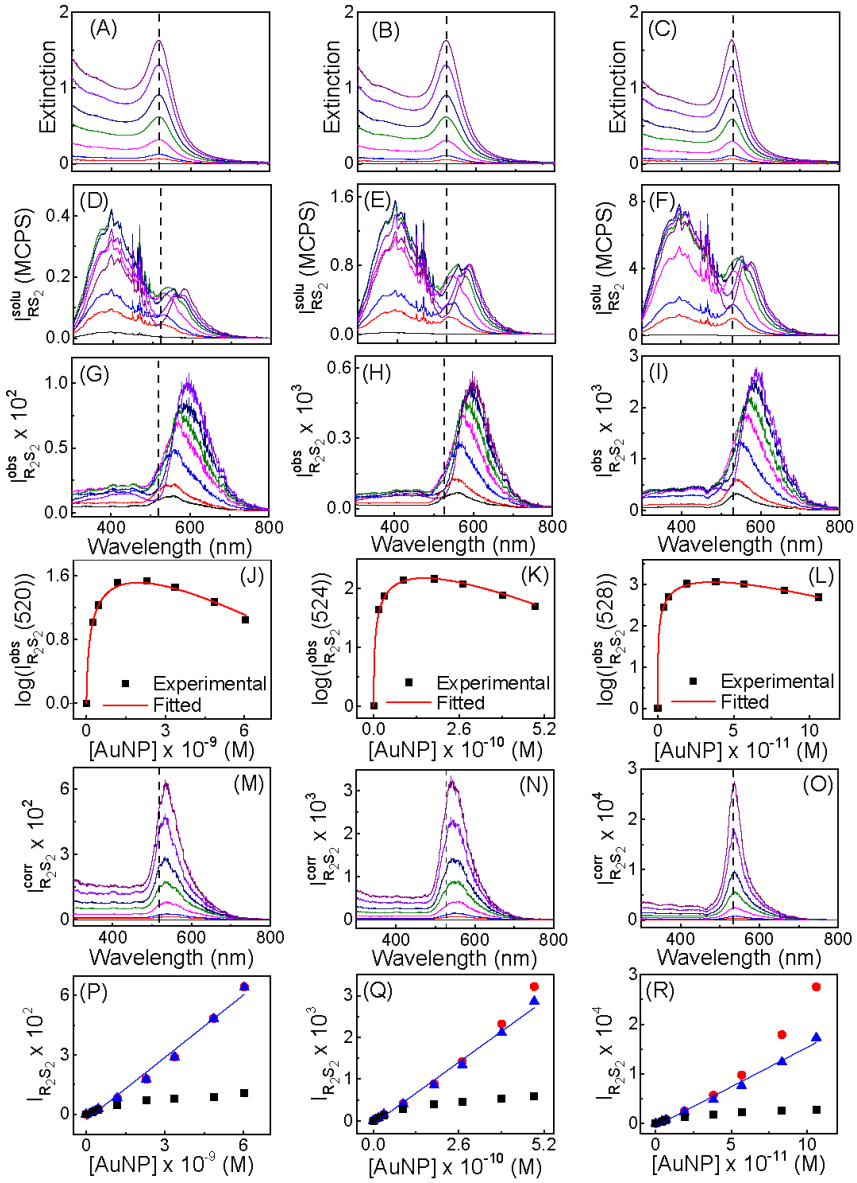

Figure 4.4 UV-vis and R_2S_2 characterization of 10, 30, and 50 nm AuNPs.

Notes: The data in the first, second, and third columns are for AuNPs with nominal diameters of 10, 30, and 50 nm, respectively. The data in the first to the fifth rows are UV-vis extinction spectra, as-acquired RS_2 spectra, experimental R_2S_2 spectra, concentration dependence of logarithm R_2S_2 intensity at the specified wavelength, the IFE-corrected R_2S_2 spectra obtained with Eq. 4.5a, and the correlation between the R_2S_2 peak intensity and AuNP concentration. The black dots represent the peak intensity without IFE-correction. The red dots are IFE-corrected R_2S_2 peak intensity in which only the UV-vis extinction is used for the IFE correction, while the blue dots are corrected with the AuNP absorbance only intensity. The vertical dash lines are for guiding the reader's view.

Since the model AuNPs do not have fluorescence activities ($\sigma_{OFE}^{NP}(\lambda) = 0$), one can determine the AuNP extinction, absorption, and scattering cross sections using a combination of the AuNP extinction spectra and R_2S_2 spectra as depicted with Eq. 4.3. The experimental UV−vis extinction cross section was determined with the AuNP UV−vis spectra, while the η(λ) derived from the curve-fitting (Figure 4.4) enables us to decompose the extinction cross section to absorption and scattering cross sections. The excellent agreement between the experimental R_2S_2 intensities and their corresponding curve- fitting data for the AuNPs of all three different sizes provides a critical validation of Eq. 4.3 for experimental decoupling of the NP UV−vis absorption and scattering contribution to the UV−vis and R_2S_2 spectra. Further validation of this method comes from the fact that the experimental extinction, absorption, and scattering cross sections deduced from the experimental η(λ) and the UV−vis extinction spectra are in excellent agreement with their counterparts computed for all AuNPs (Figure 4.5).

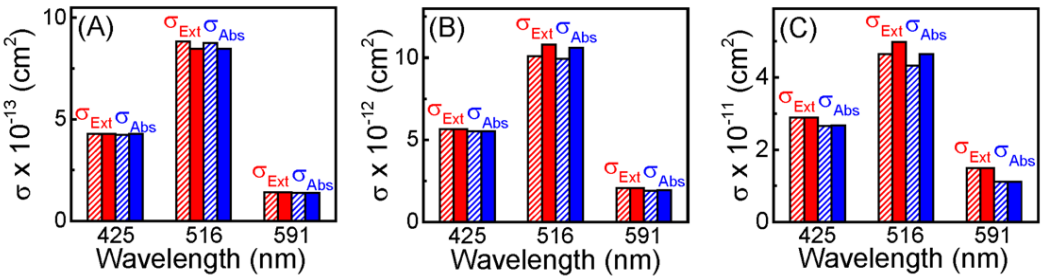

Figure 4.5 Comparison of experimental and computational extinction, absorption, and scattering cross-sections for all AuNPs at three different wavelengths.

Notes: (A), (B), and (C). Comparison of the experimental and computationally simulated cross-sections at the specified excitation wavelengths for the 10 nm, 30 nm, and 50 nm AuNPs, respectively. The solid and textured bars are theoretical and experimental cross-sections, respectively.

The IFE-corrected R_2S_2 signal intensity is nearly perfectly linearly related to the AuNP concentration when the AuNP absorbance ($\eta(\lambda)E(\lambda)$) is used for the IFE-correction in Eq. 4.5a (Figure 4.4 (P−R)). However, a large deviation from the linear dependence of the IFE-corrected R_2S_2 intensity on AuNP concentration appears if the AuNP extinction is directly used for the IFE correction. This result confirms that it is the AuNP photon absorption, not the photon scattering, that is responsible for the deviation of linearity between R_2S_2 intensity versus NP concentration.

4.5.4 NP photon absorber, emitter, and scatterer

Used in combination with UV−vis, this R_2S_2 technique paves the way for experimental quantification of on-resonance fluorescence resonance cross sections and quantum yields for both molecular and NP fluorophores (Figure 4.6). On-resonance fluorescence refers to fluorophore emission in which the energy of the emitted photon is identical to that of the excitation photon. This is in contrast to the conventional Stokes-shifted fluorescence for which the emitted photon frequency is smaller than the excitation photon frequency. Despite tremendous interest in the synthesis, characterization, and application of fluorescent NPs such as fluorescent quantum dots and fluorescent metal clusters,[155-157] there is essentially no report on the quantitative measurement of NP on-resonance fluorescence.

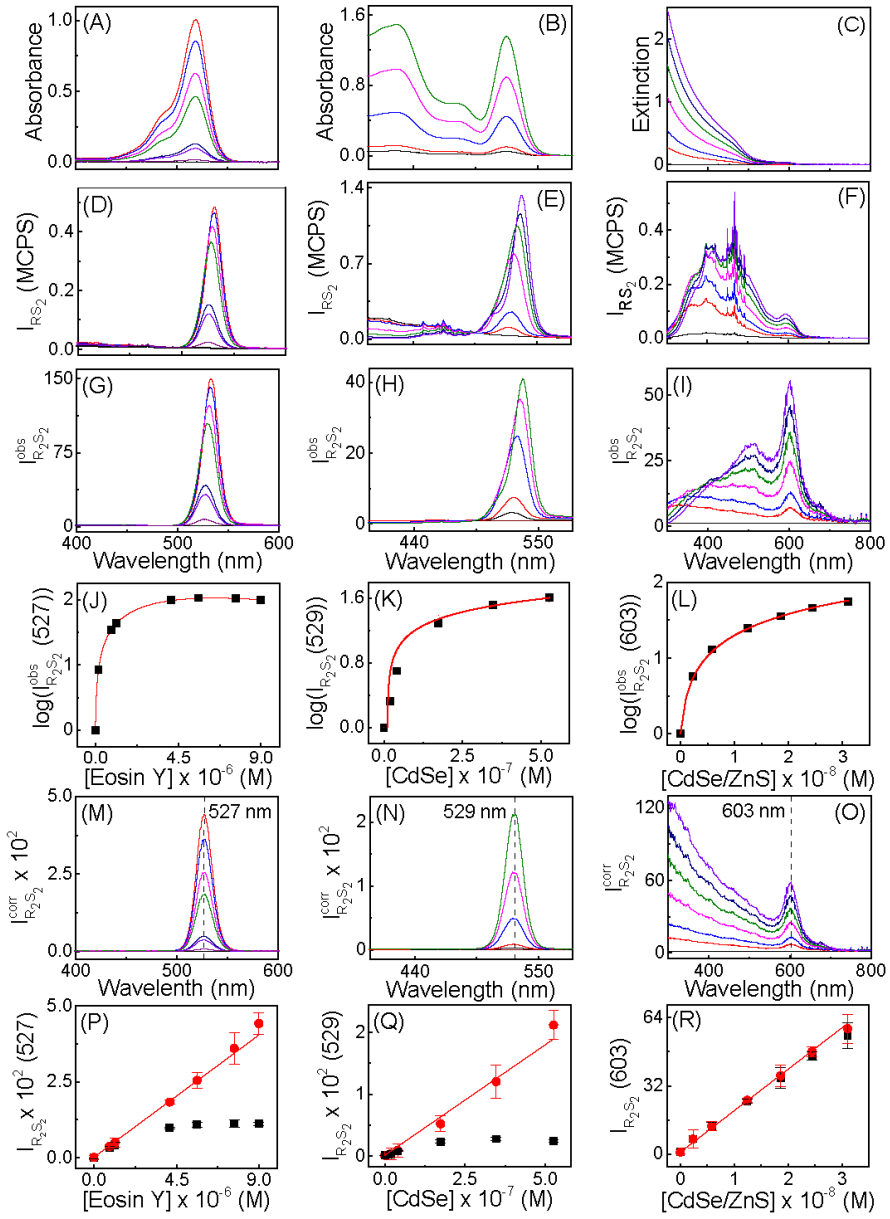

Figure 4.6 UV-vis and R_2S_2 characterization of molecular and NP fluorophores.

Notes: The data shown in the first, second, and third column are for Eosin Y, CdSe and CdSe/ZnS Qdots, respectively. (1st row) UV-vis, (2nd row) RS_2 spectra, (3rd row) as-acquired R_2S_2 spectra, (4rd row) experimental and curve-fitted correlation between the logarithm of R_2S_2 intensity and fluorophore concentration, (5th row) the IFE-corrected R_2S_2 spectra conducted with Eq. 4.5a. The dashed line corresponds to the peak wavelength. (6th row) The R_2S_2 peak intensity as a function of fluorophore concentration. The dots in black and red represents peak intensity of the R_2S_2 before and after the IFE correction.

The peak wavelength in the as-acquired R_2S_2 spectra in fluorophore-containing samples red-shifts as the fluorophore concentration increases. This is due to the interplay of fluorophore photon absorption, on-resonance fluorophore photon emission, and Rayleigh scattered light. However, the IFE-corrected R_2S_2 peak intensities are linearly dependent on the fluorophore concentration, and their peak position is totally independent of the fluorophore concentration for all samples. The IFE-corrected R_2S_2 peak wavelengths are 527, 529, and 603 nm for Eosin Y, CdSe, and CdSe/ZnS Qdots, respectively. This IFE correction was conducted with Eq. 4.5a in which $\eta(\lambda)$ was set to be 1 for all samples in Figure 4.6 on the assumption that their extinction spectra are dominated by fluorophore photon absorption with no significant photon scattering. The assumption is justified on the basis of the computational simulation that shows that peak scattering cross sections are 6, 5, and 3 orders of magnitude smaller than their respective peak absorption cross sections for Eosin Y, CdSe, and CdSe/ZnS Qdots, respectively (Figure 4.7). The excellent linearity between the corrected R_2S_2 peak intensity and the fluorophore concentration provides a critical validation to this assumption. Otherwise, the R_2S_2 intensity will be overcorrected as that has been observed by setting $\eta(\lambda)$ to 1 for the AuNP samples.

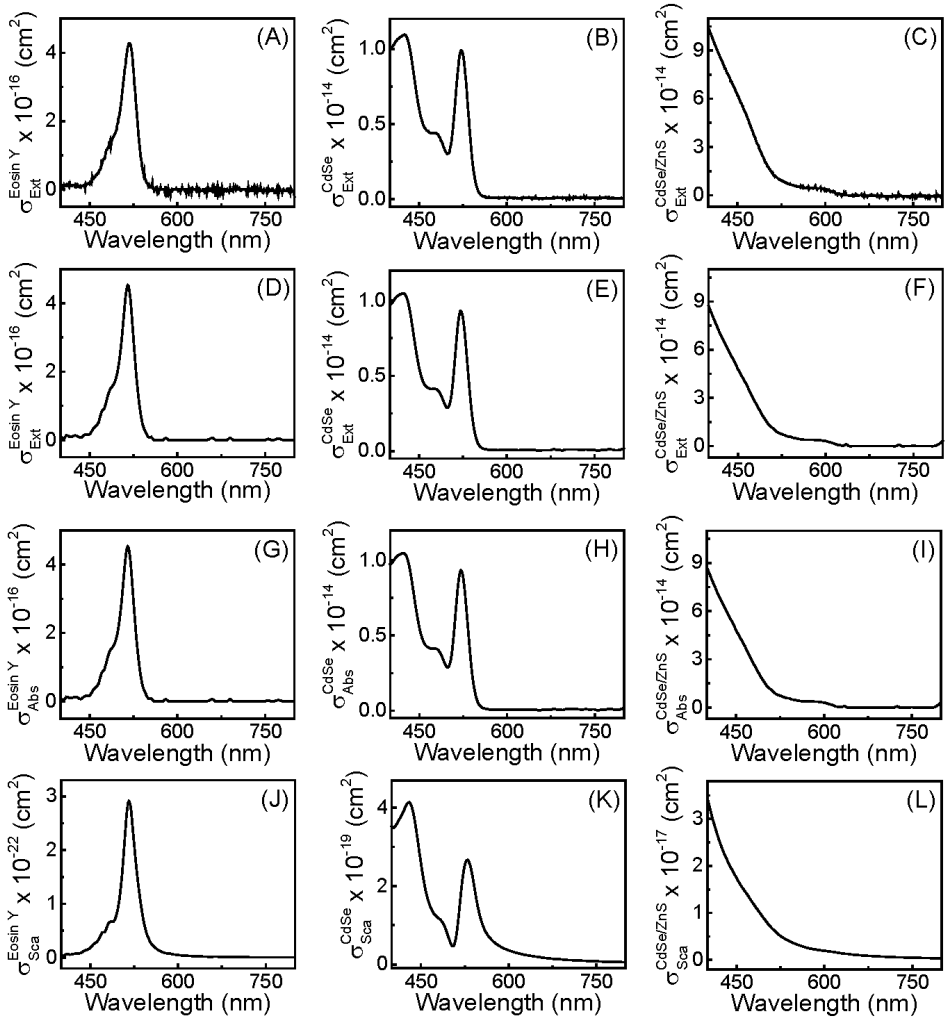

Figure 4.7 Computed extinction, absorbance, and scattering cross-sections for Eosin Y, CdSe, and CdSe/ZnS Qdots.

Notes: (1st row) Experimental and (2nd row) computed extinction cross-sections, (3rd row) computed absorption cross-section, (4th row) computed scattering cross-sections for (1st column) Eosin Y, (2nd column) CdSe Qdots, and (3rd column) CdSe/ZnS Qdots.

The sum of the fluorophore Rayleigh scattering cross sections and on-resonance fluorescence cross sections are 8.8×10^{-19}, 12.1×10^{-19}, and 260×10^{-19} cm^2 for Eosin Y, CdSe, and CdSe/ZnS Qdots, respectively, all at their respective peak R_2S_2 wavelengths. This is calculated with Eq. 4.14 derived from Eq. 4.5b. *m* in Eq. 4.14 is the slope of linear-fitted IFE-corrected R_2S_2 spectral intensity as a function of fluorophore

concentration (Figure 4.6). The solvent concentration is known, and its Rayleigh scattering cross sections over the UV−vis region can be independently determined. Therefore, this R_2S_2 technique enables the determination of the sum of the fluorophore Rayleigh and on-resonance fluorescence cross sections for the entire UV−vis region.

$$\sigma_{sca}^{NP}(\lambda) + \sigma_{OFE}^{NP}(\lambda) = m \times C_{Solv} \times \sigma_{sca}^{Solv}(\lambda) \tag{4.14}$$

In practical spectroscopic measurements of fluorophore-containing solutions, the R_2S_2 spectral signal can be dominated by the sample Rayleigh scattering or its fluorophore fluorescence or contributed simultaneously by these two optical processes. Eosin Y and CdSe Qdot R_2S_2 signals are due predominantly to fluorophore on-resonance emission with no significant fluorophore Rayleigh scattering contribution (Figure 4.8). However, both on-resonance emission and Rayleigh scattering contribute to the R_2S_2 signal in CdSe/ZnS-containing samples. This conclusion is drawn from the following experimental observation and theoretical consideration (Figure 4.8). The IFE-corrected R_2S_2 spectra of Eosin Y and CdSe overlap near perfectly with their respective multiplication product spectrum of the fluorophore absorption and emission spectra (Figure 4.8). This is consistent with the fact that on-resonance fluorescence occurs only in the wavelength region that the fluorophore both absorbs and emits. In contrast, the computed light scattering spectra show that light scattering occurs in almost the entire wavelength region where the fluorophore absorbs for both Eosin Y and CdSe Qdots (Figure 4.8 (J−L)).

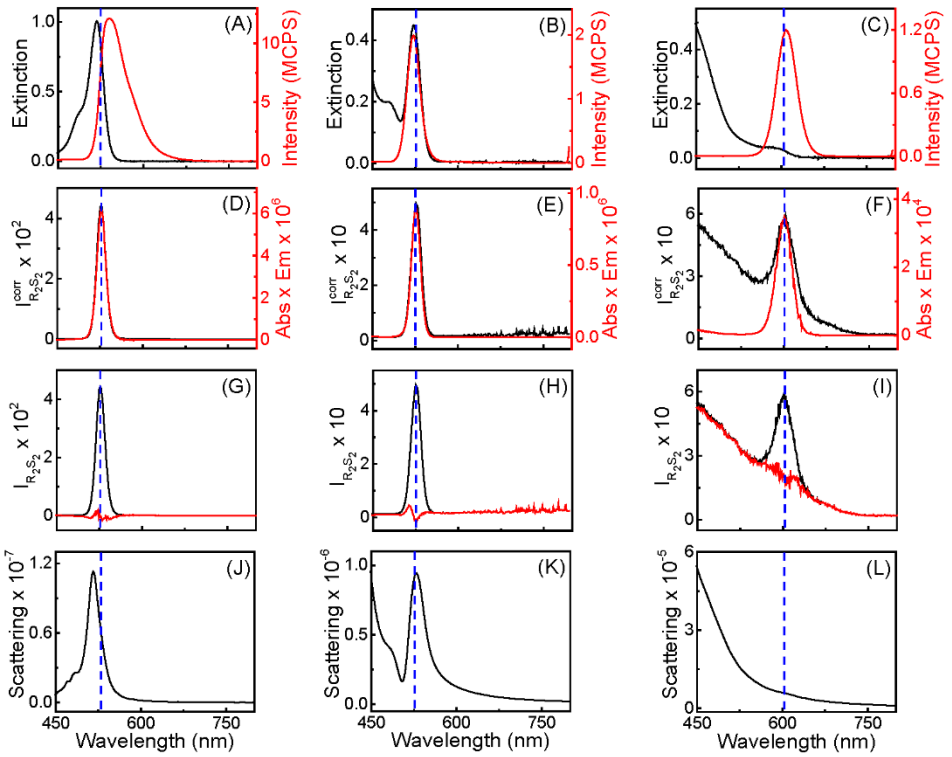

Figure 4.8 Experimental fluorophore absorbance, emission, and IFE-corrected R_2S_2 spectra compared to computational scattering spectra.

Notes: (1st column) Eosin Y, (2nd column) CdSe Qdots, and (3rd column) CdSe/ZnS Qdots. (A, B, and C) Fluorophore absorbance and emission spectra. (D, E, F) Comparison of the fluorophore IFE-corrected R_2S_2 spectra with their respective multiplication product spectrum of the absorbance and emission spectrum. (G, H, I) Difference spectrum between the two spectra shown in (D), (E), and (F), respectively. An arbitrary scaling factor was used for scaling the spectral intensity in order to facilitate comparison. (J, K, L) Computed resonance light scattering spectra of the fluorophores. The dashed lines are for guiding comparison of spectral peak positions. The fluorophore concentrations used in the experiment and simulation are 8.98 µM, 0.17 µM, and 31.0 nM for Eosin Y, CdSe Qdots, and CdSe/ZnS Qdots, respectively.

The data obtained with all three fluorophores in Figure 4.8 strongly indicate that one can use the multiplicative product spectrum of a fluorophore absorption and emission spectrum to approximate the fluorophore on-resonance spectrum. This provides a simple way to differentiate and decouple the on-resonance fluorescence from resonance light scattering (Figure 4.8). The determination of peak on-resonance fluorescence cross

sections for Eosin Y and CdSe Qdots is straightforward by considering the fact that their resonance light scattering is negligible compared to the R_2S_2 on-resonance fluorescence peak (Figure 4.8 (G, H)). Therefore, the sum of the fluorophore Rayleigh scattering cross section and on-resonance fluorescence cross section is directly assigned as the respective on-resonance fluorescence cross section (Table 4.1). Since CdSe/ZnS Qdots are simultaneous photon absorbers, scatterers, and emitters, their Rayleigh scattering and on-resonance emission cross section can be quantified only after decomposing its R_2S_2 spectra as shown in Figure 4.8 (I).

Table 4.1 Fluorophore on-Resonance Fluorescence Cross Section and Quantum Yield

Fluorophores	Peak R_2S_2 wavelength (nm)	Absorption cross-section $\times 10^{-16}$ cm^2	On-resonance emission cross-section $\times 10^{-19}$ cm^2	On-resonance fluorescence quantum yield $\times 10^{-3}$
Eosin Y	527	1.35	8.80 ± 0.26	6.51 ± 0.19
CdSe	529	3.93	12.1 ± 0.9	3.07 ± 0.24
CdSe/ZnS	603	16.1	260 ± 21	16.2 ± 1.3

The data shown in Table 4.1 is to our knowledge the first report of the on-resonance fluorescence cross sections and the on-resonance fluorescence quantum yields for any molecular and NP fluorophores. The on-resonance fluorescence quantum yield is defined as the ratio between the fluorophore on-resonance fluorescence cross section and its UV−vis absorption cross section at the specific wavelengths. Evidently, for all the NP and molecular fluorophores studied in this work, their maximum on-resonance fluorescence quantum yield is significantly lower than their respective conventional Stokes-shifted fluorescence quantum yields (all larger than 0.3).[158-160] This can be due to the difference of how the on-resonance fluorescence and Stokes-shifted fluorescence

quantum yields are defined and quantified. The on-resonance fluorescence quantum yield counts only the emitted photons that have a wavelength identical to that of the excitation photons. Any photons emitted by molecules that undergo internal conversion are excluded in the on-resonance fluorescence quantum yield calculation. In contrast, all emitted photons with wavelengths longer than the excitation wavelength were included in determining the Stokes-shifted fluorescence quantum yield.[161]

4.6 Conclusions

The presented UV−vis R_2S_2 spectroscopic technique is an extremely versatile method for experimental determination of the optical activity of molecular and NP chromophores and fluorophores. Used in combination with the UV−vis spectroscopic method, this R_2S_2 method has enabled quantification of the absolute optical cross sections for a wide range of molecules and NPs that include the Rayleigh scattering cross sections of various solvents, absorption and resonance light scattering cross sections for plasmonic AuNPs, and the additional on-resonance fluorescence cross sections for molecular and NP fluorophores. The reagents range optically from pure photon scatterers to pure photon absorbers, simultaneous photon absorbers and scatterers, photon absorbers and emitters, and all the way to photon absorbers, scatterers, and emitters. The insight and methodology presented in this work should be of broad significance in physical, biological, and chemical research and analysis that involves photon/matter interactions.

REFERENCES

(1) Skoog, D. A.; Holler, F. J.; Crouch, S. R. *Principles of Instrumental Analysis, 6th Ed.* Belmont, CA, 2007.

(2) Grove, R. E.; Wu, F. Y.; Ezekiel, S. *Phys. Rev. A* **1977**, *15*, 227.

(3) Haake, F.; Haus, J. W.; Rzążewski, K. *Zeitschrift für Physik B Condensed Matter* **1982**, *48*, 175.

(4) Mollow, B. R. *Phys. Rev. A* **1972**, *5*, 2217.

(5) Pasternack, R.; Collings, P. *Science* **1995**, *269*, 935.

(6) Collings, P. J.; Gibbs, E. J.; Starr, T. E.; Vafek, O.; Yee, C.; Pomerance, L. A.; Pasternack, R. F. *J. Phys. Chem. B* **1999**, *103*, 8474.

(7) Pasternack, R. F.; Bustamante, C.; Collings, P. J.; Giannetto, A.; Gibbs, E. J. *J. Am. Chem. Soc.* **1993**, *115*, 5393.

(8) Micali, N.; Mallamace, F.; Castriciano, M.; Romeo, A.; Monsú Scolaro, L. *Anal. Chem.* **2001**, *73*, 4958.

(9) Nettles, C. B.; Zhou, Y.; Zou, S.; Zhang, D. *Anal. Chem.* **2016**, *88*, 2891.

(10) Giljohann, D. A.; Seferos, D. S.; Daniel, W. L.; Massich, M. D.; Patel, P. C.; Mirkin, C. A. *Angew. Chem. Int. Ed.* **2010**, *49*, 3280.

(11) Hayat, M. A. *Collodial gold: principles, methods, and applications*; Academic Press: San Diego, CA, 1989.

(12) Bohren, C. F.; Huffman, D. R. *Absorption and Scattering by Small Particles*; Wiley-Interscience: New York, 1983.

(13) Kelly, K. L.; Coronado, E.; Zhao, L. L.; Schatz, G. C. *J. Phys. Chem. B* **2003**, *107*, 668.

(14) Halas, N. J.; Lal, S.; Chang, W.-S.; Link, S.; Nordlander, P. *Chem. Rev.* **2011**, *111*, 3913.

(15) Jain, P. K.; Huang, X.; El-Sayed, I. H.; El-Sayed, M. A. *Acc. Chem. Res.* **2008**, *41*, 1578.

(16) Jain, P. K.; Lee, K. S.; El-Sayed, I. H.; El-Sayed, M. A. *J. Phys. Chem. B* **2006**, *110*, 7238.

(17) Lee, K.-S.; El-Sayed, M. A. *J. Phys. Chem. B* **2006**, *110*, 19220.

(18) Liu, B.-J.; Lin, K.-Q.; Hu, S.; Wang, X.; Lei, Z.-C.; Lin, H.-X.; Ren, B. *Anal. Chem.* **2015**, *87*, 1058.

(19) van de Hulst, H. C. *Light Scattering by Small Particles*; Dover Publications, 1981.

(20) Mie, G. *Ann. Phys.* **1908**, *330*, 377.

(21) Sun, D.; Tian, Y.; Zhang, Y.; Xu, Z.; Sfeir, M. Y.; Cotlet, M.; Gang, O. *ACS Nano* **2015**.

(22) Sorokin, A. V.; Zabolotskii, A. A.; Pereverzev, N. V.; Bespalova, I. I.; Yefimova, S. L.; Malyukin, Y. V.; Plekhanov, A. I. *J. Phys. Chem. C* **2015**, *119*, 2743.

(23) Schneider, G.; Decher, G.; Nerambourg, N.; Praho, R.; Werts, M. H. V.; Blanchard-Desce, M. *Nano Lett.* **2006**, *6*, 530.

(24) Contreras-Caceres, R.; Alonso-Cristobal, P.; Mendez-Gonzalez, D.; Laurenti, M.; Maldonado-Valdivia, A.; Garcia-Blanco, F.; López Cabarcos, E.; Fernandez-Barbero, A.; Lopez-Romero, J. M.; Rubio-Retama, J. *Langmuir* **2014**, *30*, 15560.

(25) Anger, P.; Bharadwaj, P.; Novotny, L. *Phys. Rev. Lett.* **2006**, *96*, 113002.

(26) Song, J.-H.; Atay, T.; Shi, S.; Urabe, H.; Nurmikko, A. V. *Nano Lett.* **2005**, *5*, 1557.

(27) Fraiji, L. K.; Hayes, D. M.; Werner, T. C. *J. Chem. Ed.* **1992**, *69*, 424.

(28) Clapp, A. R.; Medintz, I. L.; Mattoussi, H. *ChemPhysChem* **2006**, *7*, 47.

(29) Lakowicz, J. R.; Shen, Y.; D'Auria, S.; Malicka, J.; Fang, J.; Gryczynski, Z.; Gryczynski, I. *Anal. Biochem.* **2002**, *301*, 261.

(30) Shaikh, A. J.; Rabbani, F.; Sherazi, T. A.; Iqbal, Z.; Mir, S.; Shahzad, S. A. *J. Phys. Chem. A* **2015**, *119*, 1108.

(31) Ang, Y. S.; Yung, L. Y. L. *Nanoscale* **2014**, *6*, 12515.

(32) Han, H.; Valle, V.; Maye, M. M. *J. Phys. Chem. C* **2012**, *116*, 22996.

(33) Zhang, D.; Nettles, C. B. *J. Phys. Chem. C* **2015**, *119*, 7941.

(34) Shang, L.; Jin, L.; Dong, S. *Chem. Comm.* **2009**, 3077.

(35) Ameer, F. S.; Ansar, S. M.; Hu, W.; Zou, S.; Zhang, D. *Anal. Chem.* **2012**, *84*, 8437.

(36) Ameer, F. S.; Hu, W.; Ansar, S. M.; Siriwardana, K.; Collier, W. E.; Zou, S.; Zhang, D. *J. Phys. Chem. C* **2013**, *117*, 3483.

(37) Brandt, R.; Olsen, M. J.; Cheronis, N. D. *Science* **1963**, *139*, 1063.

(38) Janin, J. *Proteins: Struct., Funct., Bioinf.* **1997**, *28*, 153.

(39) Sen, T.; Mandal, S.; Haldar, S.; Chattopadhyay, K.; Patra, A. *J. Phys. Chem. C* **2011**, *115*, 24037.

(40) Tsai, D.-H.; DelRio, F. W.; Keene, A. M.; Tyner, K. M.; MacCuspie, R. I.; Cho, T. J.; Zachariah, M. R.; Hackley, V. A. *Langmuir* **2011**, *27*, 2464.

(41) Yang, J. A.; Johnson, B. J.; Wu, S.; Woods, W. S.; George, J. M.; Murphy, C. J. *Langmuir* **2013**, *29*, 4603.

(42) Zheng, M.; Xie, Z.; Qu, D.; Li, D.; Du, P.; Jing, X.; Sun, Z. *ACS Appl. Mater. Interfaces* **2013**, *5*, 13242.

(43) Albinsson, B. *J. Am. Chem. Soc.* **1997**, *119*, 6369.

(44) Lakowicz, J. R. *Principles of Fluorescence Spectroscopy*; Kluwer Academic/Plenum Publishers: Dordrecht, The Netherlands, 2004.

(45) Niranjan, Y.; Ungureanu, D.; Hammarén, H.; Sanz-Sanz, A.; Westphal, A. H.; Borst, J. W.; Silvennoinen, O.; Hilhorst, R. *Anal. Biochem.* **2013**, *442*, 213.

(46) Parker, C. A. *Photoluminescence of Solutions*; Elsevier Publishing Company: Amsterdam, 1968.

(47) Svanvik, N.; Nygren, J.; Westman, G.; Kubista, M. *J. Am. Chem. Soc.* **2001**, *123*, 803.

(48) Christmann, D. R.; Crouch, S. R.; Holland, J. F.; Timnick, A. *Anal. Chem.* **1980**, *52*, 291.

(49) Fanget, B.; Devos, O.; Draye, M. *Anal. Chem.* **2003**, *75*, 2790.

(50) Holland, J. F.; Teets, R. E.; Kelly, P. M.; Timnick, A. *Anal. Chem.* **1977**, *49*, 706.

(51) Leese, R. A.; Wehry, E. L. *Anal. Chem.* **1978**, *50*, 1193.

(52) Lutz, H.-P.; Luisi, P. L. *Helv. Chim. Acta.* **1983**, *66*, 1929.

(53) Mendonça, A.; Rocha, A. C.; Duarte, A. C.; Santos, E. B. H. *Anal. Chim. Acta* **2013**, *788*, 99.

(54) Nettles, C. B.; Hu, J.; Zhang, D. *Anal. Chem.* **2015**, *87*, 4917.

(55) Ohno, T. *Environ. Sci. Technol.* **2002**, *36*, 742.

(56) Zhang, C.; Liu, M. S.; Han, B.; Xing, X.-H. *Anal. Biochem.* **2009**, *390*, 197.

(57) Devi, L. B.; Das, S. K.; Mandal, A. B. *J. Phys. Chem. C* **2014**, *118*, 29739.

(58) Zhai, W.; Wang, C.; Yu, P.; Wang, Y.; Mao, L. *Anal. Chem.* **2014**, *86*, 12206.

(59) Li, J.; Li, X.; Shi, X.; He, X.; Wei, W.; Ma, N.; Chen, H. *ACS Appl. Mater. Interfaces* **2013**, *5*, 9798.

(60) Abadeer, N. S.; Brennan, M. R.; Wilson, W. L.; Murphy, C. J. *ACS Nano* **2014**, *8*, 8392.

(61) Hogan, N. J.; Urban, A. S.; Ayala-Orozco, C.; Pimpinelli, A.; Nordlander, P.; Halas, N. J. *Nano Lett.* **2014**, *14*, 4640.

(62) Tseng, W.-H.; Chiu, C.-Y.; Chou, S.-W.; Chen, H.-C.; Tsai, M.-L.; Kuo, Y.-C.; Lien, D.-H.; Tsao, Y.-C.; Huang, K.-Y.; Yeh, C.-T.; He, J.-H.; Wu, C.-I.; Huang, M. H.; Chou, P.-T. *J. Phys. Chem. C* **2015**, *119*, 7554.

(63) Atwater, H. A.; Polman, A. *Nat Mater* **2010**, *9*, 205.

(64) van Dijk, M. A.; Tchebotareva, A. L.; Orrit, M.; Lippitz, M.; Berciaud, S.; al., e. *Phys. Chem. Chem. Phys.* **2006**, *8*, 3486.

(65) Xiao, M.; Chen, H.; Ming, T.; Shao, L.; Wang, J. *ACS Nano* **2010**, *4*, 6565.

(66) Bergman, D. J.; Stockman, M. I. *Phys. Rev. Lett.* **2003**, *90*, 027402.

(67) Eastham, D. A. *Atomic Physics of Lasers*; Taylor & Francis Inc.: Philadelphia, PA, 1986.

(68) Müller, M. G.; Georgakoudi, I.; Zhang, Q.; Wu, J.; Feld, M. S. *Appl. Opt.* **2001**, *40*, 4633.

(69) Brewer, S. H.; Glomm, W. R.; Johnson, M. C.; Knag, M. K.; Franzen, S. *Langmuir* **2005**, *21*, 9303.

(70) Goy-López, S.; Juárez, J.; Alatorre-Meda, M.; Casals, E.; Puntes, V. F.; Taboada, P.; Mosquera, V. *Langmuir* **2012**, *28*, 9113.

(71) Iosin, M.; Canpean, V.; Astilean, S. *J. Photochem. Photobiol. A* **2011**, *217*, 395.

(72) Lacerda, S. H. D. P.; Park, J. J.; Meuse, C.; Pristinski, D.; Becker, M. L.; Karim, A.; Douglas, J. F. *ACS Nano* **2009**, *4*, 365.

(73) Saraswat, S.; Desireddy, A.; Zheng, D.; Guo, L.; Lu, H. P.; Bigioni, T. P.; Isailovic, D. *J. Phys. Chem. C* **2011**, *115*, 17587.

(74) Shang, L.; Wang, Y.; Jiang, J.; Dong, S. *Langmuir* **2007**, *23*, 2714.

(75) Yang, W.; Sun, L.; Weng, J.; Chen, L.; Zhang, Q. *IET Nanobiotechnol* **2012**, *6*, 26.

(76) Boulos, S. P.; Davis, T. A.; Yang, J. A.; Lohse, S. E.; Alkilany, A. M.; Holland, L. A.; Murphy, C. J. *Langmuir* **2013**, *29*, 14984.

(77) Cañaveras, F. M., R.; Sevilla, J. M.; Blázquez, M.; Pineda, T. *J. Phys. Chem. C* **2012**, *116*.

(78) Chakraborty, S.; Joshi, P.; Shanker, V.; Ansari, Z. A.; Singh, S. P.; Chakrabarti, P. *Langmuir* **2011**, *27*, 7722.

(79) Huang, R.; Carney, R. P.; Ikuma, K.; Stellacci, F.; Lau, B. L. T. *ACS Nano* **2014**, *8*, 5402.

(80) Roy, S.; Das, T. K. *J. Nanosci. Nanotechnol.* **2014**, *14*, 4899.

(81) Sen, T.; Haldar, K. K.; Patra, A. *J. Phys. Chem. C* **2008**, *112*, 17945.

(82) Zhong, R.; Liu, Y.; Zhang, P.; Liu, J.; Zhao, G.; Zhang, F. *ACS Appl. Mater. Interfaces* **2014**, *6*, 19465.

(83) Calzolai, L.; Franchini, F.; Gilliland, D.; Rossi, F. o. *Nano Lett.* **2010**, *10*, 3101.

(84) Casals, E.; Pfaller, T.; Duschl, A.; Oostingh, G. J.; Puntes, V. *ACS Nano* **2010**, *4*, 3623.

(85) Deka, J.; Paul, A.; Chattopadhyay, A. *J. Phys. Chem. C* **2009**, *113*, 6936.

(86) Gagner, J. E.; Qian, X.; Lopez, M. M.; Dordick, J. S.; Siegel, R. W. *Biomater.* **2012**, *33*, 8503.

(87) Royer, C. A. *Chem. Rev.* **2006**, *106*, 1769.

(88) Alberty, R. A.; Hammes, G. G. *J. Phys. Chem.* **1958**, *62*, 154.

(89) Cárdenas, B.; Sánchez-Obrero, G.; Madueño, R.; Sevilla, J. M.; Blázquez, M.; Pineda, T. *J. Phys. Chem. C* **2014**, *118*, 22274.

(90) Dulkeith, E.; Morteani, A. C.; Niedereichholz, T.; Klar, T. A.; Feldmann, J.; Levi, S. A.; van Veggel, F. C. J. M.; Reinhoudt, D. N.; Möller, M.; Gittins, D. I. *Phys. Rev. Lett.* **2002**, *89*, 203002.

(91) Dulkeith, E.; Ringler, M.; Klar, T. A.; Feldmann, J.; Muñoz Javier, A.; Parak, W. J. *Nano Lett.* **2005**, *5*, 585.

(92) Hernández, F. E.; Yu, S.; García, M.; Campiglia, A. D. *J. Phys. Chem. B* **2005**, *109*, 9499.

(93) Kühn, S.; Håkanson, U.; Rogobete, L.; Sandoghdar, V. *Phys. Rev. Lett.* **2006**, *97*, 017402.

(94) Lakowicz, J. R. *Anal. Biochem.* **2005**, *337*, 171.

(95) Muskens, O. L.; Giannini, V.; Sánchez-Gil, J. A.; Gómez Rivas, J. *Nano Lett.* **2007**, *7*, 2871.

(96) Reed, A. M. W.; Metallo, S. J. *Langmuir* **2010**, *26*, 18945.

(97) Schmelzeisen, M.; Zhao, Y.; Klapper, M.; Müllen, K.; Kreiter, M. *ACS Nano* **2010**, *4*, 3309.

(98) Du, J.; Jin, J.; Liu, Y.; Li, J.; Tokatlian, T.; Lu, Z.; Segura, T.; Yuan, X.-b.; Yang, X.; Lu, Y. *ACS Nano* **2014**, *8*, 9964.

(99) Freeman, R. G.; Hommer, M. B.; Grabar, K. C.; Jackson, M. A.; Natan, M. J. *J. Phys. Chem.* **1996**, *100*, 718.

(100) Zhang, D.; Ansar, S. M. *Anal. Chem.* **2010**, *82*, 5910.

(101) Phillips, S. L. *Anal. Chem.* **1966**, *38*, 1714.

(102) Qin, W.; Shah, R. A.; Guyot-Sionnest, P. *ACS Nano* **2011**, *6*, 912.

(103) Gabor, G.; Walt, D. R. *Anal. Chem.* **1991**, *63*, 793.

(104) Gil, D. B.; de la Peña, A. M.; Arancibia, J. A.; Escandar, G. M.; Olivieri, A. C. *Anal. Chem.* **2006**, *78*, 8051.

(105) Gu, Q.; Kenny, J. E. *Anal. Chem.* **2008**, *81*, 420.

(106) Fonin, A. V.; Sulatskaya. A. I.; Kuznetsova, I. M.; Turoverov, K. K. *PLoS ONE* **2014**, *9*, e103878.

(107) Larsson, T. W., M.; Turner, D. *Anal. Chim. Acta* **2007**, *583*, 357.

(108) Luciani, X.; Mounier, S.; Redon, R.; Bois, A. *Chemometr. Intell. Lab.* **2009**, *96*.

(109) MacDonald, B. C. L., S. J.; Patterson, H. *Anal. Chim. Acta* **1997**, *338*.

(110) Palmier, M. O.; Van Doren, S. R. *Anal. Biochem.* **2007**, *371*, 43.

(111) Victor, M. A. C., S. R. *Appl. Spectrosc.* **1995**, *49*.

(112) Atrahimovich, D.; Vaya, J.; Tavori, H.; Khatib, S. *J. Agric. Food Chem.* **2012**, *60*, 3679.

(113) Ding, F.; Diao, J.-X.; Sun, Y.; Sun, Y. *J. Agric. Food Chem.* **2012**, *60*, 7218.

(114) Abe, R.; Ohashi, H.; Iijima, I.; Ihara, M.; Takagi, H.; Hohsaka, T.; Ueda, H. *J. Am. Chem. Soc.* **2011**, *133*, 17386.

(115) Bai, D.-R.; Wang, S. *Organometallics* **2006**, *25*, 1517.

(116) Cao, X.; Meng, L.; Li, Z.; Mao, Y.; Lan, H.; Chen, L.; Fan, Y.; Yi, T. *Langmuir* **2014**, *30*, 11753.

(117) Lindenburg, L. H.; Malisauskas, M.; Sips, T.; van Oppen, L.; Wijnands, S. P. W.; van de Graaf, S. F. J.; Merkx, M. *Biochem.* **2014**, *53*, 6370.

(118) Wang, G.; Chang, X.; Peng, J.; Liu, K.; Zhao, K.; Yu, C.; Fang, Y. *Phys. Chem. Chem. Phys.* **2015**, *17*, 5441.

(119) Cabrerizo, F. M.; Arnbjerg, J.; Denofrio, M. P.; Erra-Balsells, R.; Ogilby, P. R. *ChemPhysChem* **2010**, *11*, 796.

(120) Kumar, A.; Gupta, R. D.; Gupta, T. *RSC Adv.* **2013**, *3*, 390.

(121) Lawaetz, A. J.; Stedmon, C. A. *Appl. Spectrosc.* **2009**, *63*, 936.

(122) Loethen, Y. L. K., G. M.; Davis, B.; Gudihal, R.; Davisson, V. J.; Ben-Amotz, D. *J. Proteome Res.* **2007**, *7*, 1371.

(123) Sivaprakasam, V.; Killinger, D. K. *J. Opt. Soc. Am. B* **2003**, *20*, 1980.

(124) Xu, C.; Shear, J. B.; Webb, W. W. *Anal. Chem.* **1997**, *69*, 1285.

(125) Linic, S.; Aslam, U.; Boerigter, C.; Morabito, M. *Nat. Mater.* **2015**, *14*, 567.

(126) Liu, Y.; Tang, A.; Zhang, Q.; Yin, Y. *J. Am. Chem. Soc.* **2015**, *137*, 11327.

(127) Razgoniaeva, N.; Lambright, S.; Sharma, N.; Acharya, A.; Khon, E.; Moroz, P.; Razgoniaev, A.; Ostrowski, A.; Zamkov, M. *J. Phys. Chem. C* **2015**, *119*, 15562.

(128) Unlu, I.; Soares, J. W.; Steeves, D. M.; Whitten, J. E. *Langmuir* **2015**, *31*, 8718.

(129) Cherukuri, P.; Glazer, E. S.; Curley, S. A. *Adv. Drug Delivery Rev.* **2010**, *62*, 339.

(130) Dreaden, E. C.; Mackey, M. A.; Huang, X.; Kang, B.; El-Sayed, M. A. *Chem. Soc. Rev.* **2011**, *40*, 3391.

(131) O'Neal, D. P.; Hirsch, L. R.; Halas, N. J.; Payne, J. D.; West, J. L. *Cancer Lett. (Amsterdam, Neth.)* **2004**, *209*, 171.

(132) Chen, G.; Damasco, J.; Qiu, H.; Shao, W.; Ohulchanskyy, T. Y.; Valiev, R. R.; Wu, X.; Han, G.; Wang, Y.; Yang, C.; Agren, H.; Prasad, P. N. *Nano Lett.* **2015**, Ahead of Print.

(133) Dang, X.; Qi, J.; Klug, M. T.; Chen, P.-Y.; Yun, D. S.; Fang, N. X.; Hammond, P. T.; Belcher, A. M. *Nano Lett.* **2013**, *13*, 637.

(134) Hensel, J.; Wang, G.; Li, Y.; Zhang, J. Z. *Nano Lett.* **2010**, *10*, 478.

(135) Siefermann, K. R.; Pemmaraju, C. D.; Neppl, S.; Shavorskiy, A.; Cordones, A. A.; Vura-Weis, J.; Slaughter, D. S.; Sturm, F. P.; Weise, F.; Bluhm, H.; Strader, M. L.; Cho, H.; Lin, M.-F.; Bacellar, C.; Khurmi, C.; Guo, J.; Coslovich, G.; Robinson, J. S.; Kaindl, R. A.; Schoenlein, R. W.; Belkacem, A.; Neumark, D. M.; Leone, S. R.; Nordlund, D.; Ogasawara, H.; Krupin, O.; Turner, J. J.; Schlotter, W. F.; Holmes, M. R.; Messerschmidt, M.; Minitti, M. P.; Gul, S.; Zhang, J. Z.; Huse, N.; Prendergast, D.; Gessner, O. *J. Phys. Chem. Lett.* **2014**, *5*, 2753.

(136) He, L.; Wang, M.; Ge, J.; Yin, Y. *Acc. Chem. Res.* **2012**, *45*, 1431.

(137) Ota, S.; Wang, S.; Wang, Y.; Yin, X.; Zhang, X. *Nano Lett.* **2013**, *13*, 2766.

(138) Otelaja, O. O.; Ha, D.-H.; Ly, T.; Zhang, H.; Robinson, R. D. *ACS Appl. Mater. Interfaces* **2014**, *6*, 18911.

(139) Stamplecoskie, K. G.; Kamat, P. V. *J. Phys. Chem. Lett.* **2015**, *6*, 1870.

(140) Cunningham, J. C.; Kogan, M. R.; Tsai, Y.-J.; Luo, L.; Richards, I.; Crooks, R. M. *ACS Sens.* **2016**, *1*, 40.

(141) Inci, F.; Filippini, C.; Baday, M.; Ozen, M. O.; Calamak, S.; Durmus, N. G.; Wang, S. Q.; Hanhauser, E.; Hobbs, K. S.; Juillard, F.; Kuang, P. P.; Vetter, M. L.; Carocci, M.; Yamamoto, H. S.; Takagi, Y.; Yildiz, U. H.; Akin, D.; Wesemann, D. R.; Singhal, A.; Yang, P. L.; Nibert, M. L.; Fichorova, R. N.; Lau, D. T. Y.; Henrich, T. J.; Kaye, K. M.; Schachter, S. C.; Kuritzkes, D. R.; Steinmetz, L. M.; Gambhir, S. S.; Davis, R. W.; Demirci, U. *Proc. Natl. Acad. Sci. U. S. A.* **2015**, *112*, E4354.

(142) Jiang, Z.; Le, N. D. B.; Gupta, A.; Rotello, V. M. *Chem. Soc. Rev.* **2015**, *44*, 4264.

(143) Joshi, G. K.; Deitz-McElyea, S.; Liyanage, T.; Lawrence, K.; Mali, S.; Sardar, R.; Korc, M. *ACS Nano* **2015**, *9*, 11075.

(144) Rowland, C. E.; Susumu, K.; Stewart, M. H.; Oh, E.; Makinen, A. J.; O'Shaughnessy, T. J.; Kushto, G.; Wolak, M. A.; Erickson, J. S.; Efros, A. L.; Huston, A. L.; Delehanty, J. B. *Nano Lett.* **2015**, *15*, 6848.

(145) Lane, L. A.; Qian, X.; Nie, S. *Chem. Rev. (Washington, DC, U. S.)* **2015**, *115*, 10489.

(146) Paul, A. M.; Fan, Z.; Sinha, S. S.; Shi, Y.; Le, L.; Bai, F.; Ray, P. C. *J. Phys. Chem. C* **2015**, *119*, 23669.

(147) Petefish, J. W.; Hillier, A. C. *Anal. Chem. (Washington, DC, U. S.)* **2015**, *87*, 10862.

(148) Huang, C. Z.; Li, K. A.; Tong, S. Y. *Anal. Chem.* **1996**, *68*, 2259.

(149) Wu, L. P.; Li, Y. F.; Huang, C. Z.; Zhang, Q. *Anal. Chem.* **2006**, *78*, 5570.

(150) Cox, A. J.; DeWeerd, A. J.; Linden, J. *Am. J. Phys.* **2002**, *70*, 620.

(151) Watts, B. *Opt. Express* **2014**, *22*, 23629.

(152) Amani, M.; Lien, D.-H.; Kiriya, D.; Xiao, J.; Azcatl, A.; Noh, J.; Madhvapathy, S. R.; Addou, R.; KC, S.; Dubey, M.; Cho, K.; Wallace, R. M.; Lee, S.-C.; He, J.-H.; Ager, J. W.; Zhang, X.; Yablonovitch, E.; Javey, A. *Science* **2015**, *350*, 1065.

(153) Chen, H.; Lin, L.; Li, H.; Li, J.; Lin, J.-M. *ACS Nano* **2015**, *9*, 2173.

(154) Chen, K.; Chou, L. Y. T.; Song, F.; Chan, W. C. W. *Nano Today* **2013**, *8*, 228.

(155) Cadusch, J. J.; Panchenko, E.; Kirkwood, N.; James, T. D.; Gibson, B. C.; Webb, K. J.; Mulvaney, P.; Roberts, A. *Nanoscale* **2015**, *7*, 13816.

(156) Copp, S. M.; Schultz, D. E.; Swasey, S.; Gwinn, E. G. *ACS Nano* **2015**, *9*, 2303.

(157) Zagorovsky, K.; Chan, W. C. W. *Nat Mater* **2013**, *12*, 285.

(158) Gerion, D.; Pinaud, F.; Williams, S. C.; Parak, W. J.; Zanchet, D.; Weiss, S.; Alivisatos, A. P. *J. Phys. Chem. B* **2001**, *105*, 8861.

(159) Penzkofer, A.; Beidoun, A.; Daiber, M. *J. Lumin.* **1992**, *51*, 297.

(160) Willard, D. M.; Carillo, L. L.; Jung, J.; Van Orden, A. *Nano Lett.* **2001**, *1*, 469.

(161) Grabolle, M.; Spieles, M.; Lesnyak, V.; Gaponik, N.; Eychmüller, A.; Resch-Genger, U. *Anal, Chem.* **2009**, *81*, 6285.

APPENDIX A

COPYRIGHT PERMISSION

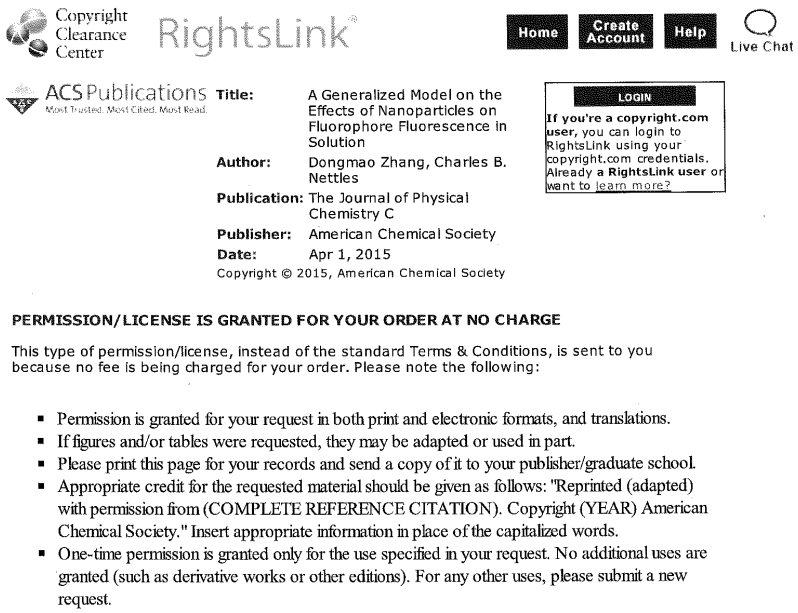

Copyright Clearance Center RightsLink®

Home | Create Account | Help | Live Chat

ACS Publications
Most Trusted. Most Cited. Most Read.

Title: A Generalized Model on the Effects of Nanoparticles on Fluorophore Fluorescence in Solution

Author: Dongmao Zhang, Charles B. Nettles

Publication: The Journal of Physical Chemistry C

Publisher: American Chemical Society

Date: Apr 1, 2015

Copyright © 2015, American Chemical Society

LOGIN

If you're a copyright.com user, you can login to RightsLink using your copyright.com credentials. Already a **RightsLink user** or want to learn more?

PERMISSION/LICENSE IS GRANTED FOR YOUR ORDER AT NO CHARGE

This type of permission/license, instead of the standard Terms & Conditions, is sent to you because no fee is being charged for your order. Please note the following:

- Permission is granted for your request in both print and electronic formats, and translations.
- If figures and/or tables were requested, they may be adapted or used in part.
- Please print this page for your records and send a copy of it to your publisher/graduate school.
- Appropriate credit for the requested material should be given as follows: "Reprinted (adapted) with permission from (COMPLETE REFERENCE CITATION). Copyright (YEAR) American Chemical Society." Insert appropriate information in place of the capitalized words.
- One-time permission is granted only for the use specified in your request. No additional uses are granted (such as derivative works or other editions). For any other uses, please submit a new request.

Figure A.1 Copyright permission form for Chapter II

Notes: The content covered in Chapter II contains material previously published by the American Chemical Society in The Journal of Physical Chemistry C. Content is referenced as Zhang, D.; Nettles, C. B., A Generalized Model on the Effects of Nanoparticles on Fluorophore Fluorescence in Solution. *J. Phys. Chem. C,* **2015**; *119*: 7941-7948

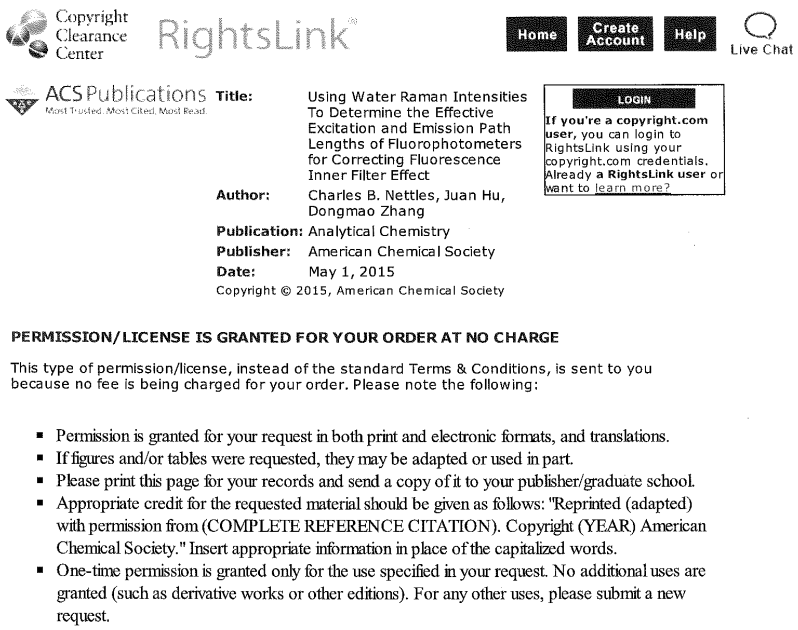

Copyright Clearance Center RightsLink

Home | Create Account | Help | Live Chat

ACS Publications
Most Trusted. Most Cited. Most Read.

Title: Using Water Raman Intensities To Determine the Effective Excitation and Emission Path Lengths of Fluorophotometers for Correcting Fluorescence Inner Filter Effect

Author: Charles B. Nettles, Juan Hu, Dongmao Zhang

Publication: Analytical Chemistry

Publisher: American Chemical Society

Date: May 1, 2015

Copyright © 2015, American Chemical Society

LOGIN

If you're a copyright.com user, you can login to RightsLink using your copyright.com credentials. Already a RightsLink user or want to learn more?

PERMISSION/LICENSE IS GRANTED FOR YOUR ORDER AT NO CHARGE

This type of permission/license, instead of the standard Terms & Conditions, is sent to you because no fee is being charged for your order. Please note the following:

- Permission is granted for your request in both print and electronic formats, and translations.
- If figures and/or tables were requested, they may be adapted or used in part.
- Please print this page for your records and send a copy of it to your publisher/graduate school.
- Appropriate credit for the requested material should be given as follows: "Reprinted (adapted) with permission from (COMPLETE REFERENCE CITATION). Copyright (YEAR) American Chemical Society." Insert appropriate information in place of the capitalized words.
- One-time permission is granted only for the use specified in your request. No additional uses are granted (such as derivative works or other editions). For any other uses, please submit a new request.

Figure A.2 Copyright permission form for Chapter III

Notes: The content covered in Chapter III contains material previously published by the American Chemical Society in Analytical Chemistry. Content is referenced as Nettles, C. B.; Hu, J.; Zhang, D., Using Water Raman Intensities to Determine the Effective Excitation and Emission Path Lengths of Fluorophotometers for Correcting Fluorescence Inner Filter Effect. *Anal. Chem.,* **2015**; *87*: 4917-4924

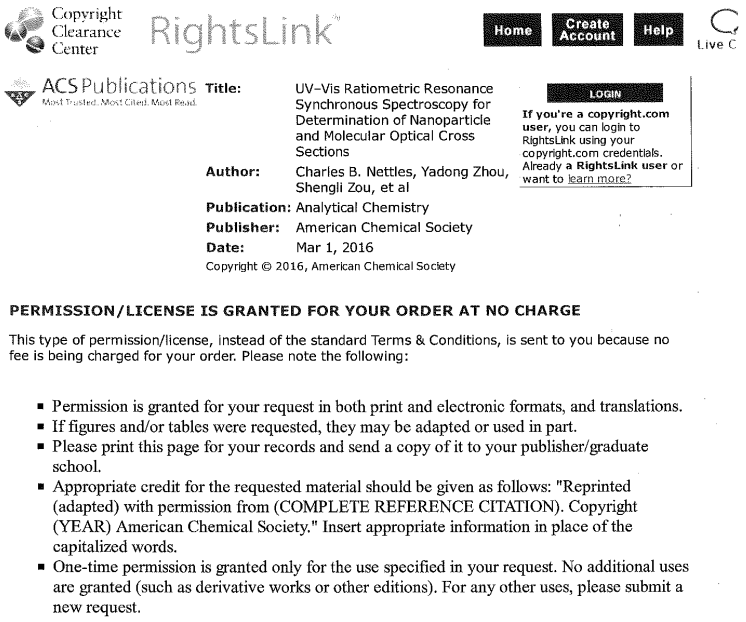

Copyright Clearance Center RightsLink

Home | Create Account | Help | Live C

ACS Publications
Most Trusted. Most Cited. Most Read.

Title: UV–Vis Ratiometric Resonance Synchronous Spectroscopy for Determination of Nanoparticle and Molecular Optical Cross Sections

Author: Charles B. Nettles, Yadong Zhou, Shengli Zou, et al

Publication: Analytical Chemistry

Publisher: American Chemical Society

Date: Mar 1, 2016

Copyright © 2016, American Chemical Society

LOGIN

If you're a copyright.com user, you can login to RightsLink using your copyright.com credentials. Already **a RightsLink user** or want to learn more?

PERMISSION/LICENSE IS GRANTED FOR YOUR ORDER AT NO CHARGE

This type of permission/license, instead of the standard Terms & Conditions, is sent to you because no fee is being charged for your order. Please note the following:

- Permission is granted for your request in both print and electronic formats, and translations.
- If figures and/or tables were requested, they may be adapted or used in part.
- Please print this page for your records and send a copy of it to your publisher/graduate school.
- Appropriate credit for the requested material should be given as follows: "Reprinted (adapted) with permission from (COMPLETE REFERENCE CITATION). Copyright (YEAR) American Chemical Society." Insert appropriate information in place of the capitalized words.
- One-time permission is granted only for the use specified in your request. No additional uses are granted (such as derivative works or other editions). For any other uses, please submit a new request.

Figure A.3 Copyright permission form for Chapter IV

Notes: The content covered in Chapter IV contains material previously published by the American Chemical Society in Analytical Chemistry. Content is referenced as Nettles, C. B.; Zhou, Y.; Zou, S.; Zhang, D., UV-Vis Ratiometric Resonance Synchronous Spectroscopy for Determination of Nanoparticle and Molecular Optical Cross Sections. *Anal. Chem.,* **2016**; *88*: 2891-2898